ABSTRACT

Title of Dissertation: RELIABILITY ASSESSMENT OF OPTICAL FIBERS UNDER TENSION AND BENDING LOADS

Yubing Yang, Doctor of Philosophy, 2003

Dissertation Directed by: Professor D. Barker
Department of Mechanical Engineering

The mechanical failure of optical fibers must be avoided to ensure reliability of fiber-based systems. The first stress event in a fiber's lifetime is the proof test. The proof test will alter the fiber's strength distribution for all subsequent processing and applications. Thus it is critical to know the fiber strength distribution after proof test (post-proof strength distribution). It is generally assumed that the proof test truncates the strength distribution at the proof test stress level. But, many users are concerned because they know that theoretically it has been shown that after proof test the strength of fiber may be much less than the proof test stress level, and that the minimum post-proof strength is determined only by the unloading rate during the proof test. But this theoretical result is not consistent with historical field data. Historically no one has documented failures stresses below the proof stress level. This dissertation resolves this apparent contradiction by reviewing the theory and conducting a probabilistic

assessment.

As optical fibers are used more and more in computer and switching gear backplanes, a new potential mechanical reliability problem arises due to the necessary bends introduced in optical fibers. Previous researchers were concerned with the uniform stress optical fibers saw in long haul underground applications, but bending places a non-uniform stress along the fiber surface. So it is inaccurate to borrow fiber usage mechanical guidelines from long-haul application. This dissertation reviews existing theories and then develops a new analytic approach to assess the mechanical reliability of optical fibers under bending loads and static fatigue conditions. This new analytic approach is verified through a simple static two-point bend experiment. Finally the newly developed reliability assessment method is used to develop new guidelines for bending application and examples are presented to show how the approach can be used to attack some very common mechanical reliability problems with optical fibers.

RELIABILITY ASSESSMENT OF OPTICAL FIBERS UNDER TENSION AND BENDING LOADS

by

Yubing Yang

Thesis submitted to the Faculty of the Graduate School of the
University of Maryland, College Park in partial fulfillment
of the requirements for the degree of
Doctor of Philosophy
2003

Advisory Committee:

Professor Donald Barker, ME Dept., Chairman / Advisor
Professor Abhijit Dasgupta, ME
Professor Christopher C. Davis, ECE
Associate Professor Bongtae Han, ME
Associate Professor F.Patrick McCluskey, ME

DEDICATION

To my father and mother, who have encouraged me to pursue the best and supported me with all their heart, and to my husband Ling, who has spiritually supported me and academically helped me with his wit.

ACKNOWLEDGEMENTS

When I started my first day in school, I could never imagine I would make it so far. Now I did it, but not without help and support from so many others.

Thank you teachers at the elementary and secondary schools in my local hometown. You have been doing your best with limited resources.

Thank you Tsinghua University for embracing me at the best university of China. During tight years, you used your unique harsh way to help me establish a solid foundation for my further study.

Thank you University of Maryland for welcoming me from the other side of Earth. You gave me the opportunity to see a different world, experience different cultures, and have some different thoughts. Also you supported me with your advanced facilities and abundant resources. This four year study was rewarding. I have learned so much from teachers and students.

Thank you Dr. Mead for accepting me in the first place.

Thank you Dr. Davis. Your courses showed me the wonderful world of Electro-Optics.

Thank you Siva and Keita for teaching me how to use lab equipment and be patient with all my questions.

And most of all, thank you Dr. Barker. You guided me with your knowledge, kindness and patience through these three years. I appreciate more than words can say.

TABLE OF CONTENTS

LIST OF FIGURES

LIST OF TABLES

Chapter 1

INTRODUCTION

1.1 Problem Statement

Currently, optical fiber based telecommunication networks are major information transmission systems. Optical fiber encircles the globe, in both terrestrial and marine installations. Mechanical failure of optical fiber must be avoided to ensure reliability of fiber-based system.

Before installation there is a flaw size distribution along the fiber surface. During the component's field lifetime, these flaws will grow over time under stress. If the stress is sufficiently high, a flaw will grow large enough to cause catastrophic failure. This classic flaw growth behavior and the models used to estimate failure have been studied for several decades. The power law is widely used to predict fiber lifetime. However, there are some subtle but important issues needing clarification. The proof test is one of them.

The proof test is the first stress event in a fiber's lifetime. It will alter the fiber strength distribution for all subsequent process and application events. Knowing the fiber strength distribution after proof test (post-proof strength distribution) is important. The assumption has been made that the proof test truncates the strength distribution at the proof test stress level. But, theoretically it has been shown that after proof test the

strength of fiber may be much less than the proof test stress value, and the minimum post-proof strength is determined only by the unloading rate during the proof test [Fuller Jr.,1980, Hanson,1997, Bubnov,1998]. This theoretical conclusion is not consistent with historical field data. According to Glaesemann [Glaesemann, 1991a], 'no failures below proof stress were recorded'. Why is the theoretical analysis not consistent with practical experience? Is the proof test useful for eliminating weak fibers out or is it harmful because it degrades the fiber strength too much? This study aims to answer these questions.

Another problem drawing attention currently is the mechanical reliability of fibers in bending. With the trend of using optical fibers in backplanes, optical fiber often finds itself in the situation where it is coiled in a tight space, routed through a package or bent as it connects devices together. Furthermore, the trend in the industry is to make components smaller and smaller. Tight bends can place high levels of stress on the fiber, posing a possible reliability risk; different from the long-haul application, bending places a non-uniform stress along the fiber surface. So it is inaccurate to borrow guidelines from long-haul application. Bending is a relatively new topic in the subject of optical fiber reliability. Some basic theories have been derived, such as the instantaneous reliability assessment for fibers in bending (without fatigue), but improvement is needed to give solutions for more meaningful and complicated situations, such as fibers in bending with static fatigue, and guidelines for industrial applications.

1.2 Research Contribution

After understanding theoretical analysis from various researchers, the emphasis of this research will be placed on the following topics:

- Reliability assessment for optical fibers after proof testing
- Reliability assessment for optical fibers in bending with static fatigue

For the proof testing problem, there is a contradiction between theory and practice which needs to be clarified. Based on the analysis method for pure bending without strength degradation presented by Methewson and Glaesemann, a method for reliability assessment after strength degradation will be established.

Besides the theory clarification and development, what is more important is to give more physical meaning to theoretical analysis, and assembly them into a thorough guideline for optical fiber reliability assessment, which could be used in industrial application.

Chapter 2

BACKGROUND

2.1 Fiber Defects

The fiber surface can be damaged before the coating is applied during the drawing process. The most common form of surface damage is through the fiber coating during post processing or handling steps. Ritter et al. [Ritter, 1998] claimed that for large abrasion flaws in bulk silica glass, the radial crack would always control failure. It is not known if the smaller abrasion type flaws in optical fiber can be generated in this fashion. A deeper understanding of flaw morphologies related to specific handling events is needed.

The other basic flaw type for optical fiber is embedded particles [K. Yoshida, 1996]. Particulates can be entirely contained within the fiber preform or exist partially embedded on the fiber surface. The frequency of these flaws has decreased over the years as manufacturing processes have improved.

The distinction between internal and external flaw is important in that internal flaws will not grow subcritically over time due to the absence of molecular water [Glaesemann, 1999]. For the fiber strength degradation issues, what concerns us is the surface flaws caused by previous mechanical handling.

2.2 Stress Intensity Factor

A well-defined sharp surface crack locally amplifies the applied stress at the crack tip. When a piece of fiber with a surface crack of length a is subjected to an applied stress σ_a, the actual stress field ahead of the crack tip is given by Eq.(2-1), and schematically shown in Figure 2.1 ,

$$\sigma = \frac{K_I}{\sqrt{2\pi r}} \tag{2-1}$$

where r is the distance from the crack tip, and K_I is the stress-intensity factor. The stress will not reach infinity because it is limited by the material yield strength.

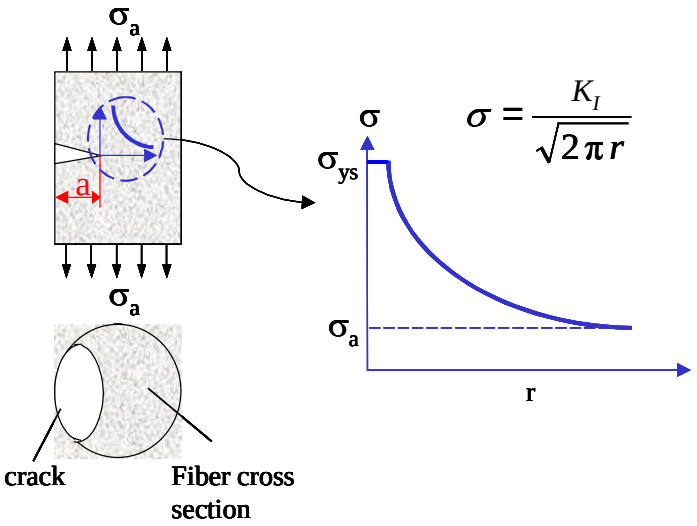

Figure 2.1 Stress field ahead of a crack tip

In Fracture Mechanics, the stress-intensity factor, K_I, instead of stress is used to analyze the stress field ahead of a sharp crack. The critical value of stress-intensity factor is K_{Ic}, called the critical stress intensity factor. When the crack length grows, K_I increases accordingly. If K_I reaches K_{Ic}, the intrinsic strength of the material is exceeded and catastrophic failure occurs.

K_I is determined by the applied stress, the crack size, and shape.

$$K_I = \sigma_a Y \sqrt{a} \tag{2-2}$$

where Y is the geometry factor which describes the crack shape, and the typical value of 1.294 [W. Griffioen, 1992] is used in the dissertation. a is the crack length. σ_a is the applied stress.

The value of K_{Ic} is determined by the material property, fracture toughness; for silica glass fiber, the typical value is 0.8 MPa·m$^{1/2}$ [W. Griffioen, 1992]. There is no evidence indicates the degradation of K_{Ic}, which has been observed in some ceramics. So it is assumed in this dissertation that K_{Ic} is constant.

When a fiber with a crack of length a is subjected to a stress S, which satisfies $S \cdot Y\sqrt{a} = K_{Ic}$, the fiber will break immediately without crack growth. This stress S is called the *inert strength* of the fiber. For simplification purposes, the word “strength” instead of “inert strength” is used in following discussions.

2.3 Subcritical Crack Growth (Strength Degradation)

The combined influence of stress at the crack tip, and reactive species in the environment, particularly water, cause subcritical crack growth of fiber. There are several alternative kinetics models proposed in the literature [Matthewson, 1999, Bubel, 1991, Armstrong, 2000]. Because of its good fitness to fatigue life data and analytical simpleness, the one-region model is mainly used for crack growth model for subcritical crack growth.

2.3.1 One- Region Model

The subcritical crack growth rate is normally assumed to follow a one-region power law model (Figure 2.2)

$$\dot{a} = AK_I^{\,n} \tag{2-3}$$

where A and n are stress corrosion constants. For glass fiber, n is 20~25 [Bubnov, 1998].

Therefore, according to Eq.(2-2) and (2-3) the applied stress causes the crack to extend, in turn increasing K_I, leading to an increase in the growth rate, so the crack will grow faster. This eventually causes K_I to reach the critical value K_{Ic} and failure ensues. The strength of the fiber, $S = K_{Ic}/(Y\sqrt{a})$, will degrade because of increasing crack length, a. Fiber strength degradation under a sustained stress is called static fatigue; otherwise dynamic fatigue. Static fatigue happens during the service life of fibers, and dynamic fatigue happens during fiber strength measurement test and proof test.

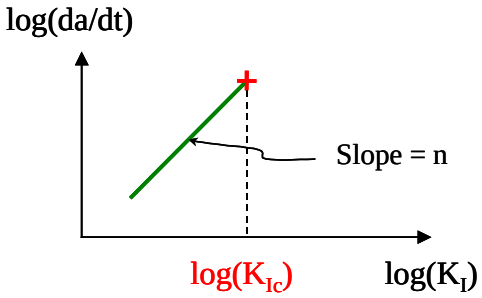

Figure 2.2 Schematic drawing of the one-region crack growth model

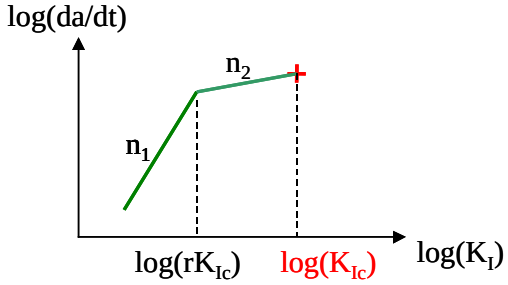

Figure 2.3 Schematic drawing of the two-region crack growth model

Combining Eq.(2-2) and (2-3), for any load cycle, an expression between the initial strength, S_i, and the degraded strength at any time during the load cycle, $S(t)$, can be derived, provided the applied stress is known as a function of time [E.R. Fuller Jr., et.al., 1980].

$$S(t)^{n-2} = S_i^{n-2} - \frac{1}{B}\int_0^t \sigma(t)^n \, dt \qquad (2\text{-}4)$$

where $1/B = (n-2)AY^2 K_{Ic}^{n-2}/2$.

For static fatigue problems, during service life, where the applied stress is a constant, σ_a, it is easy to get the commonly used life prediction equation which employs the one-region crack growth model:

$$t_f = BS_i^{n-2}\sigma_a^{-n} \qquad (2\text{-}5)$$

2.3.2 Two-Region Model

In recent years, it has become increasingly apparent that a single region of crack

growth was insufficient to explain crack growth during both high-speed and long-term low-stress events. Hanson and Glasesemann argued by experiment that the incorporation of the well known Region II (Figure 2.3) into the crack growth model is helpful. Their experiment showed contradictions surrounding the B value as well as previously observed non-linear dynamic fatigue behavior [Hanson and Glaesemann, 1997]. They argued for high-speed events, such as the proof test, and Region II crack growth plays a significant role in establishing the post-proof strength distribution. The proof test problem will be discussed in Chapter 3.

In the two-region model the crack growth model is

$$\dot{a} = A_1 K_I^{\,n_1}, \quad \text{For } \frac{K_I}{K_{Ic}} < \text{r}$$
$$\dot{a} = A_2 K_I^{\,n_2}, \quad \text{For } \frac{K_I}{K_{Ic}} > \text{r} \tag{2-6}$$

where rK_{Ic} is the K_I value in the *da/dt-K* curve where Region I and II intersect. A_1 and n_1 are stress corrosion constants in region I, and A_2 and n_2 are stress corrosion constants in region II. The integration in Eq.(2-4) would be applicable within each region of crack growth, with appropriate values of *A* and *n* being used. Thus, if the crack goes from region I to region II, then Eq.(2-4) needs to be evaluated in two steps.

2.4 Optical Fiber Strength Distribution

The fiber strength distribution is a key element for mechanical reliability models attempting to predict optical fiber lifetime. The fiber strength distribution curve gives the probability of breaking a fiber under a specific loading stress. This probability is equal to the probability of finding a crack whose strength is less than the loading stress. Fiber strength is not a material property, but rather a statistical parameter reflecting the distribution of crack sizes along the fiber surface.

2.4.1 The Weakest Link Theory for Fiber Reliability

The failure of a piece of fiber is actually a cumulative result of all unit areas along its surface. For a unit area surface, ΔA_1, its failure probability can be described by the Weibull model [Matthewson, 1986, Glaesemann, 1991b].

$$F_{\Delta A_1} = 1 - \exp\left(-\left(\frac{\sigma_{\Delta A_1}}{\sigma_o}\right)^m\right) \tag{2-7}$$

Where $\sigma_{\Delta A_1}$ is the actual applied stress on area ΔA_1. According to the weakest link theory, the failure probability of the whole surface area is

$$F = 1 - R_{\Delta A_1} \cdot R_{\Delta A_2} \cdots\cdots \tag{2-8}$$

$$F = 1 - \exp\left(-\left(\frac{\sigma_{\Delta A_1}}{\sigma_o}\right)^m\right) \cdot \exp\left(-\left(\frac{\sigma_{\Delta A_2}}{\sigma_o}\right)^m\right) \cdots\cdots \tag{2-9}$$

$$F(\sigma) = 1 - \exp(-\int_A \frac{1}{A_0}\left(\frac{\sigma(A)}{\sigma_o}\right)^m dA) \tag{2-10}$$

The total failure probability of a piece of fiber under a nominal stress, σ, is the integration result of the actual stress over the whole surface of fiber, shown by Eq.(2-10). In Eq.(2-10), A_0 is a constant to keep dimensional consistency.

2.4.2 Fiber Length Influence on Strength Distribution

For a straight fiber of length L_t, under a uniform tensile stress σ_t, it is easy to get a analytical solution of strength distribution, i.e. the failure probability vs. stress, from Eq.(2-10)

$$F(\sigma_t) = 1 - \exp(-\frac{2\pi rL_t}{A_o}\left(\frac{\sigma_t}{\sigma_o}\right)^m) \tag{2-11}$$

Here r is the radius of fiber cladding.

Conceptually, the length of the fiber plays an important role in the strength distribution of fibers. For a piece of fiber with a longer length, there is a higher probability of finding a crack whose strength is less than σ_t, thus, there will be a corresponding shift of the strength distribution curve. This relationship can be seen from Eq.(2-11). Mathematically, it can be proven that at a low failure probability level, the failure probability is directly proportional to the fiber length. Because from mathematics

$$\text{For } 1 - e^{-p}, \text{ if } p << 1, \text{ then } 1 - e^{-p} \cong p \tag{2-12}$$

When $1-e^{-p}=0.1$, the exact value of p is 0.105. So when p is less than 0.1, Eq.(2-12) is a good approximation. So for $F(\sigma_t) < 0.1$, then

$$F(\sigma_t) = \frac{2\pi r}{A_o}\left(\frac{\sigma_t}{\sigma_o}\right)^m \cdot L_t \tag{2-13}$$

For fibers of the same quality, constants A_0 and σ_0 will not change, then the failure probability will only be proportional to fiber length L_t. Figure 2.4 shows a picture from Coring. Corning did the tensile strength distribution test for 20 m long fiber, then they can shift the curve to get the distribution of fibers of different lengths.

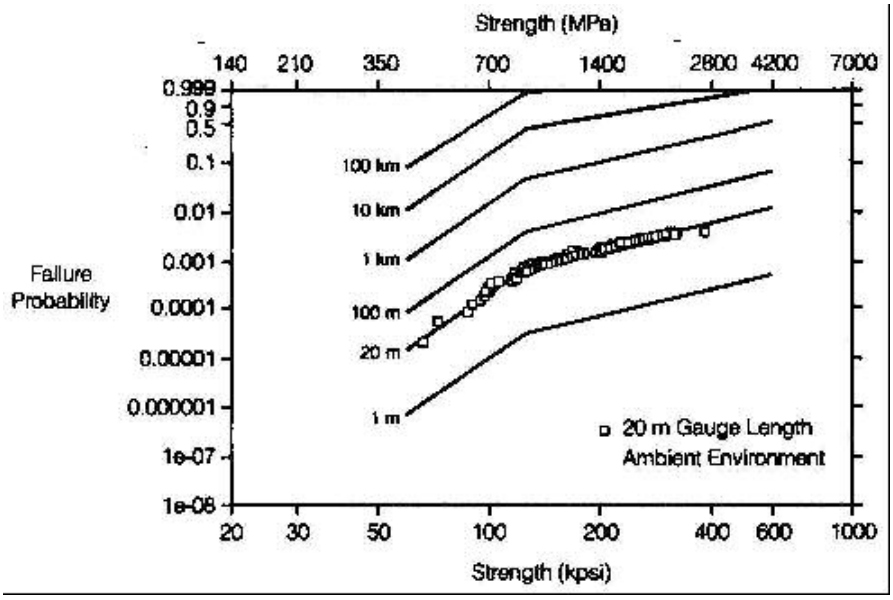

Figure 2.4 Length influence plot by Corning [Glaesemann, 1991b]

2.4.3 Corning's 20 m Optical Fiber Strength Distribution

Figure 2.5 is a strength distribution of optical fiber proof tested to 50 ksi (350MPa) tested by Corning in 1986, using 20 m gauge length [Glaesemann, 1991b]. The test was performed under ambient conditions, and a total of 17 km of fiber were tested.

The distribution is not unimodal and generally can be described by two regions. The two regions that are observed are: a high strength mode, which is very narrow, and a much broader low strength tail. The high strength or "intrinsic" region extends to the 5% failure probability level and a strength of approximately 500 ksi (3450 MPa). The low strength region extends from some point above the proof test stress level to 500 ksi gradually. Therefore, the fiber has essentially a very high strength, except for occasional weak defects, which have a broad range of possible strengths. There is a region III in Figure 2.5 that is plotted by the dashed line. It is the predicted truncation of the proof testing at 50 ksi, because no failures were observed below 75 ksi (520 MPa). Whether this predicted truncation is correct or not will be discussed in detail in Chapter 3. Region III is imposed on the strength distribution by proof test, whereas the first two regions reflect the distribution of flaws induced by manufacturing and handling prior to proof test.

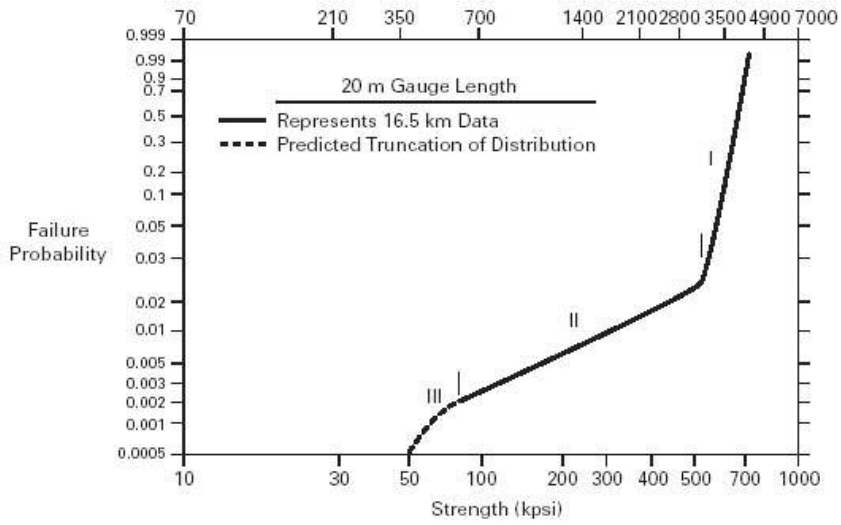

Figure 2.5 Strength distribution of standard silica-clad fiber under ambient conditions [Glaesemann, 1991b]

Normally people will fit the tensile strength data into a two-parameter Weibull distribution curve like

$$F(\sigma_t) = 1 - \exp(-\left(\frac{\sigma_t}{\beta_t}\right)^{m_t}) \tag{2-14}$$

Here m_t and β_t are the Weibull parameters, referred to as the *shape parameter* and the *scale parameter*, respectively.

Comparing Eq.(2-11) and (2-14) it is easy to get

$$m = m_t$$

$$A_0 \sigma_0^{\ m} = 2\pi r L_t \beta_t^{\ m} \tag{2-15}$$

Based on the tensile test data of fibers, of length L_t, it is easy to get the fiber

quality constants, like A_0, σ_0, and m. Then calculate the probability of fibers of different lengths and/or under different loading situations, like bending, which will be discussed in Chapter 4.

In 1991, Corning Inc. tested 386 kilometers of titania-doped silica-clad fiber proofed to 50 ksi (350 MPa) to a maximum stress level of 350 ksi (2450 MPa). The number of recorded failures below 350 ksi was 106 out of a total 19,300 individual 20 meter tests [Glaesemann, 1991b]. Corning did their newest test in 2000. This time 3800 kilometers of 100 ksi proofed single-mode fiber was tested [Castilone, 2000].

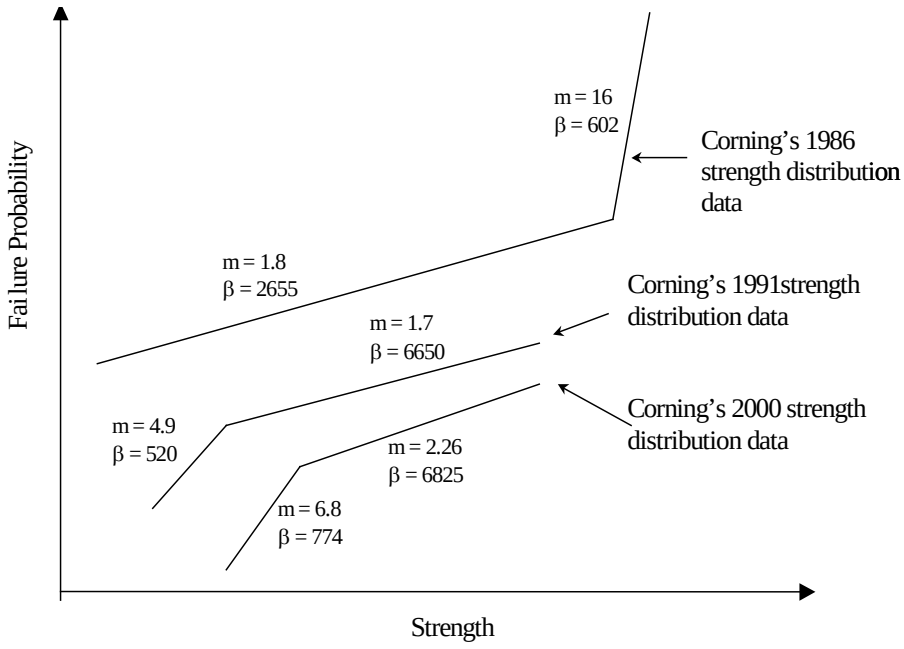

Figure 2.6 Optical fiber tensile test result from Corning

2.5 Summary

Subcritical crack growth is the behavior of discrete cracks. The strength distribution of failure probability, of a piece of fiber, is an integration result of all the crack strength or degraded strength distributed along the fiber surface using the weakest link theory. The idea of using the weakest link theory in fiber strength distribution is so important that one cannot fully understand the fiber strength distribution without understanding the theory and this is the basis for solving the bending problem. This is the first time the proportional relationship between the failure probability and the fiber length is being explicitly proposed and mathematically proven.

Chapter 3

RELIABILITY ASSESSMENT FOR FIBERS AFTER PROOF TEST

3.1 Optical Fibers Proof Test

The idea of the proof test is to load the fibers to a pre-selected tensile stress level for a measured time period to limit flaw size, by breaking the fibers with unacceptably large flaws. For a typical proof test, a fiber is loaded at a constant loading rate, $\dot{\sigma}_l = \sigma_p / t_l$, held at the proof load, σ_p, for a time t_p, and then unloaded at a constant rate, $\dot{\sigma}_u = \sigma_p / t_u$. Figure 3.1 shows a typical proof test profile. A schematic diagram of the proof tester used by the optical fiber manufacture Corning Inc. is given in Hanson's paper [Hanson, 1994]. The typical proof test stress level in industry now is 100 ksi (0.69 GPa).

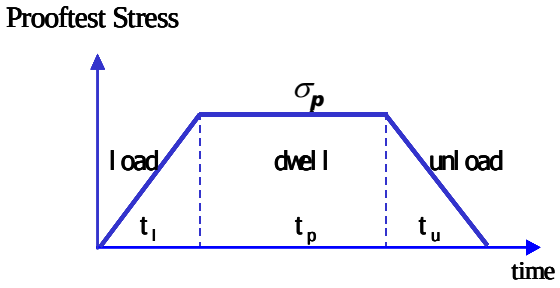

Figure 3.1 Typical proof test stress profile

It has been assumed that the fibers that survive the proof test have a minimum tensile strength of the proof test stress level. Then the minimum lifetime after the proof test under an applied static loading, σ_a, is given by Eq.(3-1) according to the one-region crack growth model.

$$t_{f\,\min} = B\sigma_p^{\,n-2}\sigma_a^{\,-n} \tag{3-1}$$

t_{fmin} is the minimum life time guaranteed after the proof test without worrying about a failure. Does the proof test really guarantee the minimum lifetime? Or, does the proof test really guarantee a post-proof strength not lower than the proof test stress value? One can contend conceptually, an actual brittle material will experience strength degradation during the proof test, as shown in Figure 3.2. As the stress is removed during unloading, the flaw still has the opportunity to continue growing as stress still exists. Thus, the post-proof strength, S_f, might be less than the proof stress, σ_p.

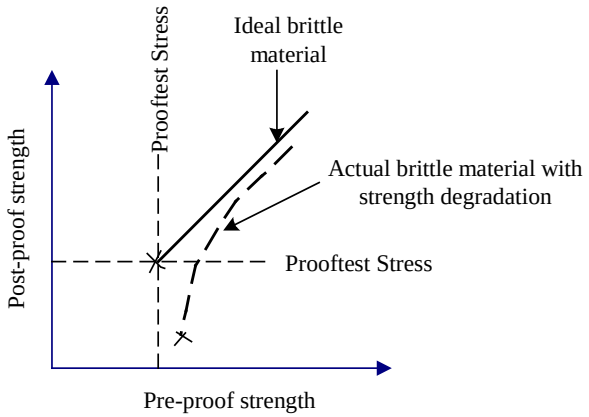

Figure 3.2 Schematic plot of post-proof strength vs. pre-proof strength of an actual brittle material

Is the post-proof fiber strength distribution just truncated at the proof stress level from the pre-proof strength distribution? Do those high strength fibers that pass the proof test also undergo strength degradation to some extent? How does this influence the post-proof strength distribution? Also, the development of adequate proof test procedures for optical fiber requires the strength distribution after proof test to be well characterized, especially in the low strength regime.

These questions will be answered in this chapter.

3.2 Fiber Strength Degradation Behavior during Proof Test

During the proof test, the loading stress as a function of time, $\sigma(t)$, is known if given the proof test parameters, σ_p, t_p, t_l, t_u. For a given pre-proof strength S_i, fiber strength degradation behavior through the whole proof test process can be traced.

a) load, $S^{n-2}(t) = S_i^{n-2} - \frac{1}{B} \cdot \frac{\sigma_p^n}{t_l^n} \cdot \frac{t^{n+1}}{n+1}$, when $t \le t_l$

b) dwell, $S^{n-2}(t) = S_i^{n-2} - \frac{1}{B} \cdot \sigma_p^n \cdot \frac{t_l}{n+1} - \frac{1}{B} \cdot \sigma_p^n \cdot (t - t_l)$,

when $t_l < t \le t_l + t_p$ (3-2)

c) unload, $S^{n-2}(t) = S_i^{n-2} - \frac{1}{B} \cdot \sigma_p^n \cdot (t_p + \frac{t_l + t_u}{n+1}) + \frac{1}{B} \cdot \sigma_p^n \cdot \frac{(t_l + t_p + t_u - t)^{n+1}}{(n+1) \cdot t_u^n}$,

when $t_l + t_p < t \le t_l + t_p + t_u$

and the post-proof strength is given by

$$S_f^{\,n-2} = S_i^{\,n-2} - \frac{1}{B} \cdot \sigma_p^{\,n} \cdot \left(t_p + \frac{t_l + t_u}{n+1}\right) \tag{3-3}$$

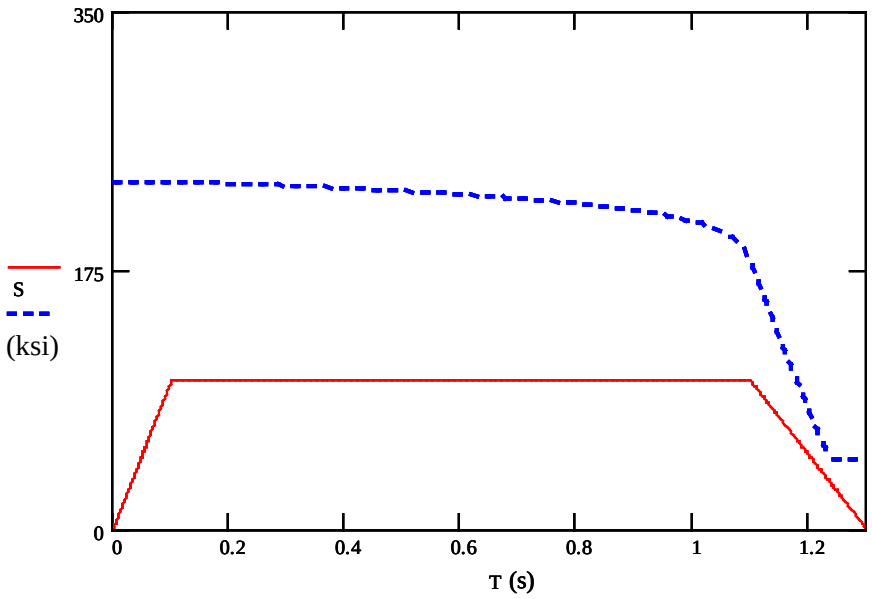

Figure 3.3 A computer simulation result of strength degradation behavior during proof test

Figure 3.3 shows an actual strength degradation behavior during proof test by computer simulation. The proof test parameters used in this simulation are: σ_p = 100 ksi, t_p = 1 sec, t_l = 0.1 sec, t_u = 0.2 sec. The one-region model crack growth constants are: n = 25, $B = 10^{-7}$ GPa^2·s. And the initial strength is S_i = 235.13943573054 ksi. In this simulation, to display the strength degradation during the unloading period, the

unloading time is elongated to 0.2 seconds; normally it is much shorter than this value.

Equation (3-2) and (3-3) are from the one-region crack growth model. Simulation, based on the two-region crack growth model, will result in the similar strength degradation curve like Figure 3.3. But, no simple analytical expressions like Eq.(3-2) could be found for the two-region model; a numeric method has to be employed. Given an initial strength, S_i, which corresponds to an initial crack length, a, for a time increment, dt, the change in crack length, da, during this period of time is determined from the crack velocity da/dt. The new crack length, $a+da$, is used to calculate a new strength. Then the new crack length is used in the next cycle, dt, as the initial crack length. By repeating this calculation cycle many times, one can get the degraded strength at every time increment, dt. At the end of each cycle, a comparison is made to determine the correct crack growth region, so the corresponding constants can be used. Finally if the condition $S = \sigma$ is reached, then fracture is assumed to occur. A Mathcad program to demonstrate this two-region model calculation is given in Appendix A, as well as a strength degradation curve from this simulation.

It is helpful to look at the time derivative of $S(t)$, dS / dt, to understand where those bends (the drop off and the level up) in Figure 3.3 come from. dS / dt gives the slope of the strength degradation curve at any point. Beginning with $S = \frac{K_{Ic}}{Y\sqrt{a}}$, the time derivative calculation yields

$$\frac{dS}{dt} = -\frac{1}{B(n-2)} \cdot S^3 \cdot \left(\frac{\sigma}{S}\right)^n \tag{3-4}$$

The detailed derivation procedure is given in Appendix B.

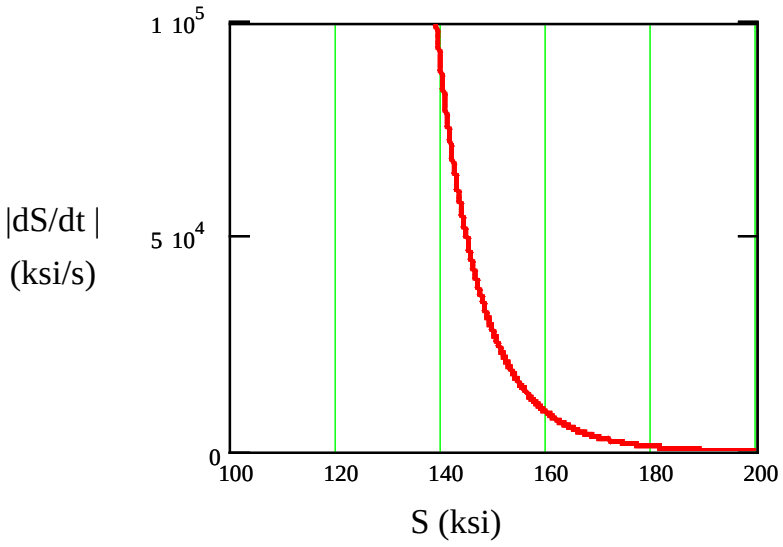

Figure 3.4 Time derivative of strength during proof test

Figure 3.4 shows the calculation result of dS/dt. The constants used in the calculation are: n = 25, $B = 1\times10^{-7}$ GPa^2·s = 2.1×10^{-3} ksi^2·s, σ_p = 100 ksi. From Figure 3.4, at strength of approximately 160 ksi strength, the absolute value of the time derivative of strength begins to increase dramatically, which explains the rapid strength drop off in Figure 3.3. During the unloading period, due to the high speed of unloading, the speed of strength degradation drops greatly, leading to the second bend (the level up) of the curve.

From the computer proof test simulation four cases could happen during a proof test, shown schematically in Figure 3.5. Fiber 'a' passes the proof test with little strength degradation because of its high pre-proof strength; fiber 'd' fails the proof test because of its lower pre-proof strength. 'b' and 'c' are two critical cases in the middle. Fiber 'b' passes the proof test, and with a post-proof strength equal to the proof stress, i.e. $S_{fb} = \sigma_p$. Fiber 'c' just survives the proof test, but with a post-proof strength much less than the proof test stress level. Thus, S_{ic} is the minimum pre-proof strength that can pass the proof test and S_{fc} is the minimum post-proof strength.

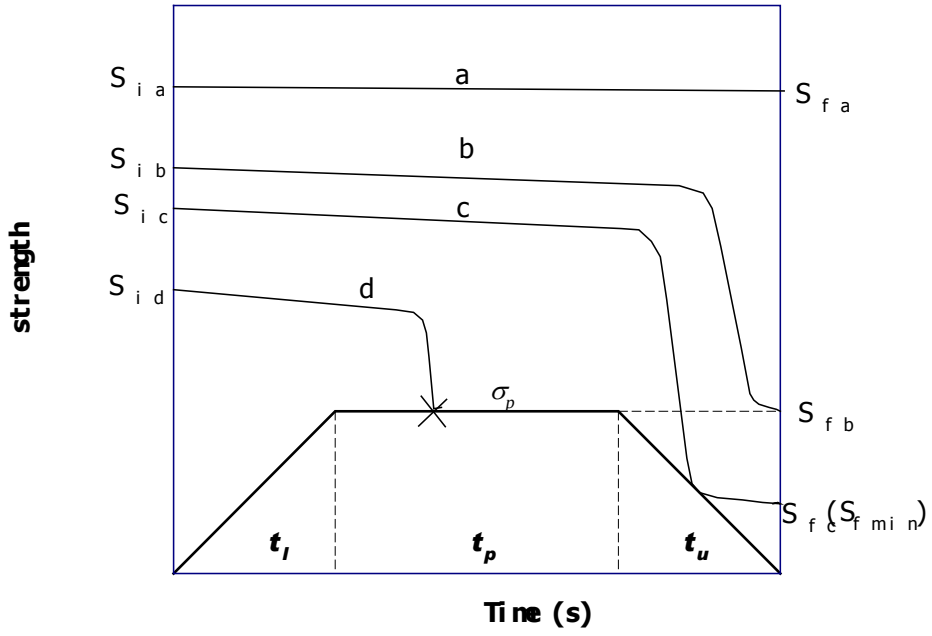

Figure 3.5 Schematic strength degradation behaviors during proof test

Actually these four strength degradation behaviors have been shown in literature [Bubnov, 1998]. But there are still many questions that need to be asked.

From Figure 3.5, it can be seen that for strong fibers like 'a', they will not experience noticeable strength degradation during the proof test. But, how strong do the fibers need to be to have negligible strength degradation? And how many fibers pass the proof test but with a substantial strength degradation like fiber 'b' does?

Redrawing Figure 3.2 but with an actual curve for an optical fiber from a computer simulation gives a curve shown in Figure 3.6. The constants used in the calculation are: $n = 20$, $B = 1\times10^{-7}$ GPa^2·s $= 2.1\times10^{-3}$ ksi^2·s, $\sigma_p = 100$ ksi, $t_l = 0.1$ sec, $t_p = 0.3$ sec, $t_u = 0.001$ sec.

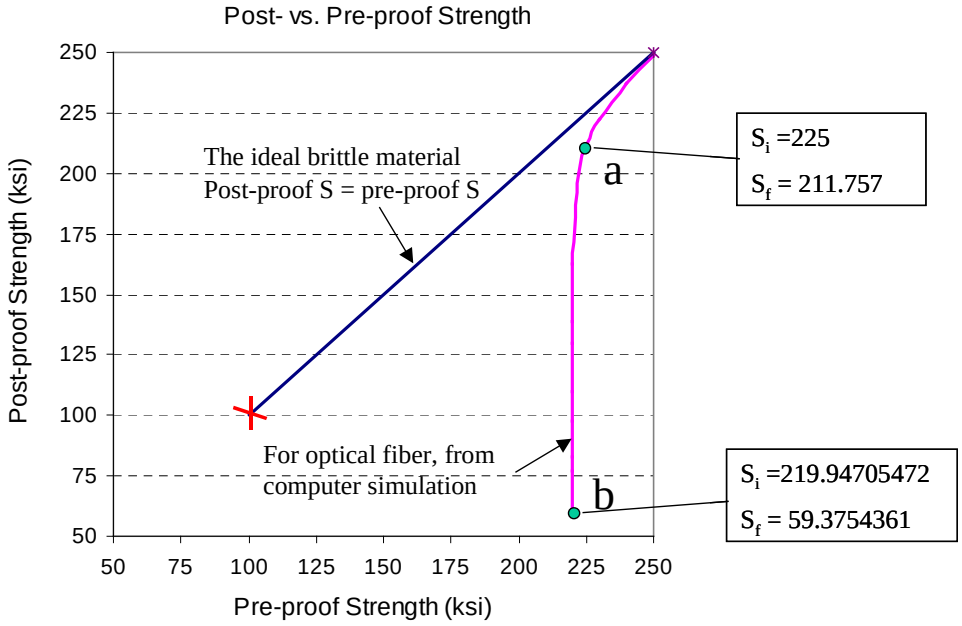

Figure 3.6 Practical strength plot after proof test simulation

At high S_i level (>250 ksi), from Figure 3.6, the curve overlaps with the straight line of the ideal brittle material, whose $S_f = S_i$. With the decrease of S_i, the actual S_f degrades from S_i, first slowly but below approximately 225 ksi this degradation becomes dramatic. From point 'a' to 'b', S_i only drops by 5 ksi, but it causes S_f to drop from 211.757 ksi to 59.3754361 ksi. It is important to specify the many significant figures of S_i of point 'b' (219.94705472). Because if S_i = 219.94705471, the fiber will break during the proof test. Theoretically, one can get a minimum S_f, which is much less than the proof test stress 100 ksi, from a S_i, which is between 219.94705471 and 219.94705472. But, actually it is limited by the capacity of the computer. There are analytical methods that can be used to find this minimum post-proof strength, S_{fmin}.

3.3 The Theoretical Minimum Post-proof Strength (S_{fmin})

Fuller, et. al., analytically calculated the minimum post-proof strength, $S_{f\min}$, based on the one-region model [Fuller Jr.,1980]. The basic idea from Fuller's method is to determine the strength of the tangent point, $S_{*\min}$, of the 'just survive' case, then determine $S_{f\min}$ from $S_{*\min}$. His procedure is given here.

According to Eq.(3-4) the time derivative of strength along the proof test profile is

$$\frac{dS}{dt} = -\frac{1}{2} AY^2 K_{Ic}{}^{n-2} (\frac{\sigma}{S})^n S^3 \tag{3-5}$$

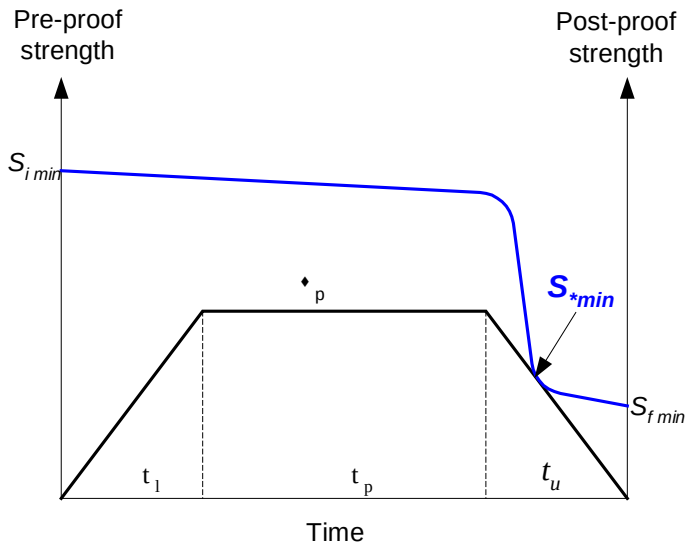

Figure 3.7 The 'just survive' situation

For the 'just survival' situation shown in Figure 3.7, there is a point where the *S(t)* curve is tangent to the unloading stress profile named $S_{*\min}$

$$\frac{dS}{dt} = -\dot{\sigma}_u \tag{3-6}$$

$$S(t) = \sigma(t) = S_{*\min} \tag{3-7}$$

Substituting Eq.(3-6) and (3-7)into Eq.(3-5) yields

$$S_{*\min} = \sqrt[3]{(n-2)B\dot{\sigma}_u} \tag{3-8}$$

Then, determining $S_{f\min}$ from $S_{*\min}$. According to Eq.(2-4)

$$S_{f\min}{}^{n-2} = S_{*\min}{}^{n-2} - \frac{1}{B}\int_0^{S_{*\min}/\dot{\sigma}_u} (S_{*\min} - \dot{\sigma}_u \cdot t)^n \, dt \tag{3-9}$$

Fuller's final result is given by

$$S_{f\min} = [B\cdot(n-2)\cdot\dot{\sigma}_u]^{1/3}\cdot\left(\frac{3}{n+1}\right)^{1/(n-2)} \tag{3-10}$$

According to Fuller, the higher the unloading rate, the greater $S_{f\min}$ will be. But, there is one scenario missed in his analysis: what if the tangent point calculated from Eq.(3-8) is higher than the proof stress, i.e., $S_{*\min} > \sigma_p$, as curve "a" in Figure 3.8?

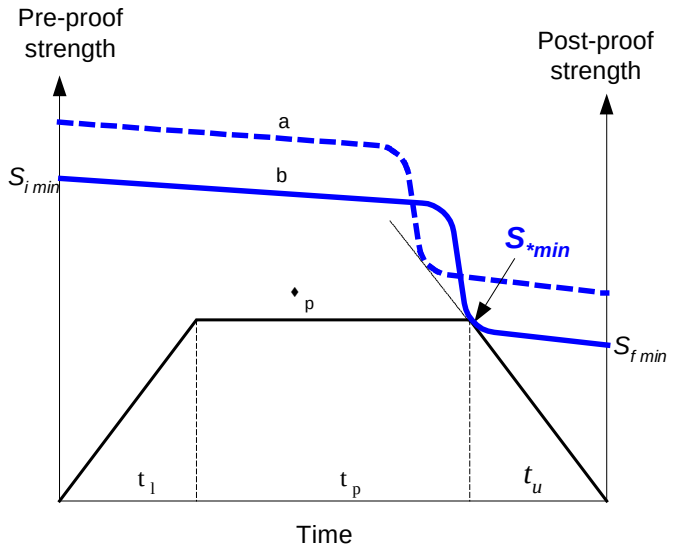

Figure 3.8 The situation that the calculated $S_{*\min}$ is higher than the proof stress

Obviously for this situation, $\sqrt[3]{(n-2)B\dot{\sigma}_u}$ does not give the correct value of $S_{*\min}$, because when Fuller calculated it, he assumed $S(t) = \sigma(t) = S_{*\min}$, for this case the assumption is not true. One can certainly lower the pre-proof strength to get a lower bend point, until the bend point reaches the proof test stress level σ_p. The curve cannot be lowered further, because the unloading rate is so high that there is no tangent point from Eq.(3-8), which is lower than the proof test stress level σ_p. So curve 'b' is the correct solution for this situation, where $S_{*\min} = \sigma_p$.

So the determination of $S_{*\min}$ depends on a parameter α, defined as

$$\alpha = \frac{{\sigma_p}^3}{B(n-2)\dot{\sigma}_u} \tag{3-11}$$

if $\alpha > 1$, then $S_{*\min} = \sqrt[3]{(n-2)B\dot{\sigma}_u}$

if $\alpha \le 1$, then $S_{*\min} = \sigma_p$

Then derive S_{fmin} from S_{*min} by Eq.(3-9), the modified final result is

if $\alpha > 1$, then $S_{f\min} = [B \cdot (n-2) \cdot \dot{\sigma}_u]^{1/3} \cdot (\frac{3}{n+1})^{1/(n-2)}$

if $\alpha \le 1$, then $S_{*\min} = \sigma_p \left(1 - \frac{{\sigma_p}^3}{B \cdot (n+1) \cdot \dot{\sigma}_u}\right)^{1/(n-2)}$

Using the same idea as Fuller, Hanson and Glaesemann analyzed $S_{f\min}$ for the

two-region model. In their analysis, the high speed unloading rate scenario is also missed. The same modification as presented for Fuller's analysis is also needed. The modified result for the two-region model will follow. The complete mathematical derivation procedure is given in Appendix C.

Also the determination of $S_{*\min}$ depends on a parameter α, defined as

$$\alpha = \frac{\sigma_p^{\,3}}{B_2(n_2-2)\dot{\sigma}_u} \tag{3-12}$$

if $\alpha > 1$, then $S_{*\min} = \sqrt[3]{B_2(n_2-2)\dot{\sigma}_u}$

if $\alpha < 1$, then $S_{*\min} = \sigma_p$

Then derive S_{fmin} from S_{*min} by two steps

$$\begin{cases} S_{*\min}^{\,n_2-2}\left[1-\dfrac{S_{*\min}^{\,3}}{B_2(n_2+1)\dot{\sigma}_u}\right] = S_r^{\,n_2-2}\left[1-\dfrac{S_r^{\,3} r^{n_2+1}}{B_2(n_2+1)\dot{\sigma}_u}\right] \\ S_{f\min}^{\,n_1-2} = S_r^{\,n_1-2} - \dfrac{(S_r r)^{n_1+1}}{B_1(n_1+1)\dot{\sigma}_u} \end{cases} \tag{3-13}$$

Where S_r is the strength when $\frac{K_I}{K_{Ic}} = r$, $B_i = \frac{2}{(n_i-2)AY^2 K_{Ic}^{\,n_i-2}}$ and

$\frac{B_1}{B_2} = r^{n_1-n_2}\frac{n_2-2}{n_1-2}$

According to Hanson and Glaesmann's high speed tensile test experiment, the two-region model is more suitable for tensile strength experiment and proof test than the one-region model [Hanson & Glaesemann, 1997, Glaesemann, 1998]. Using the result

shown above, the dependence of S_{fmin} on the unloading rate has been studied. Fitted fatigue parameters from Hanson and Glaesemann (Table 3-1) are used in the calculation, and the proof test stress is 100 ksi. The result is given in Figure 3.9. Table 3-2 lists some data from the calculation.

Table 3-1 Fitted fatigue parameters for the two-region power-law model [Glaesemann, 1998]

n_1	28
n_2	2.25
r	0.81
B_1	1.86×10^{-7} $GPa^2\cdot s$
B_2	4.39×10^{-3} $GPa^2\cdot s$

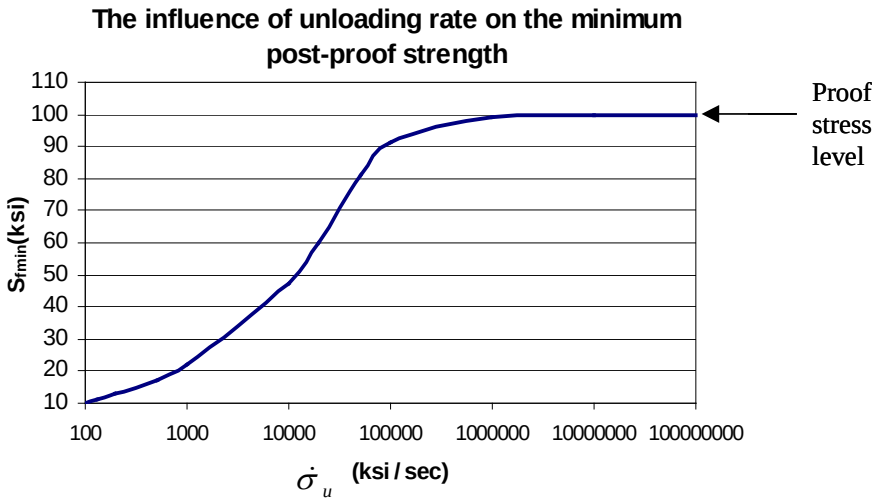

Figure 3.9 The dependence of S_{fmin} on $\dot{\sigma}_u$

Table 3-2 Calculated minimum post-proof strength for different unloading rates

Unloading time t_u(s)	Unloading Rate $\dot{\sigma}_u$ (ksi/s)	Unloading Rate $\dot{\sigma}_u$ (GPa/s)	The Minimum Post-proof strength S_{fmin} (ksi)
0.1	1000	6.9	22.06543
0.01	10000	69	47.53855
0.001	100000	690	91.45632
0.0001	1000000	6900	99.25126
0.00001	10000000	69000	99.92617

From Figure 3.9, at a low unloading rate a higher unloading rate does lead to a higher S_{fmin}, but after the unloading rate is high enough to make $\sqrt[3]{B_2(n_2-2)\dot{\sigma}_u} \geq \sigma_p$, the change of unloading rate does not cause much change in S_{fmin}. From Table 3-2 it can be seen that once the unloading rate reaches 1 000 000 ksi/s, S_{fmin} is just slightly less than the proof test stress level, 100 ksi. The difference can be neglected in reality. It is practically true to say that the proof test does guarantee a minimum strength of the proof testing stress level if a high enough unloading rate is used.

The minimum pre-proof inert strength that can pass the proof test, $S_{i\min}$, can be derived analytically from $S_{f\min}$ for the case when $\alpha < 1$,

$$S_{i\min}{}^{n-2} = S_{f\min}{}^{n-2} + \frac{1}{B}\cdot\sigma_p{}^{n}\cdot\left(t_p + \frac{t_l + t_u}{n+1}\right) \tag{3-14}$$

3.4 Strength Distribution after Proof Test

The initial strength will degrade during the proof test and weak fibers will be removed from the assembly. Thus, it is not accurate to get the strength distribution after proof test by just drawing a vertical line at the proof stress level in the initial strength distribution, although it is practically correct that the proof test truncates the initial strength distribution at the proof stress level.

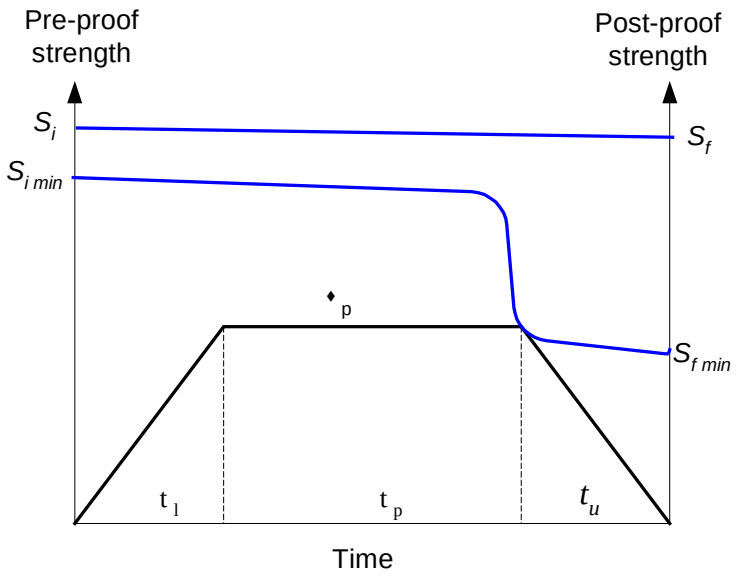

Figure 3.10 The 'just survive' situation

Through the two-region model proof test simulation, the corresponding post-proof strength, S_f, for a given pre-proof strength, S_i, could be found, as shown in Figure 3.10. The probability of post-proof strength falling in the region between S_{fmin} and S_f is equal

to the probability of pre-proof strength falling in the region between S_{imin} and S_i. But, the total assembly number change need to be taken into consideration. Thus,

$$P\{post-proofstrength \le S_f\} = \frac{P\{pre-proof\ \ strength \in (S_{i\min}, S_i)\}}{1-P\{pre-proof\ \ strength \le S_{i\min}\}} \qquad (3\text{-}15)$$

Finally

$$F_{post}(S_f) = \frac{F_{pre}(S_i) - F_{pre}(S_{i\min})}{1-F_{pre}(S_{i\min})} \qquad (3\text{-}16)$$

Conceptually, it is known how many fibers fall in the region between S_{imin} and S_i, provide the initial strength distribution is given. Because the distance between S_{imin} and S_i is very short according to Figure 3.6, the probability of finding a fiber which passes the proof test, but with a substantial strength degradation, is very low.

Corning's 2000 tensile test result is used as the pre-proof strength distribution, shown in Figure 3.11. The strength data is fitted into a two-parameter Weibull model, $F(S_i) = 1-e^{-\left(\frac{S_i}{S_0}\right)^m}$. For the low strength region, m = 2.26 and S_0 = 6825 ksi. For the region truncated by proof test, m = 6.8 and S_0 = 774 ksi. The first region is taken as the pre-proof strength distribution in the simulation, and the calculated post-proof strength distribution, using the two-region model, is shown in Figure 3.12. And Figure 3.13 shows the post- vs. pre-proof strength after proof test simulation.

It is seen from Figure 3.12 that for this 100 ksi proof test, the post-proof strength could be less than 50 ksi — theoretically it is possible that the post-proof strength is

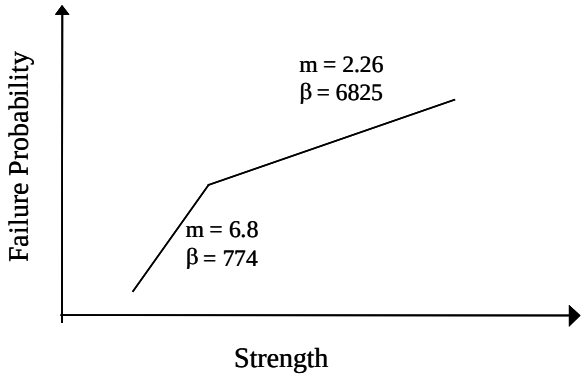

Figure 3.11 Fiber strength distribution tested by Corning Inc. 2000

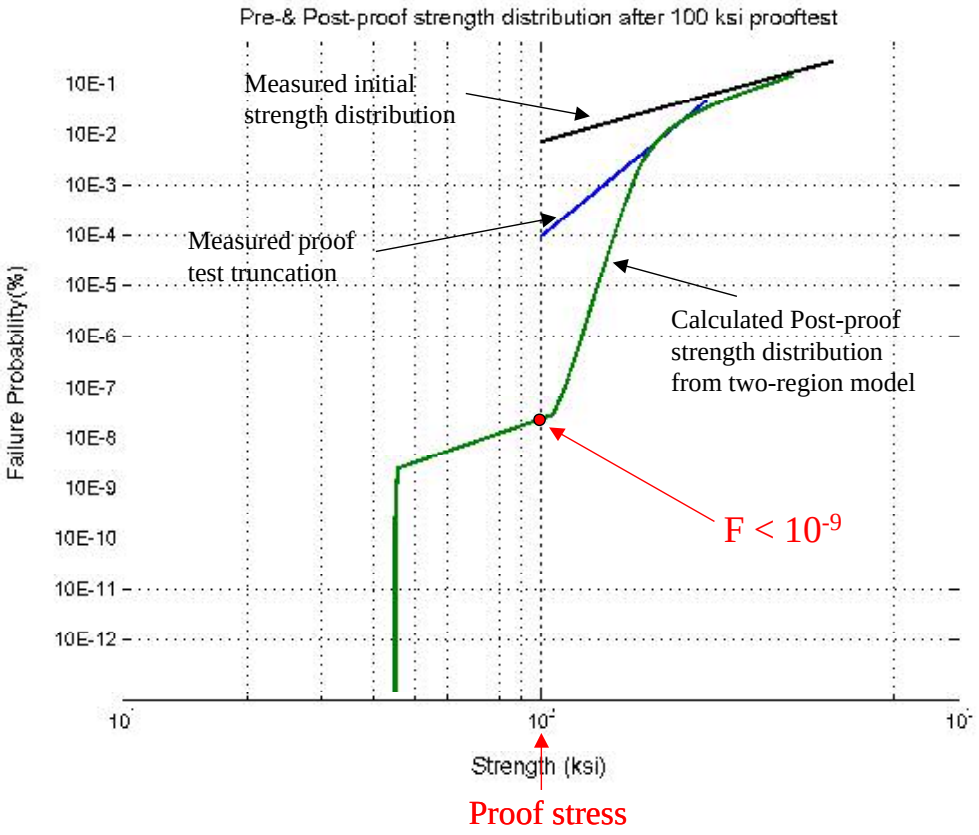

Figure 3.12 Post-proof fiber strength distribution calculated from Corning's 2000 data using the two-region model

much less than the proof test stress level, but the possibility is less than 10^{-9} — it is practically impossible to find a fiber that passes the proof test but with a post-proof strength less than the proof test stress value.

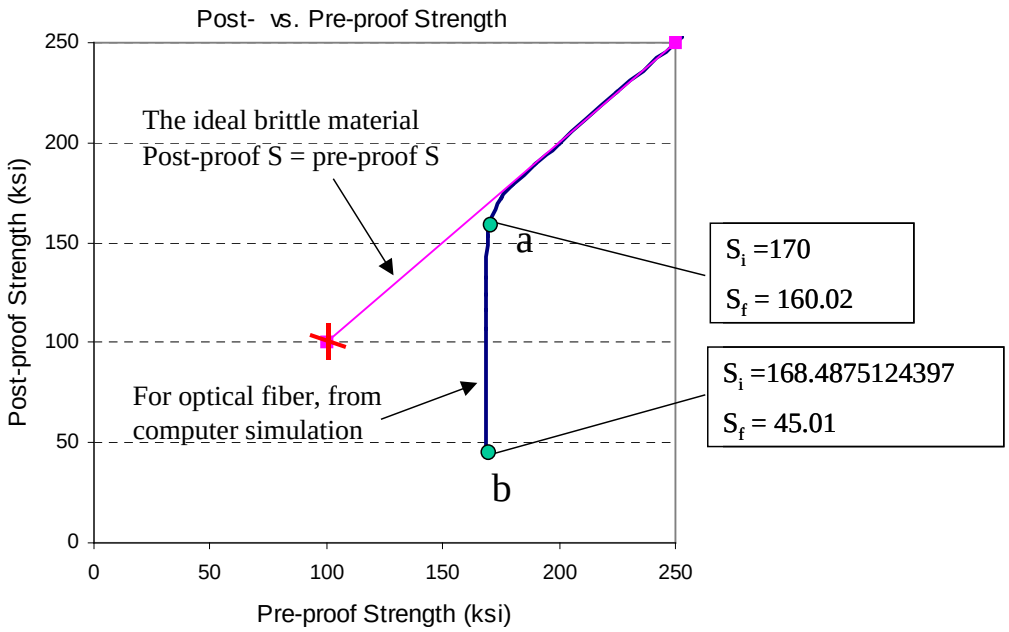

Figure 3.13 Post- vs. Pre-proof strength after proof test simulation from Corning's 2000 data using the two-region model

From Figure 3.13, for point 'a', the strength degraded from 170 ksi to 160 ksi (6% strength degradation). Fibers with pre-proof strength less than 170 ksi will experience a 6% or greater strength degradation (segment 'ab'). But from the post-proof strength distribution curve (Figure 3.12), there are about 1 out of a million fibers ($F = 10^{-6}$) that has a post-proof strength less than 160 ksi. So the probability of finding a fiber that

passes the proof test but with a 6% or greater strength degradation is 10^{-6}. So practically speaking, most fibers that pass the proof test experience negligible strength degradation.

3.5 Proof Test Parameters' Influence on Post-proof Strength Distribution

Through computer simulation, evaluation of the effect of proof test parameters (σ_p, t_p, t_l ($\dot{\sigma}_l$), t_u ($\dot{\sigma}_u$)) on the post-proof strength distribution has been done, using Corning's newest tensile test data from 2000 (Figure 2.6) as the pre-proof strength distribution (the initial strength distribution), for which m = 2.26 and S_0 = 6825 ksi.

3.5.1 Influence of Proof Stress Level

Historically, optical fiber was typically proof tested at 50 ksi, but currently the normal proof test stress is 100 ksi, where for some special cases 200 ksi proof test stress is used. Thus, 50 ksi, 100ksi and 200 ksi proof stresses are used in the simulated proof test. Other proof test parameters used are: t_l = 0.1 sec ($\dot{\sigma}_l$ = 1000 ksi/s = 6.9 GPa/s), t_p = 0.3 sec and t_u = 0.01 sec ($\dot{\sigma}_u$ = 10 000 ksi/s = 69 GPa/s).

Figure 3.14 shows the post- vs. pre-proof curves from theoretical calculation. The proof test stress substantially affects the pre-proof strength truncation value (fibers with initial strength or pre-proof strength less than this value will be eliminated). 50 ksi proof stress will eliminate fibers whose initial strength is less than approximately 80 ksi (the

accurate value would be 79.86 ksi); for a 100 ksi proof test, this truncation value is 168 ksi; for a 200 ksi proof stress, the truncation value increases to 355 ksi. The discrepancy between the proof stress and the corresponding truncation value on pre-proof strength enlarges with the increase of proof stress.

Also, proof stress greatly influences the post-proof strength distribution. In Figure 3.15, with the proof stress increasing, the post-proof strength distribution curve shifts to the right, correspondingly. With 99.999% reliability, the post-proof strength is higher than 90 ksi for 50 ksi proof stress, it is higher than 150 ksi for 100 ksi proof stress, and it is higher than 310 ksi for 200 ksi proof stress.

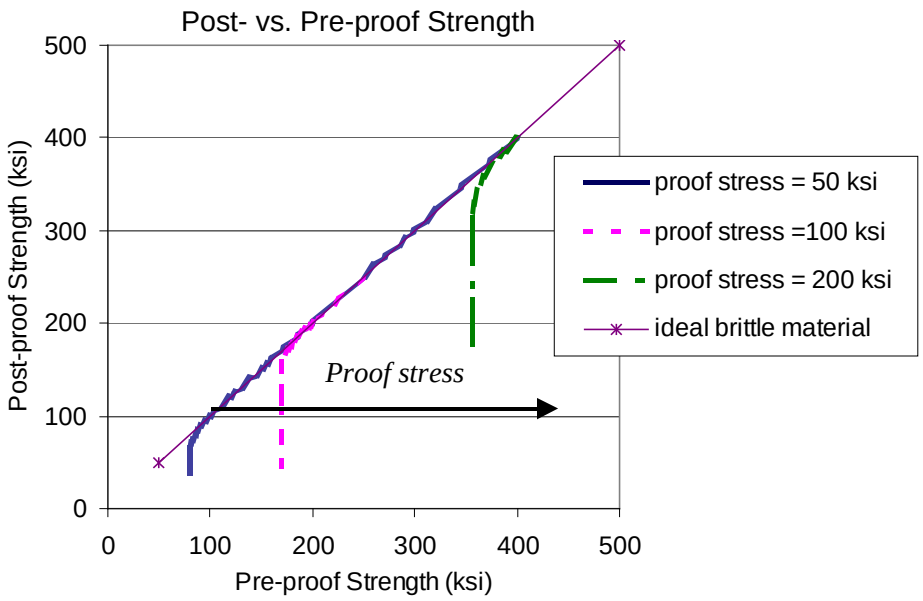

Figure 3.14 Post- vs. Pre-proof test strength under different unloading rates

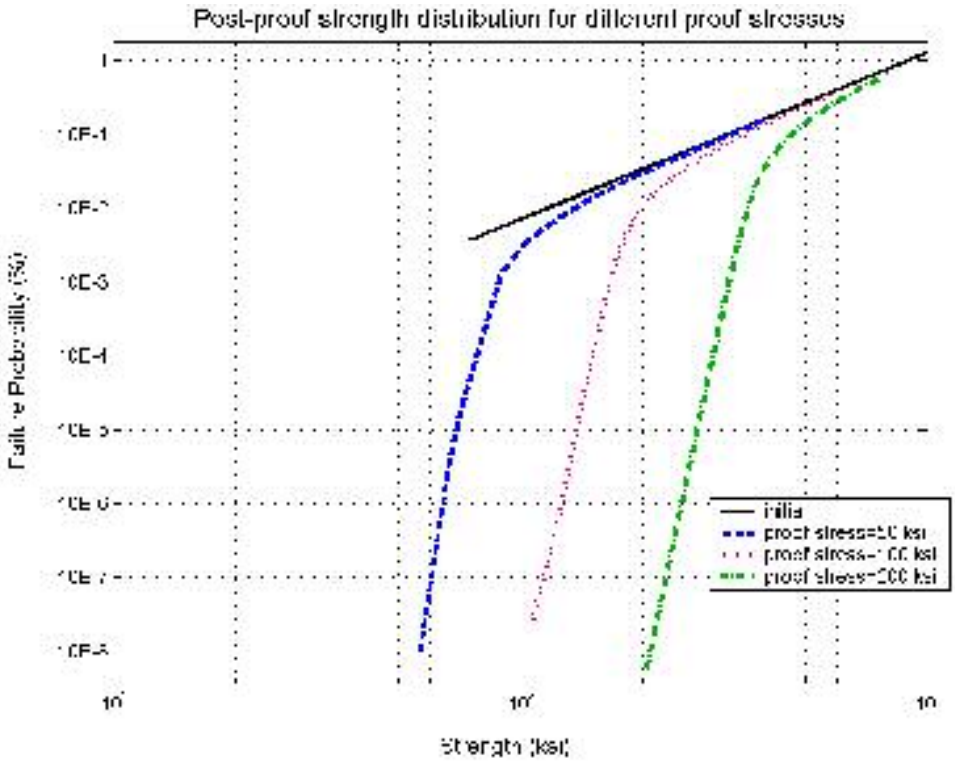

Figure 3.15 Strength distribution after proof test for different proof test stresses

High proof test stress efficiently shifts the post-proof strength distribution curve in the high strength direction at the expense of failing more fibers.

3.5.2 Influence of Dwell Time

In industry to avoid crack growth in the proof-test, it is common to decrease the dwell time, even to 0, i.e. to load the stress to σ_p and unload it immediately. Figure 3.16 compares the strength degradation curve for three different dwell times, 0 sec, 0.3 sec, 0.01 sec. Other proof-test parameters used here are: σ_p = 100 ksi, t_l = 0.1 sec ($\dot{\sigma}_l$ =

1000 ksi/s = 6.9 GPa/s), and t_u = 0.01 sec ($\dot{\sigma}_u$ = 10 000 ksi/s = 69 GPa/s).

Elongating the proof test dwell time from zero to one second led to the increase of pre-proof truncation strength from 142 ksi, to 168 ksi, to 176 ksi. The shift is not huge but still substantial. This trend is easy to understand. Holding longer at the proof stress will fail more fibers and let less pass — longer proof-test dwell time truncates the pre-proof strength at a higher value.

Consequently, elongating dwell time causes a right shift of the post-proof strength distribution curve (Figure 3.17). Although the shift is not as substantial as that caused by proof test stress change, it is still noticeable.

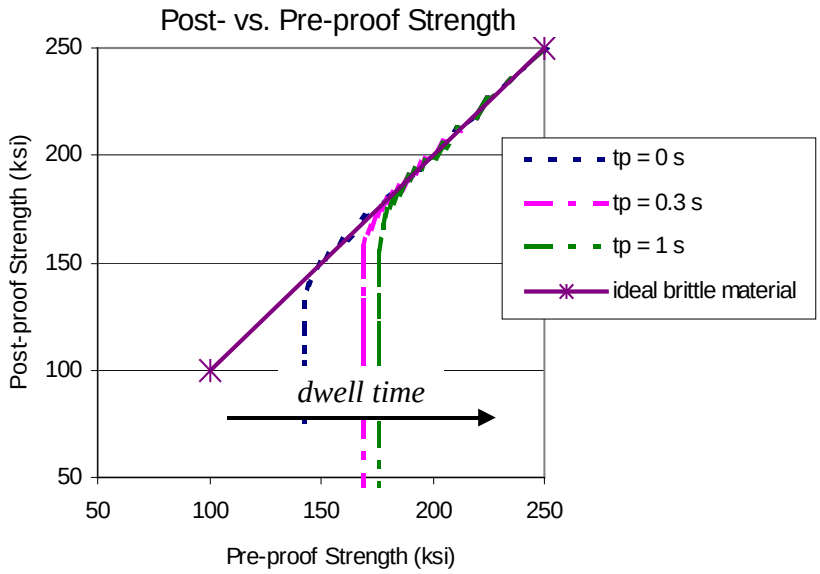

Figure 3.16 Post- vs. Pre-proof test strength under different dwell times

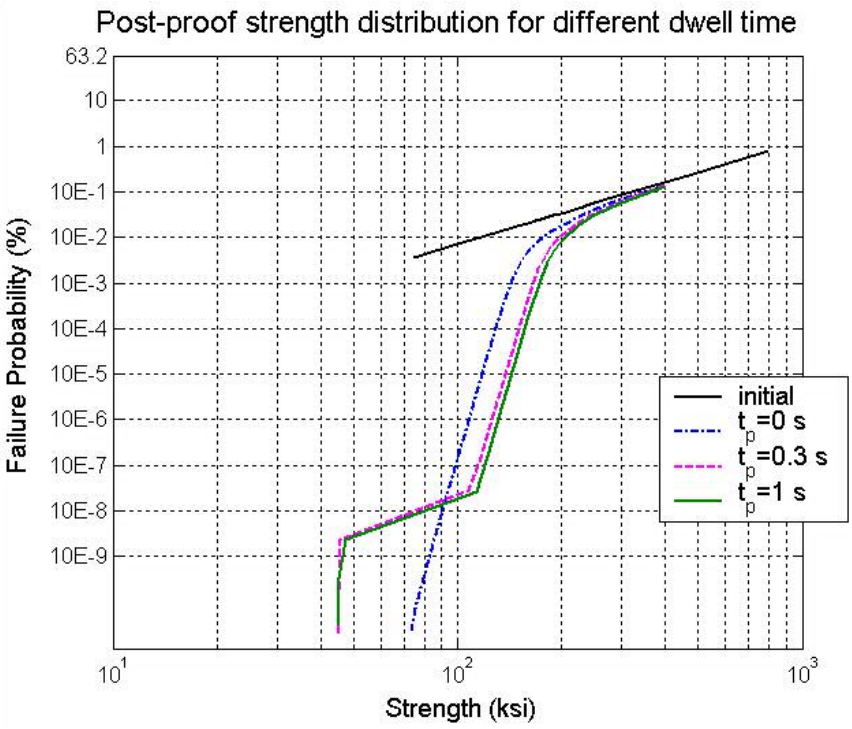

Figure 3.17 Strength distribution after proof test for different dwell times

3.5.3 Influence of Unloading Rate

Figure 3.18 shows the final strength (S_f) verse the initial strength (S_i) curves under different unloading times, 0.1 sec, 0.01 sec, 0.001 sec, corresponding to three different unloading rates, 1 000 ksi/s (6.9 GPa/s), 10 000 ksi/s (69 GPa/s), 100 000 ksi/s (690 GPa/s), respectively. Other parameters are: σ_p = 100 ksi (0.69 GPa), t_p = 0.3 sec and t_l =0.1 sec ($\dot{\sigma}_l$ = 1 000 ksi/s).

The three post-proof strength verse pre-proof strength curves in Figure 3.18 pile up to each other, it is not easy to see any differences among them, but they are not

exactly the same. If zoomed in on the pre-proof strength axis (Figure 3.19), the three curves are then visually distinguishable. From Figure 3.19, elongating the unloading time, lowering the unloading rate, will shift the curve to the right — longer unloading time (lower unloading rate) will truncate the pre-proof strength at a higher value. Another observation is that the distance between 0.01 sec and 0.001 sec is much smaller than the distance between 0.1 sec and 0.01 sec. The shift caused by the unloading rate becomes much less at a high unloading rate level.

Practically, the unloading time (unloading rate) will not cause noticeable change on the post-proof strength verse pre-proof strength curve, especially when the unloading time is already short (0.01 sec), i.e., the unloading rate is already high enough.

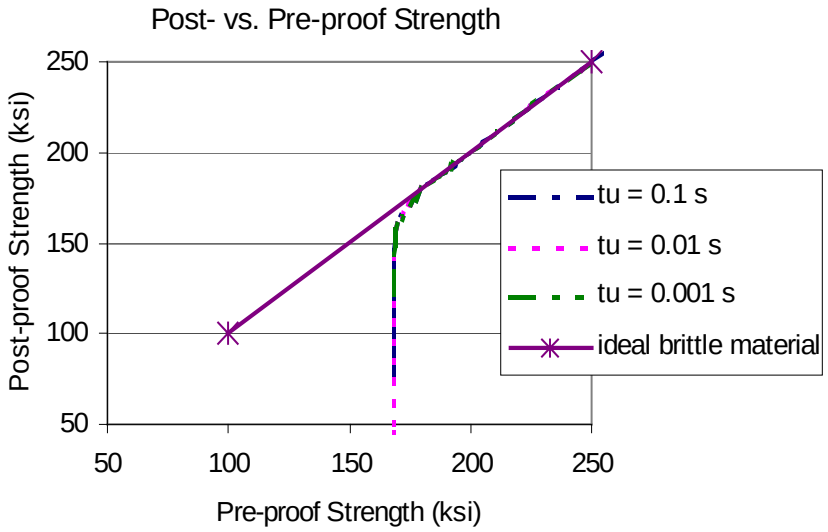

Figure 3.18 Post- vs. Pre-proof test strength under different unloading rates (1)

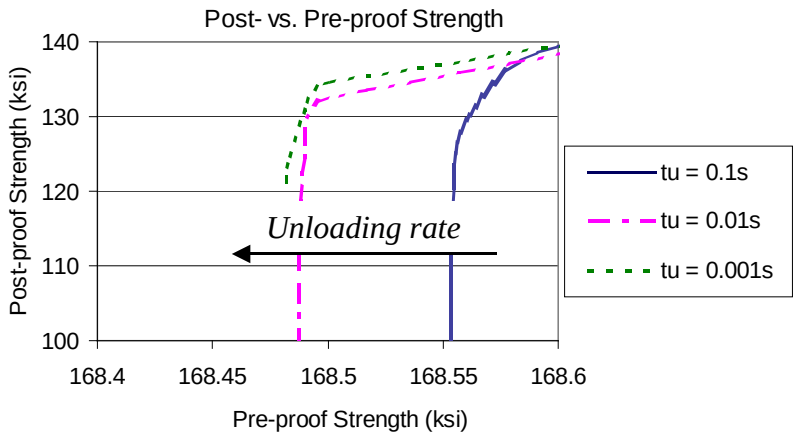

Figure 3.19 Post- vs. Pre-proof test strength under different unloading rates (2)

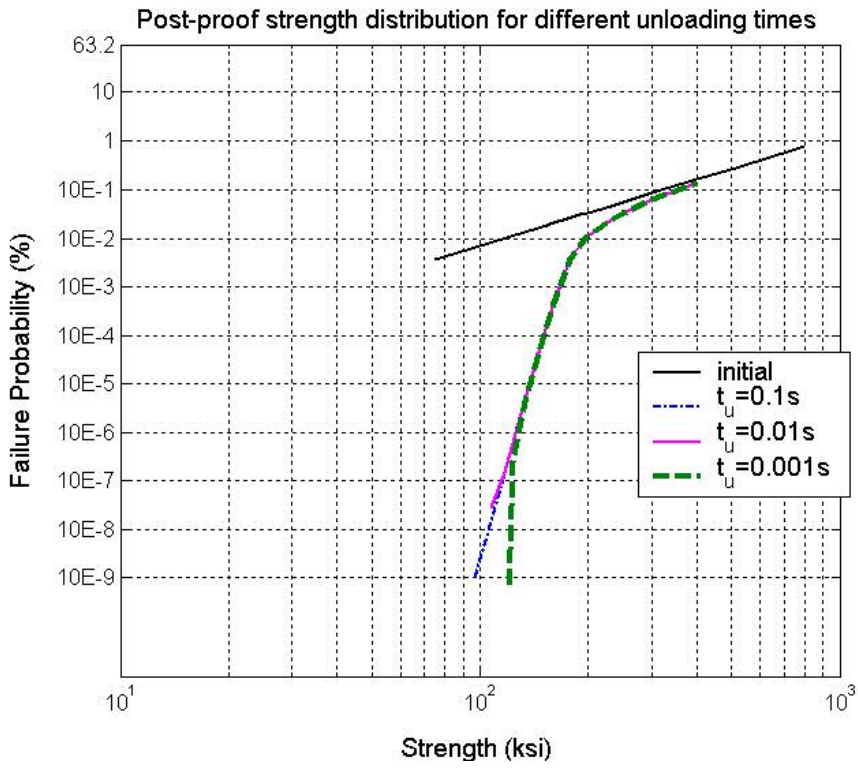

Figure 3.20 Strength distribution after proof test for different unloading rates

In the post-proof strength distribution plot (Figure 3.20), when $F>10^{-6}$ % the curves for three different unloading rates are undistinguishable. At lower F values ($F<10^{-6}$ %), the three curves begin to separate. This is consistent with the theoretical analysis in Section 3.3, that the unloading rate will influence the minimum post-proof strength (S_{fmin}), faster unloading rate guarantees a higher S_{fmin}. S_{fmin} for each unloading rate is not apparently shown in Figure 3.20 because of limitation of numerical method, but the trend is still visible. t_u = 0.001 sec curve stops at a post-proof strength of 100 ksi, and t_u = 0.01 sec and t_u = 0.1 sec curves will reach much lower post-proof strengths.

Clearly the unloading rate does determine the theoretical minimum post-proof strength, but practically it has little influence on the post-proof strength distribution. Thus, it is not helpful to increase the unloading rate at high expense.

3.5.4 Influence of Loading Rate

Keeping other proof test parameters fixed (σ_p = 100 ksi, t_p = 0.3 sec, t_u = 0.0l sec), and trying different loading rates (t_l =1 sec, 0.1 sec, 0.01 sec, 0.001 sec), leads to the similar results as unloading rate. One must zoom in pre-proof strength to see the shift of post verse pre-proof strength curve caused by different unloading rate (Figure 3.21 and Figure 3.22). Longer loading time (lower loading rate), slightly higher pre-proof truncation strength. With loading rate increasing, the difference diminishes. The loading time (loading rate) will not cause noticeable change on the post-proof strength

vs. pre-proof strength curve, and loading rate has little influence on post-proof strength distribution (Figure 3.23).

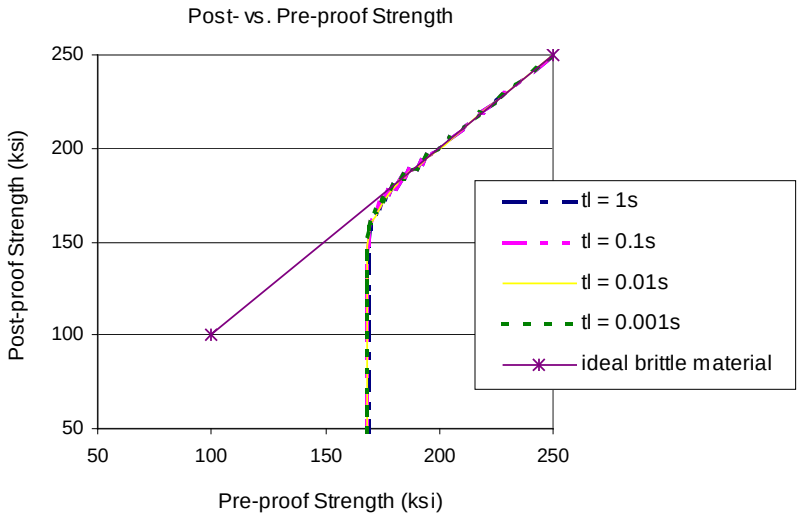

Figure 3.21 Practical post- vs. pre-proof strength for different loading times (1)

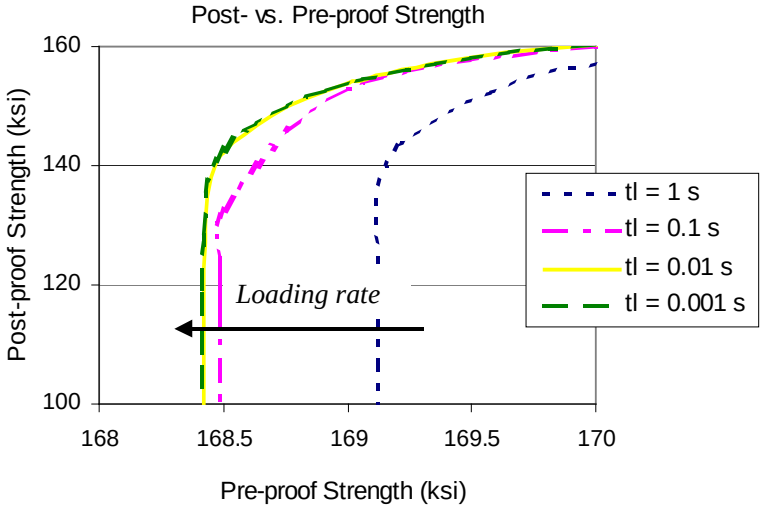

Figure 3.22 Practical post- vs. pre-proof strength for different loading times (2)

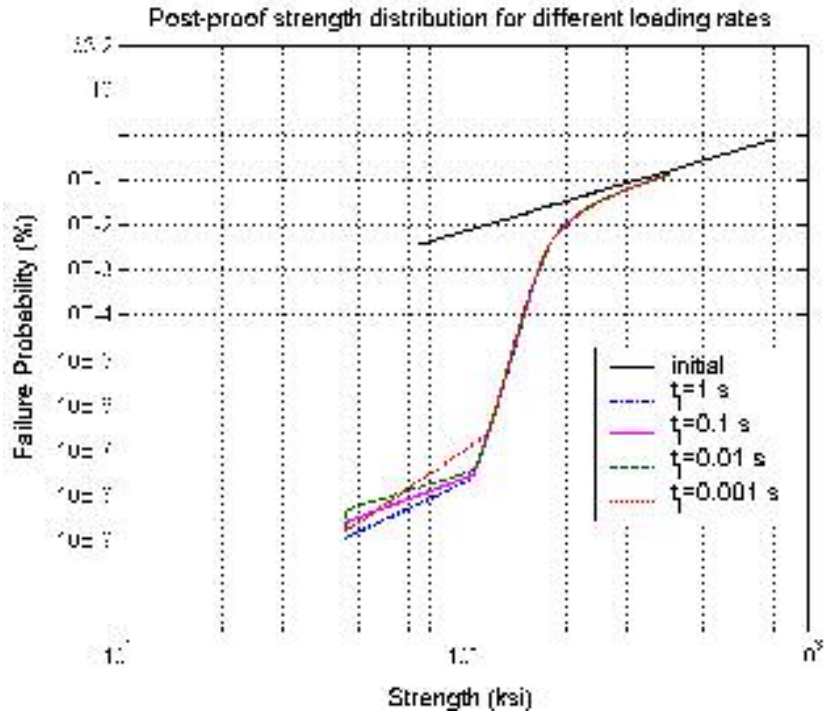

Figure 3.23 Strength distribution after proof test for different loading rates

Therefore, practically loading rate has negligible influence on the pre-proof strength truncation value and the post-proof strength distribution.

3.6 Summary

The goal of this chapter is to resolve some basic misconceptions involved with proof testing from a probability point of view. Correction and improvement on existing theories have been done, and a numerical proof test simulation has been proposed here to get the post-proof strength distribution.

According to the theoretical analysis, the post-proof strength could be much lower than the proof test stress, but practically the probability is very low (from the proof test simulation in Figure 3.12, this probability is less than 10^{-9}, and this is especially true when the unloading rate is high enough (690 GPa/s). For those fibers that pass the proof test, it is theoretically true that the proof test cause a strength degradation on all of them, but practically only 1 out of a million fiber that pass the proof test will experience 6% or greater strength degradation (Figure 3.12). Most fibers that pass the proof test experience negligible strength degradation.

Among the parameters of the proof test, proof stress has the most powerful influence on both pre- and post-proof strength; then dwell time; unloading rate and loading rate has little influence on them practically, although theoretically the minimum post-proof strength is determined by the unloading rate.

Strict proof test conditions, such as long dwell time or high proof stress, leads to high pre-proof strength truncation values, and correspondingly guarantees high strength after proof test. High post-proof strength is desired, but high pre-proof strength truncation is not because it will fail more products. Therefore, it is a tradeoff that needs to be considered carefully according to the specific situation.

Once again, it is theoretically true that optical fibers which pass the proof test may have post-proof strengths less than the proof stress, but practically this possibility is very low (less than 10^{-9}), and most fibers pass the proof test with practically negligible strength degradation.

Chapter 4

RELIABILITY ASSESSMENT FOR OPTICAL FIBERS IN BENDING

4.1 Introduction

Compared with the optical fiber reliability problem in long-haul applications, reliability assessment for optical fiber in bending is a relatively new subject. The trend of optical fiber moving from long-haul applications to backplanes is predictable. Currently, optical connection between individual computers is commercially available, and experts predict that in 2-5 years, optical interconnections will enter the computer, connecting circuit boards. The mechanical reliability assessment of fibers in bending correspondingly becomes desirable. Also the pigtails of optical devices are often bent in circles when they are stored, and to save space they are always bent very tight. People want to know how tight they can bend the fiber without degrading its strength too much. This subject will be discussed in full detail in this chapter.

The non-uniform stress situation caused by bending is much more complicated than the uniform tensile stress situation assumed in the long-haul application. Bending places a considerably smaller area under stress compared to uniaxial tension, due to the fact that only half of the fiber surface is under tensile loading. However, large stresses

along the fiber surface are easily generated due to the non-uniform stress caused by bending. But, it can be solved.

4.2 Extrapolate Instantaneous Bending Reliability From Tensile Test

For the bending situation, the actual applied stress on the fiber surface is not uniform, it is a function of position as shown in Figure 4.1.

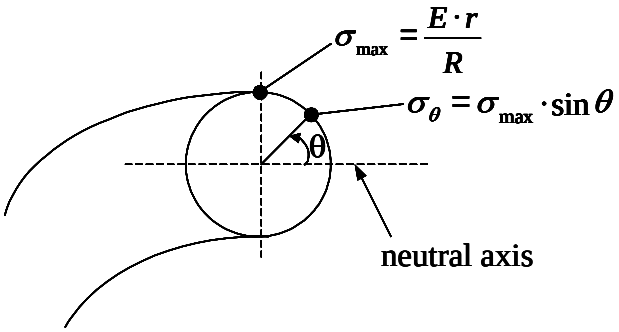

Figure 4.1 Cross section of a bent fiber

From the Weakest Link Theory discussed in Chapter 2, the failure probability under stress $\sigma_{\Delta A_1}$ (or the strength distribution) of a unit area surface, ΔA_1 is

$$F_{\Delta A_1} = 1 - \exp\left(-\left(\frac{\sigma_{\Delta A_1}}{\sigma_o}\right)^m\right) \qquad (4\text{-}1)$$

Then the failure probability of a piece of fiber under any arbitrary stress configuration along its surface is the integration result of the actual stress over the whole surface of

fiber as Eq.(4-2) shows,

$$F(\sigma) = 1 - \exp(-\int_A \frac{1}{A_0}\left(\frac{\sigma(A)}{\sigma_o}\right)^m dA) \tag{4-2}$$

For a straight fiber of length L_t under a uniform tensile stress, $\sigma(A) \equiv \sigma_t$, it is easy to get an analytical solution of strength distribution, i.e. the failure probability verse stress, from Eq.(4-3)

$$F(\sigma_t) = 1 - \exp(-\frac{2\pi rL_t}{A_o}\left(\frac{\sigma_t}{\sigma_o}\right)^m) \tag{4-3}$$

Here r is the radius of fiber cladding.

For a piece of fiber in bending, substitute the non-uniform stress caused by bending

$$\sigma_\theta = \sigma_{\max} \cdot \sin\theta \tag{4-4}$$

into Eq.(4-2) and integrate. The failure probability of a piece of fiber of length L_b, with uniform bending whose maximum bending stress is $\sigma_{\max}$ can be solved analytically, a result which has been presented by Matthewson and Glaesemann [Matthewson, 1986; Glaesemann, 1991b].

$$F(\sigma_{\max}) = 1 - \exp(-\frac{r\sqrt{\pi} \cdot L_b}{A_0 \cdot {\sigma_0}^m} \cdot \frac{\Gamma(\frac{m+1}{2})}{\Gamma(\frac{m+2}{2})} \cdot {\sigma_{\max}}^m) \tag{4-5}$$

In which $\Gamma(x)$ is the gamma function or factorial function defined by

$$\Gamma(x) = \int_0^\infty \xi^{x-1} e^{-\xi} d\xi \tag{4-6}$$

Which is readily calculated using polynomial approximations [Abramowitz, 1965].

The constants appear in Eq.(4-3) and Eq.(4-5), A_0, σ_0, and *m*, are determined by the optical fiber quality. If the fiber in bending and the fiber under tensile stress have the same strength quality, then those constants are the same for both situations. Those constants can be obtained through the tensile strength test.

Normally, through the tensile test, the strength distribution of fiber of gauge length L_t is measured and fitted into a two parameter Weibull form, as

$$F(\sigma_t) = 1 - \exp(-\left(\frac{\sigma_t}{\beta}\right)^m) \tag{4-7}$$

Comparing Eq.(4-7) and Eq.(4-3), it is easy to get

$$A_o {\sigma_o}^m = \beta^m 2\pi r L_t \tag{4-8}$$

Then substituting into the equation of bending, yields

$$F(\sigma_{\max}) = 1 - \exp(-\frac{1}{2\sqrt{\pi}\beta^m} \cdot \frac{L_b}{L_t} \cdot \frac{\Gamma(\frac{m+1}{2})}{\Gamma(\frac{m+2}{2})} \cdot {\sigma_{\max}}^m) \tag{4-9}$$

Here, L_t is the gauge length of tensile test, and *m* and β are the two parameters of the Weibull distribution curve, which the tensile test data is fitted. The tensile test data can be used to calculate the instantaneous failure probability of a piece of fiber of any arbitrary length, L_b, under uniform bending, which causes a maximum bending stress,

$\sigma_{\max}$. Eq.(4-9) can also be transformed to a form which is a function of the uniform bend radius, *R*,

$$F(R) = 1 - \exp(-\frac{E^m r^m}{2\sqrt{\pi}\beta^m} \cdot \frac{L_b}{L_t} \cdot \frac{\Gamma(\frac{m+1}{2})}{\Gamma(\frac{m+2}{2})} \cdot \frac{1}{R^m}) \tag{4-10}$$

4.3 Calculation Result and Discussion of Instantaneous Reliability

For a 360° uniform bending, L_b is dependent on bend radius, *R*, so is the maximum bending stress, $\sigma_{\max}$. Then, Eq.(4-10) can be written as an function only dependent on *R*.

$$F(R) = 1 - \exp(-\frac{\sqrt{\pi}E^m r^m}{\beta^m L_t} \cdot \frac{\Gamma(\frac{m+1}{2})}{\Gamma(\frac{m+2}{2})} \cdot \frac{1}{R^{m-1}}) \tag{4-11}$$

If constants, L_t, *m*, and β are known from tensile test data, it is easy to use Eq.(4-11) to calculate the instantaneous failure probability of a piece of fiber under 360° uniform bending of any bend radius, *R*.

Again, the data from Corning's 2000 tensile test is borrowed as the initial strength distribution. In Corning's test, the tensile stress stopped at 350 ksi, so the high strength region was not measured. It is necessary to borrow the high strength region from Corning's 1986 tensile test. The overall tensile test data used in the calculation is shown

in Figure 4.2.

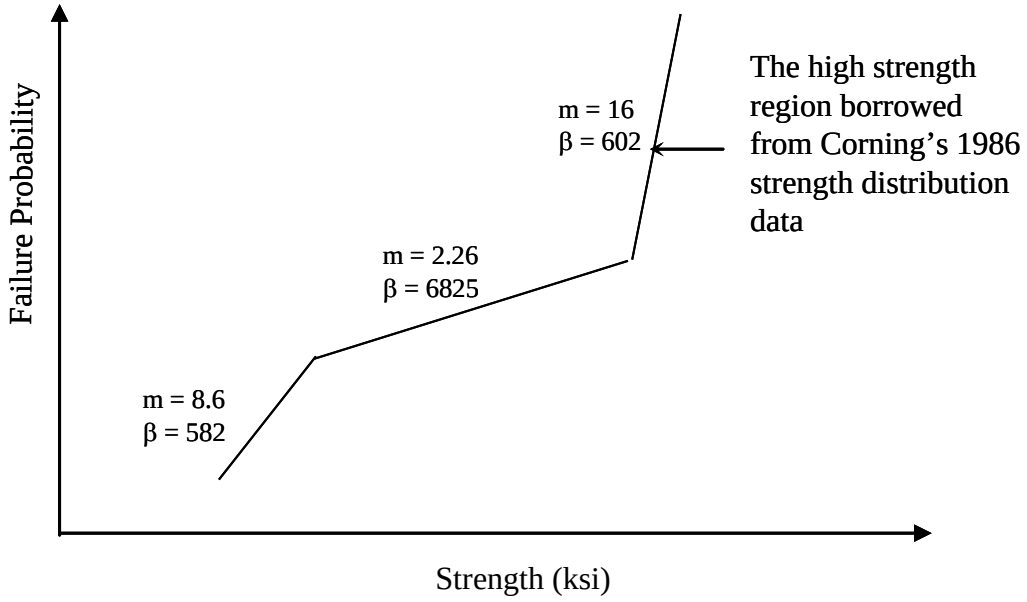

Figure 4.2 The initial strength distribution from Corning's 2000 tensile test data

Then the extrapolated instantaneous failure probability of a uniform 360^{o} bending is shown in Figure 4.3. There are three regions in Figure 4.3 , a high probability region, calculated from the high strength region of the initial strength distribution shown in Figure 4.2 (the maximum bending stress caused by a bend radius in this region is in the initial high strength region), a low probability region calculated from the low strength region of the initial strength distribution, and a third region calculated from the proof test truncation region.

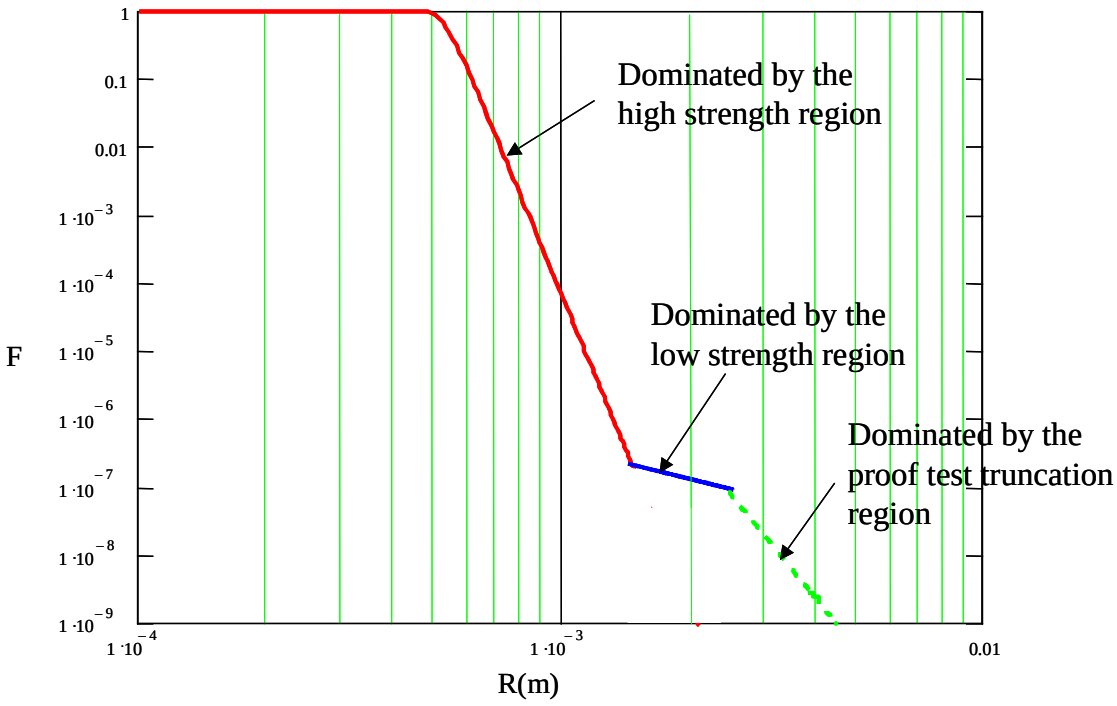

Figure 4.3 360^{o} bend instantaneous failure probability extrapolated from Corning's 2000 tensile test data (F vs. R)

For a 360^{o} bend, the high probability region, which is calculated from the initial high strength region, spreads from F = 1 to about 10^{-7}(which corresponds to a bend radius about 1.3 mm). It is the initial high strength region that matters in the reliability assessment of bending fibers. As long as the bend radius stays above 1.5 mm, the failure probability of a 360^{o} circle will stay very low.

In Figure 4.3 , at approximately 0.5 mm bend radius, the failure probability is almost 1, which is consistent with people's practical experience of breaking a piece of fiber by bending it as a circle.

Equation (4-11) can also be transformed into a function of σ_{max} (Eq.(4-12)). Correspondingly plot of F verse σ_{max} can be drawn (Figure 4.4).

$$F(\sigma_{max}) = 1 - \exp\left(-\frac{\sqrt{\pi}\cdot E\cdot r}{\beta^m L_t}\cdot\frac{\Gamma\left(\frac{m+1}{2}\right)}{\Gamma\left(\frac{m+2}{2}\right)}\cdot {\sigma_{max}}^{m-1}\right) \qquad (4\text{-}12)$$

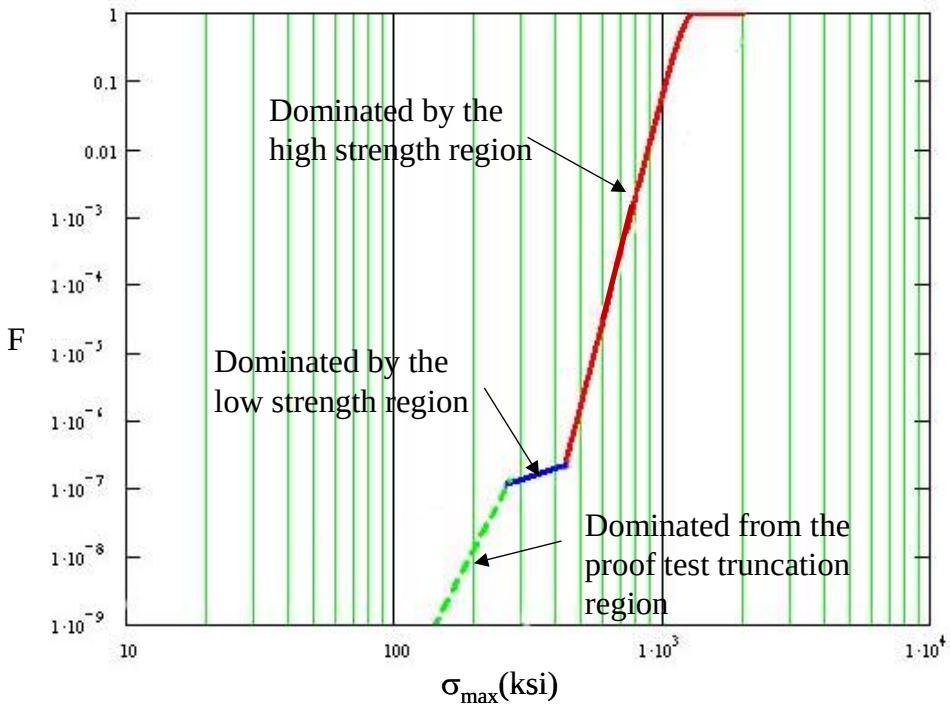

Figure 4.4 360° bend instantaneous failure probability extrapolated from Corning's 2000 tensile test data (F vs. σ_{max})

Figure 4.4 has a similar shape as Figure 4.2, the initial strength distribution curve, but not exactly the same. In Figure 4.2, the initial strength distribution curve, which is

also the failure probability of a straight 20 m optical fiber verse the uniform tensile stress curve, shows three strength regions with the Y-axis scales in ln(-ln(1-F)). But in Figure 4.4, the failure probability of a 360^{o} circle vs. the maximum bending stress, the Y-axis is plotted in log scale. If Figure 4.4 was drawn on the same axis scale as Figure 4.2, the plots of the three regions would not be straight anymore.

It is clearly seen that the initial high strength region is the important region for reliability assessment where optical fibers are bent. Only when the maximum bending stress gets into the high strength region should people begin to worry about breaking the fiber instantaneously. In terms of the bend radius, as long as the bend radius is bigger than 1.3 mm, there is a very low possibility of breaking fibers.

4.4 Reliability Assessment of Bending with Strength Degradation

Instantaneous bending failure is the failure without fatigue of strength degradation, according to the calculation done in the previous section. Generally, people do not bend fiber so tight that an instantaneous failure is a problem. Thus, the reliability assessment of fibers bent under a much more loose radius for some period of time is of more interest. This is a totally new subject, never having been discussed anywhere else. A theoretical method is developed here to solve this problem. The basic idea is similar to the method used for instantaneous failure, but now the strength degradation over time needs to be taken into consideration.

Before strength degradation caused by bending happens, there is a uniform strength distribution all along the fiber surface. During bending, the fiber surface is experiencing a non-uniform stress, that leads to a non-uniform strength degradation over the fiber surface. So after some time in bending, the strength distribution along the fiber surface is no longer uniform, as well as the current applied stress. The two non-uniform items makes the reliability with fatigue issue much more complicated than the instantaneous reliability problem discussed previously. It cannot be solved by analytical methods, a numerical method has to be employed.

At a unit surface area, ΔA_1, the applied stress under bending is constant, σ_a, the strength at time t =0 is S_0. According to the Two-Region crack growth model, under applied stress σ_a, the strength after time *t* is given by

$$S(t)^{n_i-2} = S_i^{n_i-2} - \frac{1}{B_i}\int_0^t \sigma_a^{n_i} dt \qquad (4\text{-}13)$$

Here, $i = 1$ or 2, depending on which region it is in.

At time t, the condition for failure to happen at area ΔA_1 is that the degraded strength is less than the actual applied stress, i.e., $S_t(\Delta A_1) \le \sigma_a(\Delta A_1)$, i.e.

$$F_{\Delta A_1} = P\{S_t(\Delta A_1) \le \sigma_a(\Delta A_1)\} \qquad (4\text{-}14)$$

Using the two-region crack growth model, it is easy to calculate the minimum strength at time 0, S_{0min}, which corresponds to the minimum strength at time t, $S_{tmin} = \sigma_a$ (Figure 4.5)

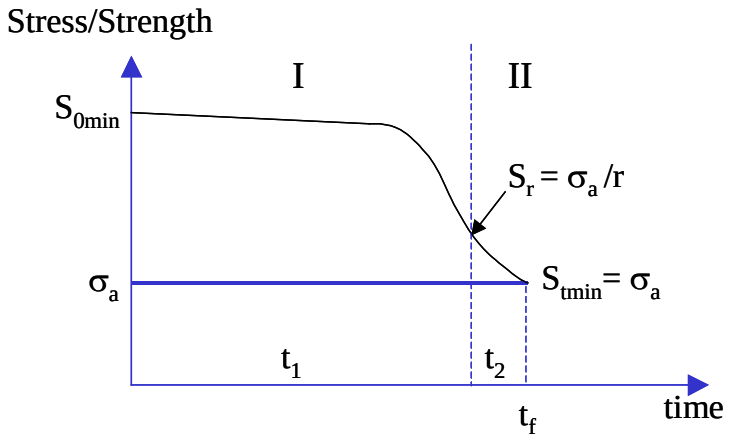

Figure 4.5 The two-region strength degradation

According to the two-region model,

In region I: $$S_r^{\,n_1-2} = S_0^{\,n_1-2} - \frac{1}{B_1}\sigma_a^{\,n_1}\cdot t_1 \tag{4-15}$$

In region II: $$S_t^{\,n_2-2} = S_r^{\,n_2-2} - \frac{1}{B_2}\sigma_a^{\,n_2}\cdot t_2 \tag{4-16}$$

And, $t_1 + t_2 = t_f$, $S_r = \sigma_a / r$

Solving Eq.(4-15) and Eq.(4-16), yields

$$S_{0\min} = \left(\left(\frac{\sigma_a}{r}\right)^{n_1-2} + \frac{1}{B_1}\sigma_a^{\,n_1}\cdot t_f - \frac{B_2}{B_1}\cdot\sigma_a^{\,n_1-n_2}\cdot\left(\frac{1}{r^{n_2-2}}-1\right)\right)^{\frac{1}{n_1-2}} \tag{4-17}$$

Then, the failure probability at area ΔA_1 at time t is equal to the probability that the initial strength is less than S_{0min}, i.e.,

$$F_{\Delta A_1} = P\{S_t(\Delta A_1) \le \sigma_a(\Delta A_1)\} = P\{S_o(\Delta A_1) \le S_{0\min}\}) \tag{4-18}$$

which is known

$$F_{\Delta A_1} = 1 - \exp(-\frac{S_{0\min}{}^m}{A_o \sigma_o{}^m} \Delta A_1) \tag{4-19}$$

Then, the total failure probability F_{total} is the cumulative result of every discrete area on fiber surface

$$F_{total} = 1 - R_{total} = 1 - \prod_{i=1}^{k} R(\Delta A_i) = 1 - \prod_{i=1}^{k} F(\Delta A_i) \tag{4-20}$$

4.5 Calculation Result and Discussion of Degraded Reliability

4.5.1 Long-Term Reliability

Corning defines long-term as 20 or 40 years. An extrapolation calculation from Corning's 2000 tensile test data (Figure 4.2) to 360^{o} bend long-term reliability has been done. The result is shown in the following figures.

Figure 4.6 shows the curves of failure probability changing with time for different bend radii. From Figure 4.6, it can be seen that for long-term reliability issues, longer bending time does not cause much higher failure probability, 20 years and 40 years almost have the same probability. This is especially true for a larger bend radius, such as 10mm in the figure. What does have a substantial influence on the reliability is the bend

radius, R. Thus, redraw the changing of F with respect to R, but just for 40 years lifetime.

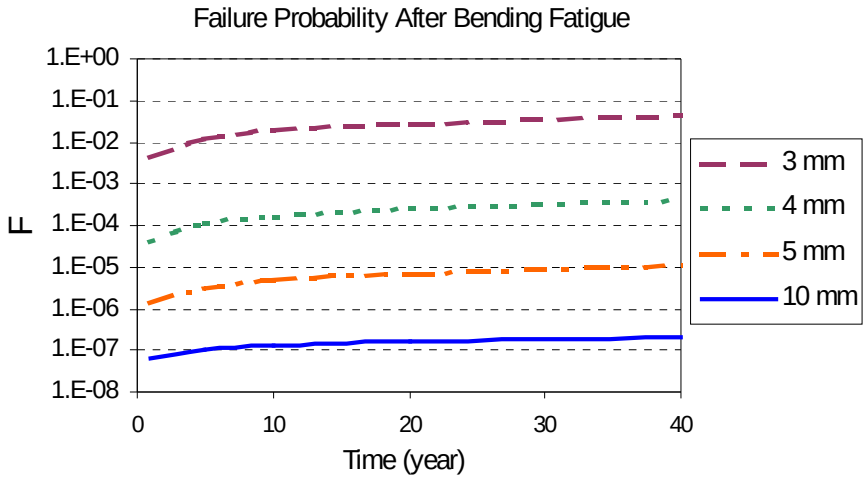

Figure 4.6 Long-term reliability of fiber in 360^{o} bend for different bend radii

.

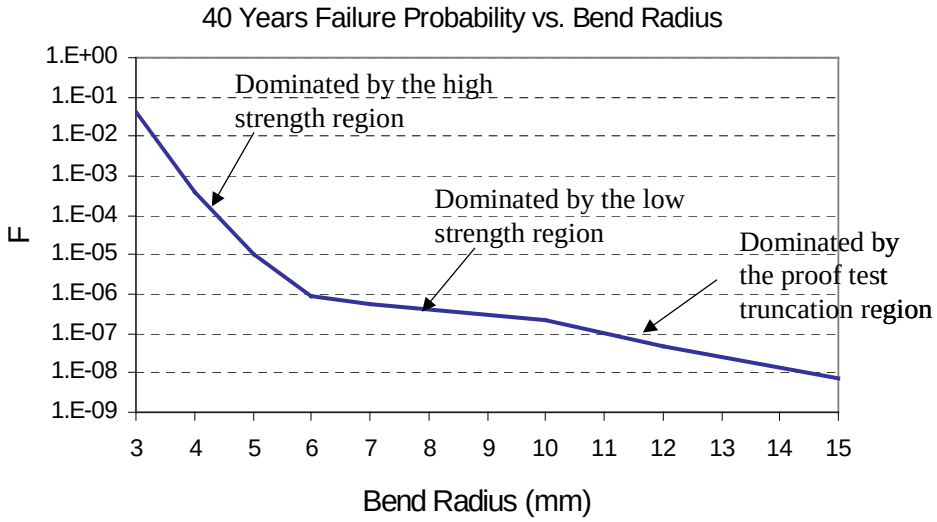

Figure 4.7 Long-term reliability of a 360^{o} bend for 40 years

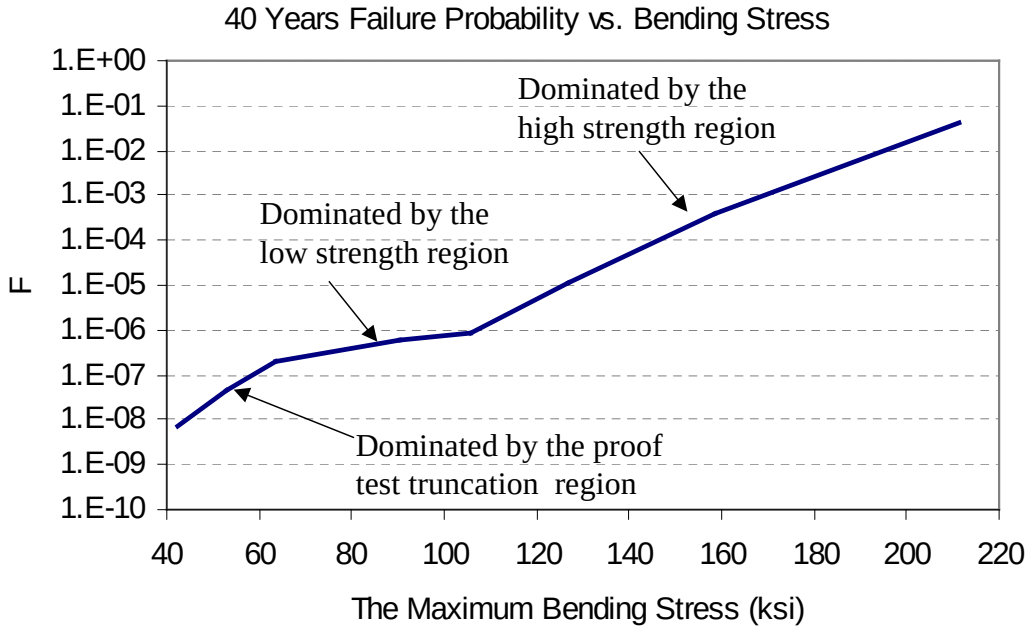

Figure 4.8 Long-term reliability of a 360^{o} bend for 40 years

Figure 4.7 and Figure 4.8 shows the curves of 40 year failure probability, changing with bend radius and the maximum bending stress, respectively. Similar to the situation of bending reliability without fatigue (Figure 4.3 and Figure 4.4), the curves have three regions, a high probability region, which is calculated from the high strength region of the initial strength distribution, a low probability region from the low strength region, and a proof test truncation region. The failure probability begins to increase rapidly with decreasing radius, if the radius is tighter than some critical bend radius value. This critical radius value, from Figure 4.7, is around 6mm; below this value a small bend radius drop will lead to a big failure probability increase. Thus, it is better to

keep the bend radius larger than 6 mm.

For 100 ksi proof tested fiber, Corning suggested that the maximum tensile stress be 20 ksi for a long-term life [Hanson, 1997]. But for a 360^{o} pure bending situation, according to the calculation, a 100 ksi maximum bending stress can guarantee a failure probability less than 10^{-6} for a 40 year lifetime. Obviously it is too conservative to use the guideline from long-haul application for bending situation.

4.5.2 Short-Term Reliability

Short-term reliability is something happens during handling and installation. Short-term defined by Corning is 1minute [Castilone, 2001], which is adopted here. Figure 4.9 and Figure 4.10 shows the curves of short-term failure probability changing with bend radius and the maximum bending stress, respectively.

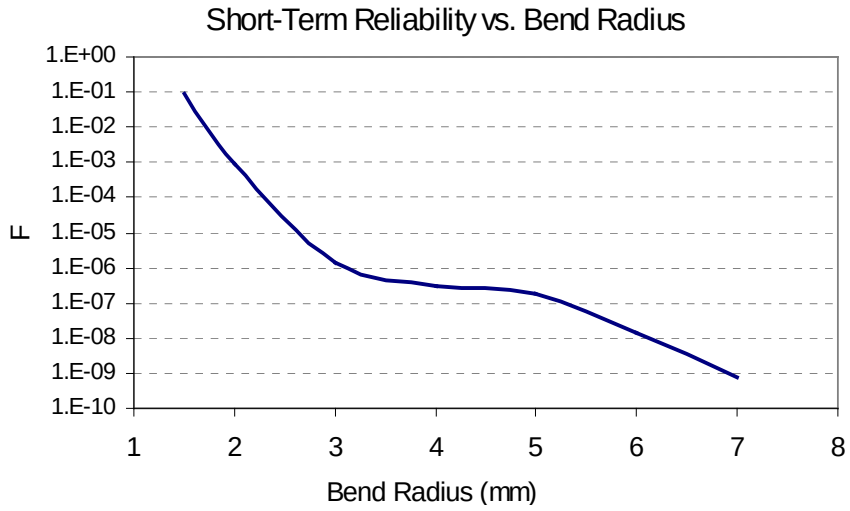

Figure 4.9 Short-term reliability of a 360^{o} bend

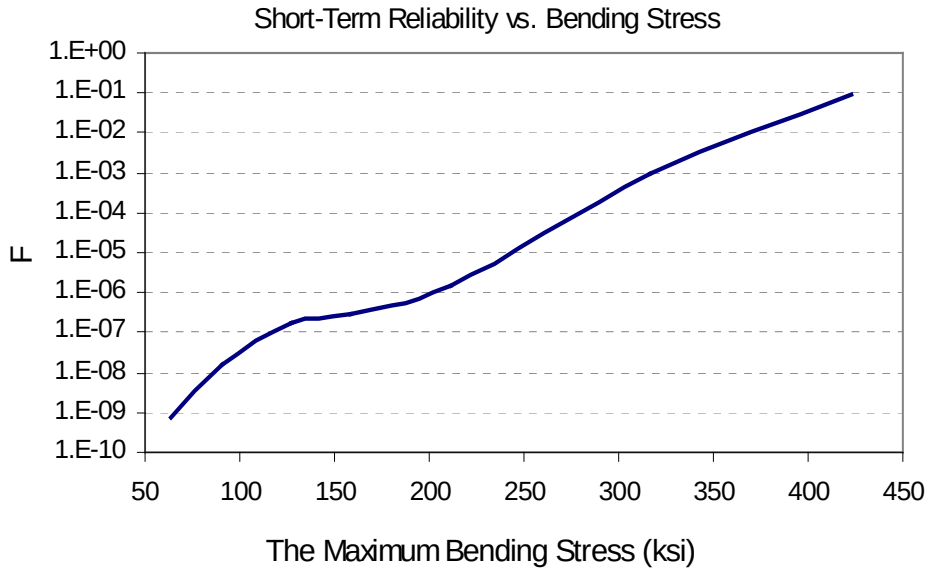

Figure 4.10 Short-term reliability of a 360^{o} bend

Similarly, curves in Figure 4.9 and Figure 4.10 have three regions, calculated from the high strength region, the low strength region and the proof test truncation region from the initial strength distribution curve, respectively. The critical value of the bend radius for short-term reliability is 3 mm, which guarantees a short-term failure probability of less than 10^{-6}.

4.6 Summary

After reviewing existing theories about the instantaneous reliability assessment of optical fiber in bending, a new analytic approach is developed to assess the mechanical reliability of optical fibers under bending loads, but take into consideration the effect of

static fatigue. The basic idea of this approach is to degrade the fiber surface strength piece by piece because of the non-uniform strength degradation caused by the non-uniform bending stress, and then use the weakest link theory to integrate along the whole surface of the fiber to get the total failure probability.

Long-term and short-term reliability calculations using the newly proposed approach have been done in this Chapter. The calculations help to understand the implications behind the mathematics. From the calculation results, the bend radius has a much stronger influence on failure probability than the factor time. There are three regions in the F verse R or F verse σ_{max} curves, calculated from the high strength region, low strength region, and the proof test truncation region of the initial strength distribution curve, respectively.

An experiment will be carried in Chapter 5 to verify the analysis approach proposed. Based on the approach, industrial guidelines will be established in Chapter 6.

Chapter 5

TWO POINTS BEND EXPERIMENT

5.1 Bending Test Techniques Introduction [M. J. Matthewson, 1999(b)]

It is desirable to do an experiment to verify the reliability assessment theory for bending. From literature there are several bending test methods, a brief introduction to them is given here.

5.1.1 Mandrel Bending Test

Mandrel or uniform bending involves wrapping the fiber around the outside of a precision diameter rod or mandrel (Figure 5.1). The fiber is then subjected to uniform curvature. Different stresses are achieved by using mandrels of different diameters. A second rod could be used to effectively isolate each turn (Figure 5.1b). The main advantages of mandrel bending are its compactness and ease of use, the principal disadvantage is the difficulty with adequately gripping the ends of the specimen. And uniform tension can be superimposed upon the bending stresses if the winding tension is too high or if the fiber coating swells due to absorption of certain species from the environment; such tensile stresses should be minimized since they are not measurable

and so cannot be compensated for.

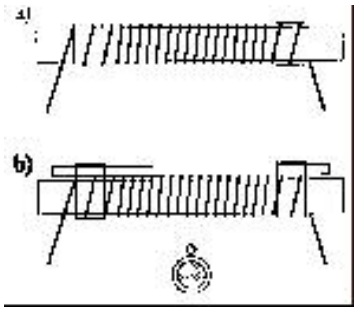

Figure 5.1 Schematic of the mandrel bending test (after Matthewson)

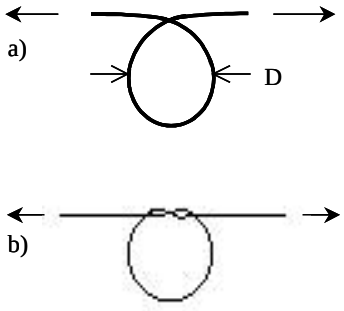

Figure 5.2 Schematic of (a) the fiber loop and (b) the fiber knot tests

5.1.2 Loop or Knot Test

Sinclair [Sinclair, 1950] describes a bending method in which the fiber is twisted into a loop (Figure 5.2 a). The ends of the fiber are pulled until the fiber breaks by bending in the loop. Sinclair showed that the breaking stress is inversely proportional to the width of the loop, D. Substantial torsion must to applied to avoid the loop untwisting. Eitel and Oberlies [Eitel and Oberlies, 1937] tie the fiber into a knot (Figure 5.2 b) which restrains the loop from unwinding. The stress distribution is then approximately uniform bending. These two techniques are crude and not particularly accurate, but they are very simple and require little in the way of an apparatus, except for a ruler in front of which to perform the experiment.

5.1.3 Two-point Bend Test

The two-point bend technique, first described by Cowap and Brown [Cowap and Brown, 1987], involves bending a short length of fiber double and inserting it into a precision-bore glass tube (Figure 5.3a). Many specimens may be inserted into one tube and the stress applied to them is determined by the tube internal diameter. Several specimens may be inserted at once using the insertion tool shown in Figure 5.3b. Usually the fiber is accurately located between the faceplates by grooves. In its dynamic form (Figure 5.4), the two faceplates are brought together by a computer-controlled steer motor, which is halted when the fiber fracture is sensed by an acoustic detector. There are no gripping problems with two-point bend, no tensile stress, and it has high accuracy, as well as other advantages, fully discussed by Matthewson [Matthewson, 1986 and 1987].

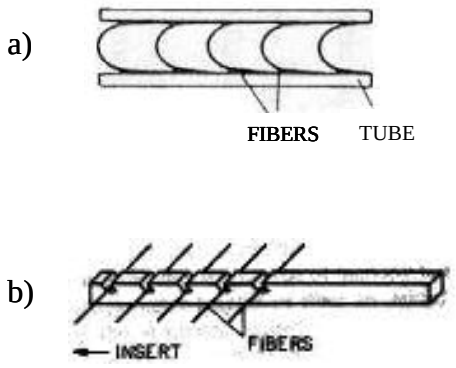

Figure 5.3 Schematic of (a) two-point bend by tube and (b) fiber insertion tool

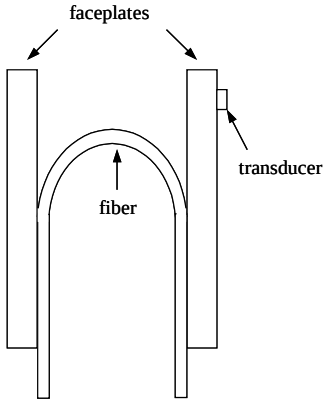

Figure 5.4 Schematic of the two-point bend test (after Matthewson)

5.1.4 Four-point Bend Test

Figure 5.5 is a schematic of the four-point bend apparatus for strength measurement, in which the specimen is supported by two outer pins and then pushed in bending by the two inner loading pins. The technique has been widely used to measure the strength of glasses and ceramics by the determining the force applied to the loading pins that produces failure. It has also been successfully applied to testing optical fibers.[Nelson, 1996; Matthewson, 1996]

Griffioen describes a version of four-point bend in which the support and load pins are mounted on two meshed gears (Figure 5.6)[Griffioen, 1993].

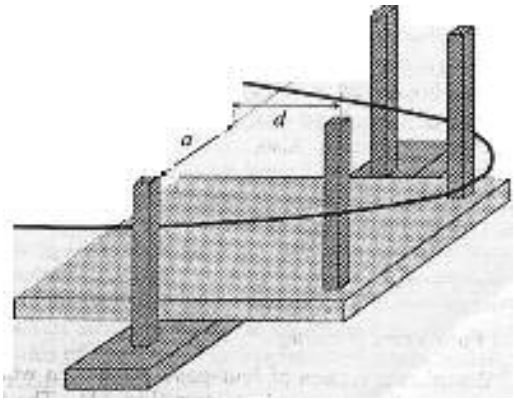

Figure 5.5 Schematic of the four-point bend apparatus (after Matthewson)

Figure 5.6 Alternative method of loading fiber in four-point bend (after Griffioen)

5.2 Static Micrometer Two-point Bend Experiment

The static two-point bend experiment is used to verify the newly developed theory. Instead of using a commercially available apparatus, a simplified apparatus shown in Figure 5.7 is used. A piece of fiber is bent between fixed plates and a moving plate. The micrometer is then twisted to move the moving plate back and forth. The bend diameter of the neutral axis is easy to measure using the micrometer. After the desirable bend diameter is reached, the micrometer is locked and the fiber is subjected to a static bending stress (no tensile stress) until it breaks. The lifetimes for samples under certain bend diameters are recorded. Knowing the bend diameter and the lifetime, according to the theory developed previously, the initial strength of the fiber can be calculated. If the fiber is bent at different diameters, the lifetimes measured will be different, but the initial strength calculated from the different diameters and lifetimes should be the same. Or one set of bend diameter and lifetime could be used to predict the lifetimes for other bend diameters.

The bend diameter is chosen so that the lifetime of the fiber under such diameter is much longer than the time that is needed to twist the micrometer to this diameter, which is several seconds. Three bend diameters are used, 2.3 mm (104 samples), 2.5 mm (97 samples) and 2.7 mm (30 samples). The lifetime of fibers for those bend diameters are on the order of 1 minute, 10 minutes and 2 hours, respectively.

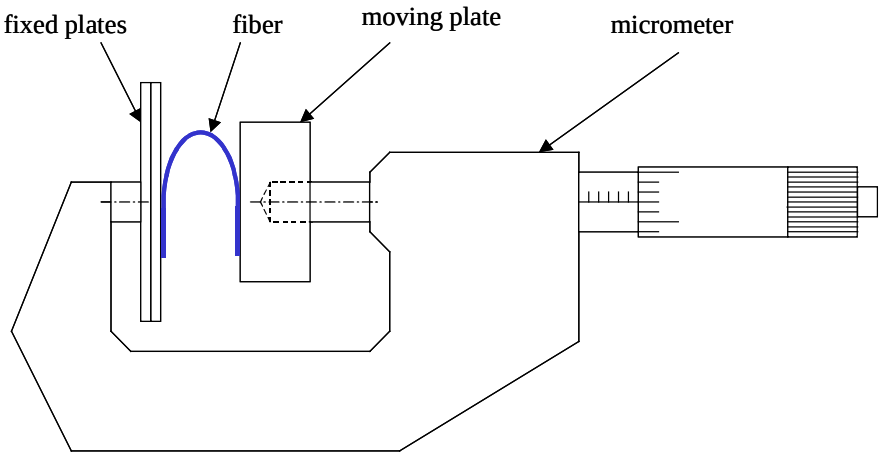

Figure 5.7 Schematic of the micrometer two-point bend apparatus

5.3 Experiment Result Analysis (Half-circle Approximation)

The stress situation of a two-point bend can be approximated by a half-circle bend. A half-circle bend causes uniform bending along the fiber length. The degraded strength, when the fiber is broken, is equal to the known bending stress, combined with the time under bending, the initial strength before bending can be calculated based on the two-region crack growth model. The initial strength distribution calculated from the three different bend diameter experiment is shown in Figure 5.8. The three initial strength distribution curves, calculated from three bend diameters, are on top of each other as expected.

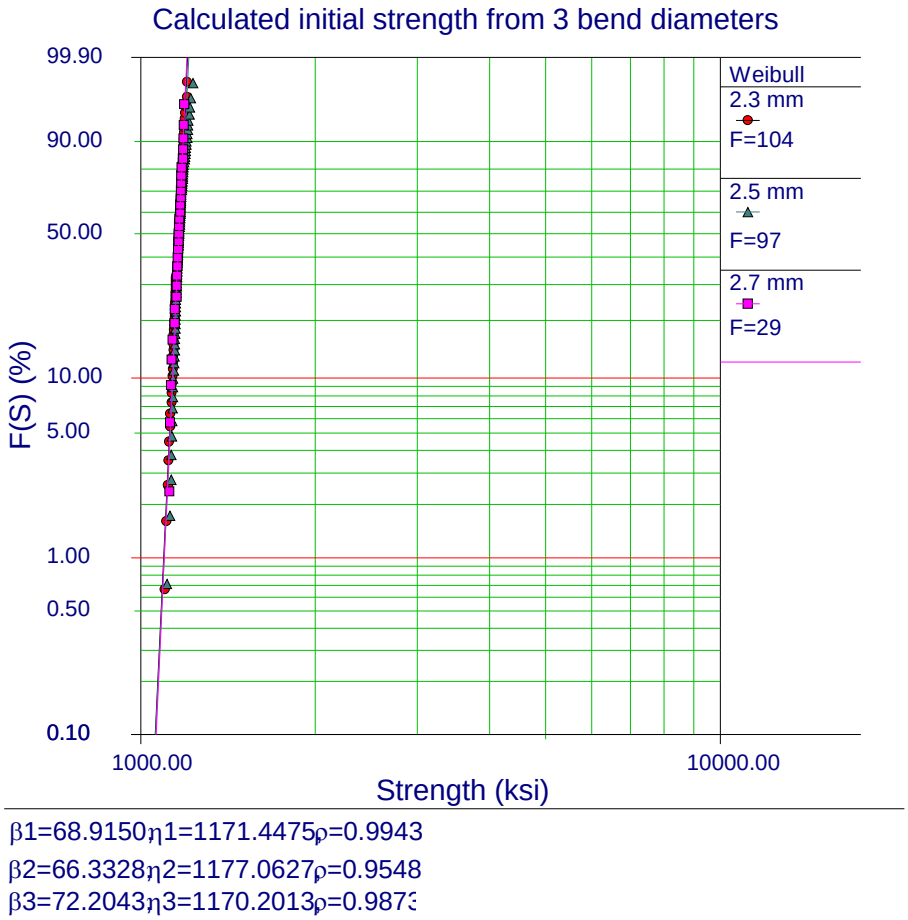

Figure 5.8 The initial strength distribution calculated from the two-point bend test result using half circle uniform stress approximation

The experiment data will be analyzed from another perspective. The lifetime data of the 104 samples of 2.3 mm diameter, and the assumed half-circle uniform bending, can give the initial strength distribution of the fiber, i.e. the quality of the fiber. Then the lifetime of 2.5 mm and 2.7 mm diameter bends can be predicted based on this calculated initial strength distribution using the method developed in Section 4.4. The process is

shown as follows.

Recall from Chapter 2, for a unit area surface, ΔA_1,

$$F_{\Delta A_1} = 1 - \exp\left(-\left(\frac{\sigma_{\Delta A_1}}{\sigma_o}\right)^m\right) \tag{5-1}$$

the total failure probability for the surface area A is

$$F_A(\sigma) = 1 - \exp\left(-\int_A \frac{1}{A_0}\left(\frac{\sigma(A)}{\sigma_o}\right)^m dA\right) \tag{5-2}$$

If surface A is small enough that it can be said that the stress on surface A is uniform, then

$$F_A(\sigma) = 1 - \exp\left(-\frac{\sigma^m(A)}{A_0 \cdot \sigma_0{}^m} \cdot A\right) \tag{5-3}$$

Glaesemann's analytical result of the failure probability for fibers under uniform bending is [Glaesemann, 1991b]

$$F(\sigma_{\max}) = 1 - \exp\left(-\frac{r\sqrt{\pi} \cdot L_b}{A_0 \cdot \sigma_0{}^m} \cdot \frac{\Gamma\left(\frac{m+1}{2}\right)}{\Gamma\left(\frac{m+2}{2}\right)} \cdot \sigma_{\max}{}^m\right) \tag{5-4}$$

Here, L_b is the length of the fiber, for a half-circle,

$$F(\sigma_{\max}) = 1 - \exp\left(-\frac{\pi\sqrt{\pi} \cdot E \cdot r^2}{A_0 \cdot \sigma_0{}^m} \cdot \frac{\Gamma\left(\frac{m+1}{2}\right)}{\Gamma\left(\frac{m+2}{2}\right)} \cdot \sigma_{\max}{}^{m-1}\right) \tag{5-5}$$

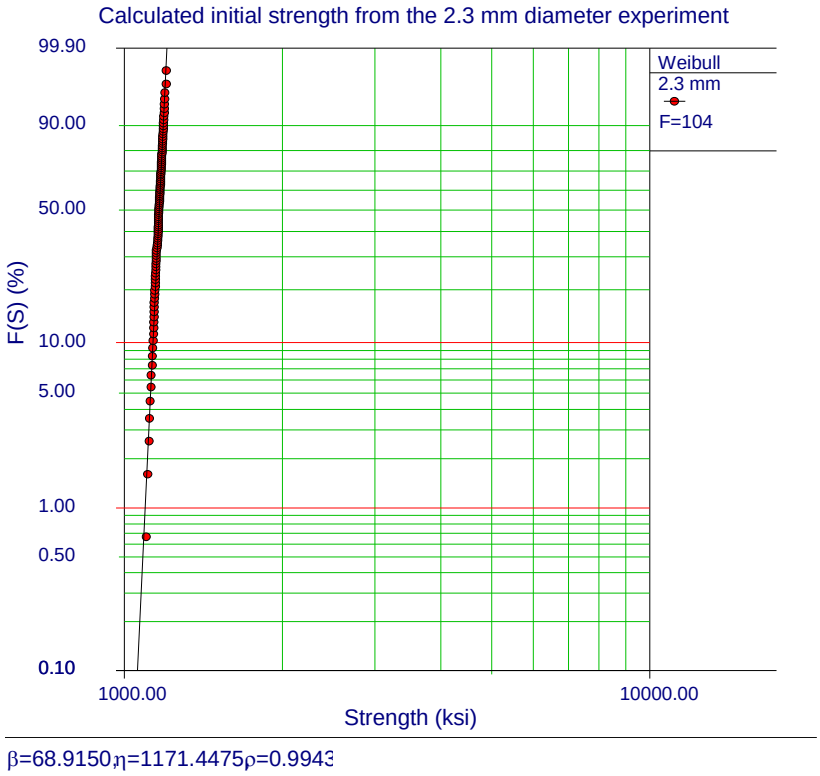

Figure 5.9 The initial strength calculated from the 2.3 mm experiment using half-circle uniform stress approximation

The Weibull parameters of the strength calculated from the 2.3 mm bend diameter experiment are (Figure 5.9): the shape parameter (β) is 68.9150, the scale parameter (η) is 1171.4475. Compared with Eq.(5-5) yields

$$m - 1 = 68.9150 \tag{5-6}$$

$$\frac{A_0 \cdot {\sigma_0}^m}{\pi\sqrt{\pi} \cdot E \cdot r^2} \cdot \frac{\Gamma(\frac{m+2}{2})}{\Gamma(\frac{m+1}{2})} = 1171.4475^{m-1} \tag{5-7}$$

Then

$$m = 69.9150 \tag{5-8}$$

$$A_0 {\sigma_0}^m = 9.363 \times 10^{206} \tag{5-9}$$

These are two parameters that are determined by the quality of the fiber. Knowing them, the reliability assessment for any arbitrary stress configuration can be done, using Eq.(5-2) or Eq.(5-3). Here, r is the radius of fiber cladding, which is 57 μm in the experiment.

Then, the lifetime of 2.5 mm and 2.7 mm diameter bends will be predicted using the method developed in Section 4.4, which is briefly repeated here.

The failure probability at area ΔA_1, at time t is equal to the probability that the initial strength is less than S_{0min}, i.e.

$$F_{\Delta A_1} = 1 - \exp(-\frac{{S_{0\min}}^m}{A_o {\sigma_o}^m} \Delta A_1) \tag{5-10}$$

Here S_{0min} is determined by lifetime, t_f, and the applied stress, σ_a.

$$S_{0\min} = \left(\left(\frac{\sigma_a}{r} \right)^{n_1 - 2} + \frac{1}{B_1} {\sigma_a}^{n_1} \cdot t_f - \frac{B_2}{B_1} \cdot {\sigma_a}^{n_1 - n_2} \cdot \left(\frac{1}{r^{n_2 - 2}} - 1 \right) \right)^{\frac{1}{n_1 - 2}} \tag{5-11}$$

Then

$$F_{total} = 1 - R_{total} = 1 - \prod_{i=1}^{k} R(\Delta A_i) = 1 - \prod_{i=1}^{k} F(\Delta A_i) \tag{5-12}$$

So the predicted data are arbitrary lifetimes and the corresponding failure probabilities. With this data, it is easy to draw the Weibull distribution curve of lifetime in the Weibull software. Figure 5.10 and Figure 5.11 compare the predicted lifetime distribution with the measured lifetime distribution of 2.5 mm and 2.7 mm bends, respectively.

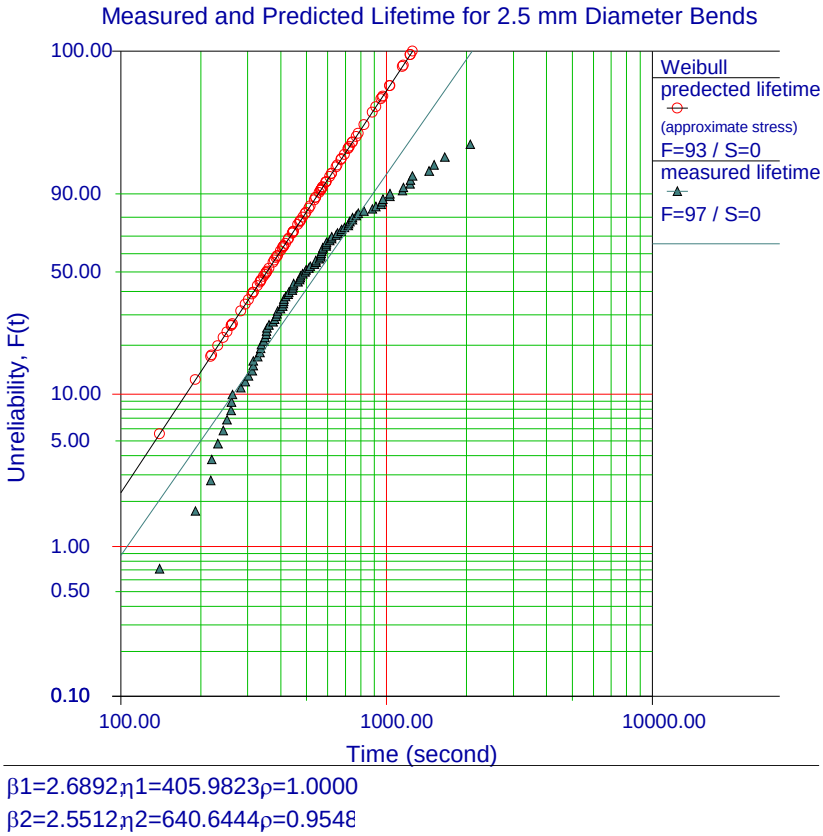

Figure 5.10 Measured and predicted lifetime for 2.5 mm bend

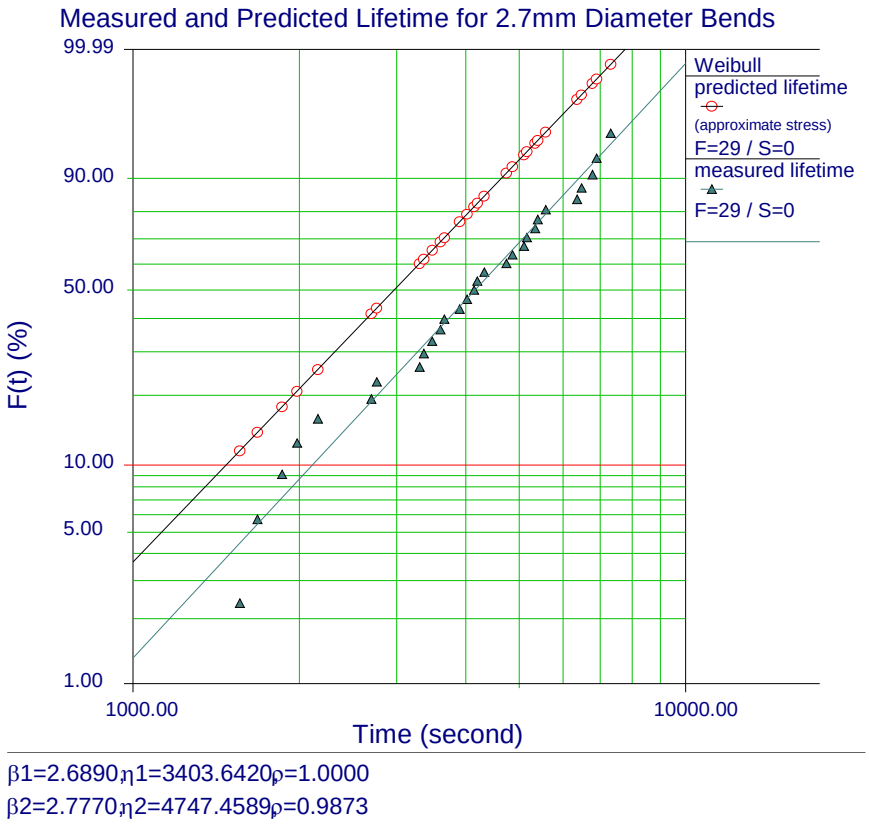

Figure 5.11 Measured and predicted lifetime for 2.7 mm bend

Table 5-1 Weibull distribution parameters from measured and predicted lifetime for 2.5 mm and 2.7 mm bends

	2.5 mm bend diameter		2.7 mm bend diameter	
	shape parameter, β	scale parameter, η	shape parameter, β	scale parameter, η
Measured	2.5512	640.6444	2.7770	4747.4589
Predicted	2.6892	405.9823	2.6890	3403.6420
Error	0.137 (5%)	245 (38%)	0.088 (3%)	1344 (28%)

From Figure 5.10 and Figure 5.11, the predicted curves have almost the exact slope as the measured curves, but are shifted left somehow. It is seen from Table 5-1, the predicted shape parameters, which influence the slope of the curve in the Weibull plot, are at most 5% away from the measured curves. But the scale parameters could be 38% less than the measured parameters.

This assessment method gives a very conservative lifetime prediction. An accurate stress analysis, instead of the approximate half-circle bend, is used next to see if more accurate predictions can be obtained.

5.4 Experiment Result Analysis (Accurate Stress Analysis)

Theoretically, the two-point bend causes non-uniform bending along fiber length (Figure 5.12). Gulati [Gulati, 1981] and France *et al.* [France, 1980] independently presented an analysis of the bending caused by two-point bend, with agreeable results.

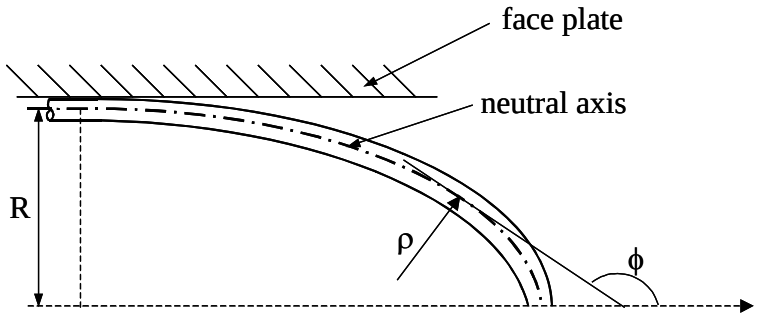

Figure 5.12 The accurate stress configuration of a two-point bend

According to Gulati and France's analysis

$$\sigma(\phi) = r\sqrt{\frac{2EF \cdot \sin\phi}{I}} \tag{5-13}$$

$$R = 0.847\sqrt{\frac{EI}{F}} \tag{5-14}$$

Eq.(5-13) and (5-14) gives

$$\sigma(\phi) = 1.198\frac{E \cdot r}{R}\sqrt{\sin\phi} \tag{5-15}$$

The maximum stress, $\sigma_{\max}$, occurs at $\phi = \pi / 2$ and is

$$\sigma_{\max} = 1.198\frac{E \cdot r}{R} \tag{5-16}$$

Compared to the half-circle bend approximation, in which $\sigma_{\max} = \frac{E \cdot r}{R}$, the accurate stress situation is more severe in the middle of the bend, but less at the ends.

From Figure 5.13, the accurate stress analysis causes a shift of the calculated strength curve of the 2.3 mm bend to the right, i.e. high strength direction. The two new Weibull parameters are: $\beta = 68.8380$, $\eta = 1423.0446$

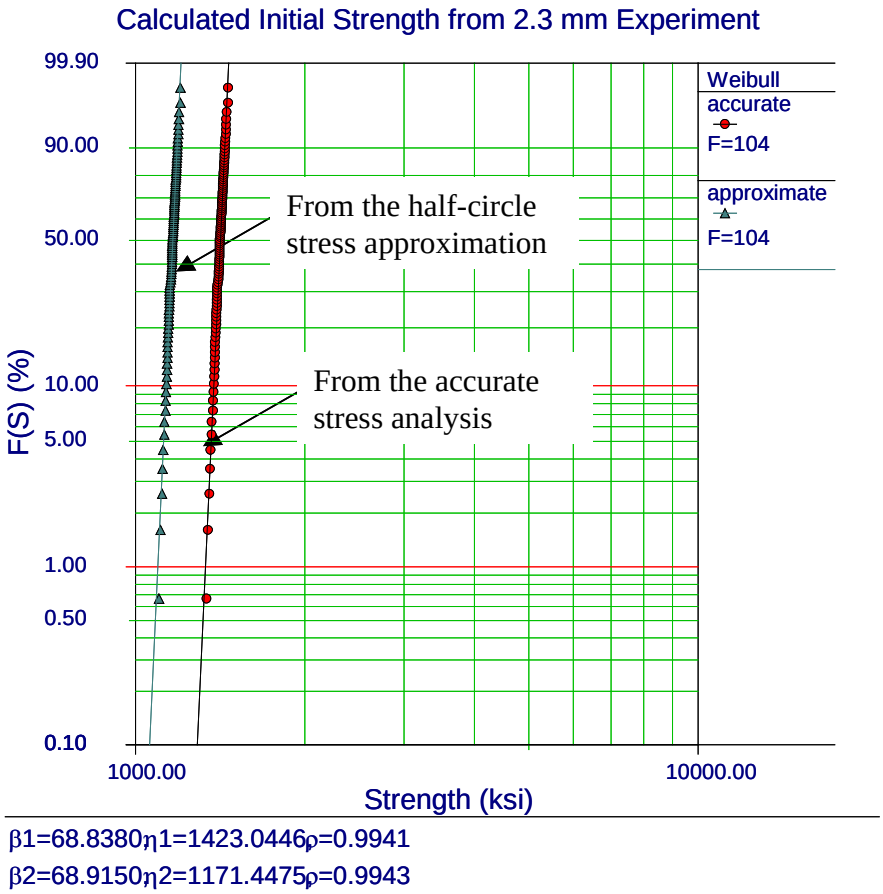

Figure 5.13 The initial strength calculated from the 2.3 mm experiment using the accurate and approximate stress analysis

Based on Eq.(5-2), and using the accurate bending stress (Eq.(5-15)), the failure probability of the two-point bend can be derived. The result from Matthewson's analysis is [Matthewson, 1986]

$$F(\sigma_{\max}) = 1 - \exp\left[-\frac{4Er^2}{A_0 \sigma_0^{\,m}} \cdot \psi\left(\frac{m-1}{2}\right) \cdot \psi(m) \cdot \sigma_{\max}^{\,m-1} \right] \qquad (5\text{-}17)$$

Here $\psi(x)$ is given as

$$\psi(x) = \frac{\sqrt{\pi}}{2} \cdot \frac{\Gamma(\frac{x+1}{2})}{\Gamma(\frac{x+2}{2})} \tag{5-18}$$

Comparing the Weibull parameters from experiment data (Figure 5.13) with Eq.(5-17), yields

$$m - 1 = 68.8380 \tag{5-19}$$

$$\frac{A_0 \cdot \sigma_0{}^m}{4Er^2} \cdot \frac{1}{\psi(\frac{m-1}{2}) \cdot \psi(m)} = 1423.0446^{m-1} \tag{5-20}$$

Then

$$m = 69.8380 \tag{5-21}$$

$$A_0 \sigma_0{}^m = 4.812 \times 10^{211} \tag{5-22}$$

Finally, lifetimes of the 2.5 mm and 2.7 mm diameter bends can be predicted using the method described in Section 5.3. The result is given in Figure 5.14 and Figure 5.15, in which solid triangles show the measured lifetime, and opened circles show the predicted lifetime.

The accurate stress analysis does shift the curve of the approximate stress analysis, to the right, but it is still left of the measured curve. Thus, the predicted lifetime from the accurate stress analysis is still conservative. Table 5-2 compares the three curves quantitatively. The two stress analysis methods get similarly shape

parameters, with acceptable error, but the accurate stress analysis decreases error of the scale parameter by 10%.

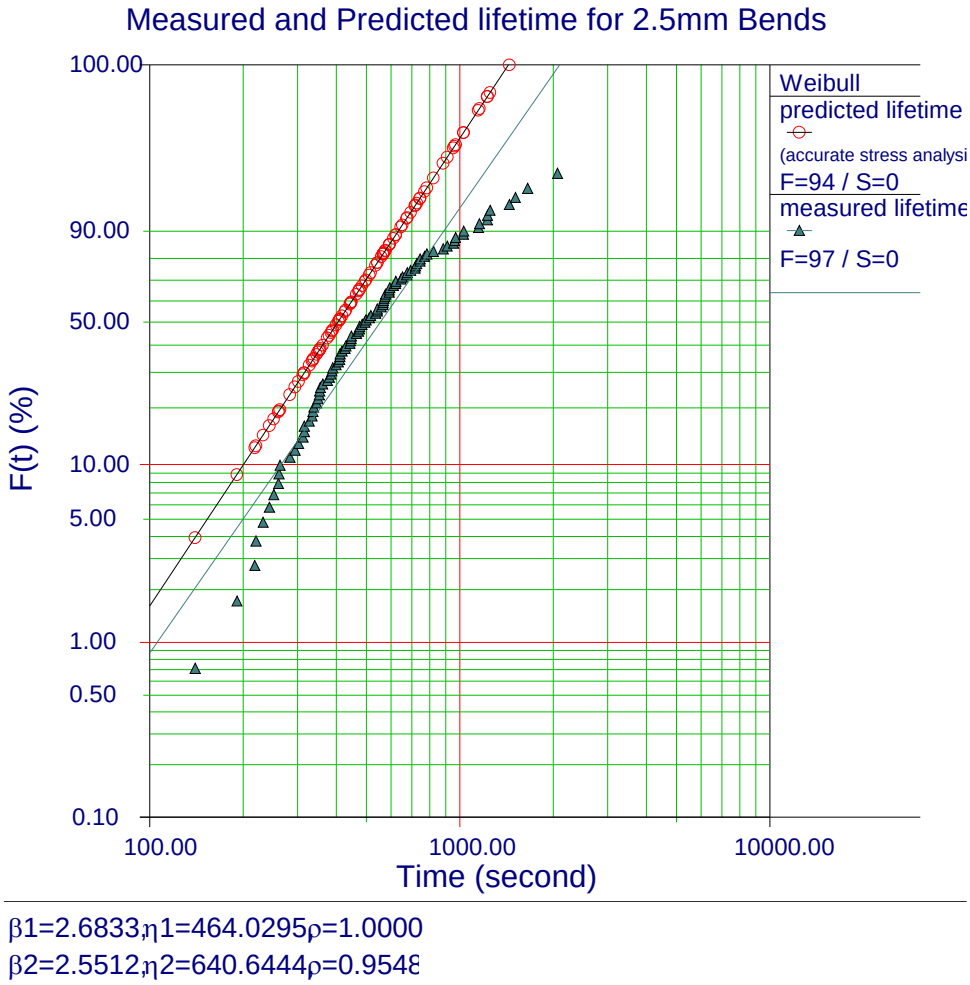

Figure 5.14 Measured and predicted lifetime for 2.5 mm bend using the accurate stress analysis

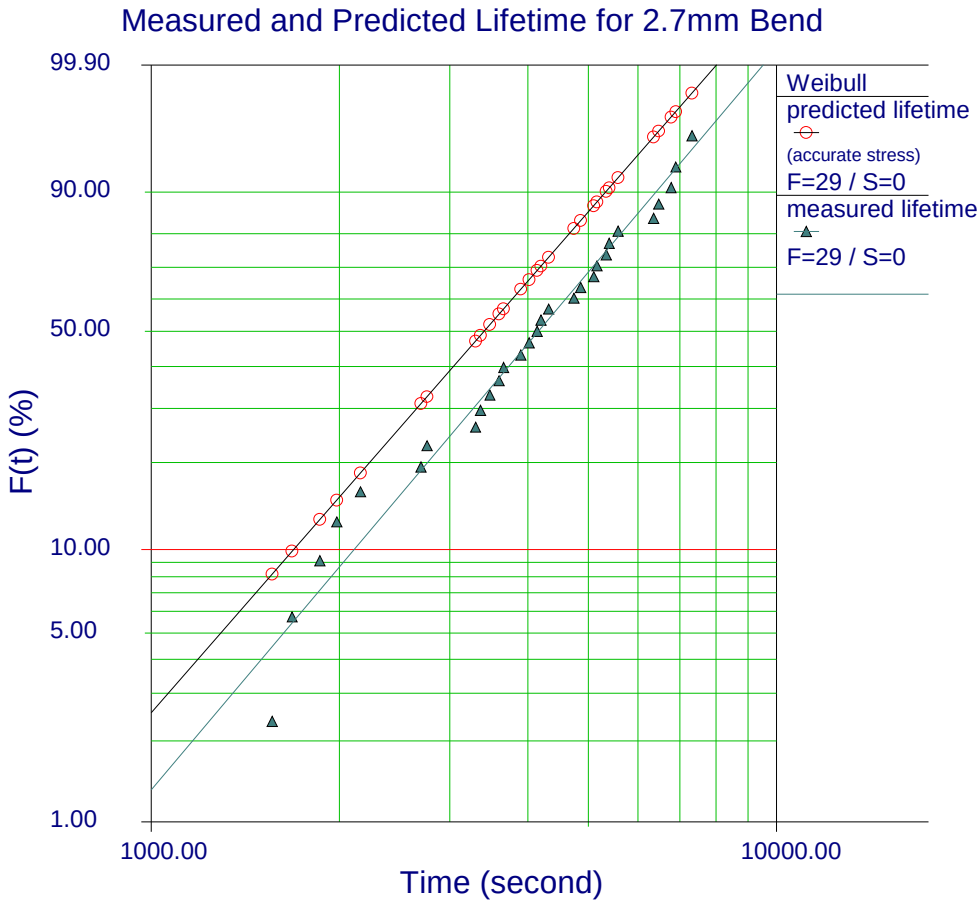

Figure 5.15 Measured and predicted lifetime for 2.7 mm bend using the accurate stress analysis

Table 5-2 Weibull distribution parameters from measured and predicted lifetime for 2.5 mm and 2.7 mm bends

	2.5 mm bend diameter		2.7 mm bend diameter	
	shape parameter, β	scale parameter, η	shape parameter, β	scale parameter, η
Measured	2.5512	640.6444	2.7770	4747.4589
Predicted (approximate stress analysis)	2.6892	405.9823	2.6890	3403.6420
	Err: 0.137 (5%)	245 (38%)	0.088 (3%)	1344 (28%)
Predicted (accurate stress analysis)	2.6833	464.0295	2.6861	3904.6873
	Err: 0.1321(5%)	176.6(28%)	0.0909(3%)	843(18%)

Notice that the measured lifetime data of 2.5 mm bends does not fit in the straight 2 parameter Weibull distribution quite well. The line from the actual data shows curves at high strength and low strength. But the curve cannot be explained by experimental uncertainty (the error caused by the measurement of R is ± 0.01 mm, the error caused by the measurement of lifetime is ± 2 sec).

The curve indicates that the measured lifetime data might be fitted by a 3-parameter Weibull distribution better than a 2-parameter Weibull distribution. Then to compare the predicted lifetime distribution with the measured lifetime distribution, the predicted lifetime data has to be fitted in a 3-parameter Weibull plot as well, which in turn requires a 3-parameter Weibull distribution of the initial strength distribution. But

generally the initial strength data is fitted in a 2-parameter Weibull distribution. So 2-parameter Weibull distribution is the lifetime distribution used in this dissertatioin.

If a 3-parameter Weibull initial strength distribution has to be used, one must redo all the theoretic work from the beginning — assume a 3-parameter Weibull initial strength distribution of a unit area along the fiber surface, and do the integration according to Eq.(2-10).

The main purpose of the two-point bend experiment is to verify the reliability assessment method developed in Chapter 4. Using the accurate stress analysis, reasonable lifetime prediction can be achieved. The experiment results supported the newly developed reliability assessment approach of bending with fatigue problem and the stress analysis by Gulati and France of two-point bend.

5.5 Summary

The static micrometer two-point bend experiment is used in this chapter to verify the reliability assessment approach of the bending fiber with static fatigue problem developed in Chapter 4. From the lifetime data of the 2.3 mm diameter samples, the initial strength distribution of the fiber can be calculated. Then the lifetime of 2.5 mm and 2.7 mm diameter bends can be predicted based on this calculated initial strength distribution using the method developed in Section 4. Compared with measured lifetime of 2.5 mm and 2.7 mm bends, the approach gives a conservative but good enough

prediction. So the result of the static two-point bend experiment verifies the reliability assessment approach of the bending fiber with static fatigue problem developed in Chapter 4.

Both approximate uniform bending stress analysis and accurate stress analysis are used in the calculation. The accurate stress analysis leads to a better lifetime prediction.

This chapter is also a demonstration of how the bending test data can be used to do reliability assessment, but not like other workers who use the bending strength directly as the initial breaking strength, some appropriate extrapolation must be utilized to get the real initial strength distribution. Also this chapter demonstrates that not all the time is a tensile test needed to get the initial strength distribution, for some applications, a simple bending test could be used. But it must be remembered that bending test data can only give a small part of the initial strength distribution.

Chapter 6

APPLICATION EXAMPLES

6.1 Industrial Guidelines for Bending

With the bending fiber reliability assessment method developed, guidelines for industrial application can be established.

6.1.1 Long-Term Reliability Guidelines

Based on Corning's 2000 tensile test the guideline for long-term application reliability has been calculated. The results are given in Table 6-1.

Table 6-1 Minimum allowed bend radius for long-term reliability (40 years)

Fiber Length	F = 1e-4 (100ppm)	F = 1e-5 (10ppm)	F = 1e-6 (1ppm)
1 m	5.4 mm	7.7 mm	11.4 mm
10 m	7.7 mm	11.4 mm	14.6 mm
100 m	11.4 mm	14.6 mm	18.8 mm

From the table, for a fiber that is 1 meter long, coiled at a 5.4 mm radius, its probability of breaking after 40 years is 100 ppm.

There are some subtleties from the guideline table that need to be pointed out. If

Table 6-1 is looked at diagonally, it is easy to see that if coil the fiber is coiled at the same R, but with a length of 1 order of magnitude longer, then the failure probability will be 1 order of magnitude higher. This is consistent with the previous mathematical analysis that at a low F level the failure probability is proportional to fiber length.

In Corning's newest publication *White Paper 3690* [Glaesemann, 2002] the allowable bend radius for a range of fiber lengths and failure probability levels are given. Table 6-1 is Corning guidelines for long-term application of fiber proof tested at 100 ksi.

Table 6-2 Allowable bend radius values for 20-40 year lifetime from Corning

Fiber Length	F = 1e-4 (100 ppm)	F = 1e-5 (10 ppm)	F = 1e-6 (1 ppm)
1 m	6 mm	10 mm	16 mm
10 m	10 mm	17 mm	26 mm
100 m	17 mm	27 mm	29 mm

Comparing Table 6-1 and Table 6-2, it is seen that Corning's guideline is more conservative than ours. If one look at Table 6-2 diagonally, a similar trend found in Table 6-1 can also be found — if the fiber is coiled at the same R, but with a length of 1 order of magnitude longer, then the failure probability will be 1 order of magnitude higher. Notice that the numbers in Corning's guideline table are rounded, this may

explain why diagonally the numbers are not exactly equal. Also notice, the number '29 mm' (F = 1e-6, L = 100 m) does not fit into Table 6-2 quite well. According to the trend of the numbers in Table 6-2, there should be a number greater than '29 mm' here. Because it has not been said how Corning come up with their guidelines, it is not possible to check what went wrong here.

6.1.2 Short-Term Reliability Guidelines

Short-term reliability guidelines has also been calculated. Again 1 minute is used here as short-term. The results are given in Table 6-3. Also Corning's guideline for short-term reliability is given in Table 6-4. Once again, Corning's guideline is more conservative than ours.

Table 6-3 Minimum allowed bend radius for short-term reliability

Fiber Length	F = 1e-4 (100 ppm)	F = 1e-5 (10 ppm)	F = 1e-6 (1 ppm)
1 m	3.0 mm	4.3 mm	6.3 mm
10 m	4.3 mm	6.3 mm	8.0 mm
100 m	6.3 mm	8.0 mm	10.3 mm

Table 6-4 Allowable bend radius values for short-term reliability from Corning

Fiber Length	F = 1e-4 (100 ppm)
1 m	3 mm
10 m	5 mm

100 m	8 mm

6.1.3 Reliability Assessment Curves

The reliability assessment approach developed in this dissertation can give more than just guidelines. In the bending reliability problem, there are four parameters, fiber length (L), bend radius (R), lifetime (t), and failure probability (F). Specifying any three of them, the fourth can be calculated. This provides more flexibility than the discrete data in the guidelines.

If L is fixed, there are three independent parameters, F, R and t. Plots of F verse t for different R (Figure 6.1) can be drawn, as well as F verse R plots for different t (Figure 6.4) for a particular L value. Then, because of the proportional relationship between F and L, which is proved in Section 2.4.2, F for other L values can be easily obtained. Figure 6.1 and Figure 6.4 shows the curves L = 1 m. For a fiber of length 100 m, the F value would be 100 times the value obtained from the curves.

Consistent with the previous conclusion, F is changing with t but not substantially. The time axis of Figure 6.1 spreads from 10^{-5} days (0.6 seconds) to 10^{6} days (2740 years), but the plot still cannot fully display the three regions of the curves. The curve of *R = 3 mm* just shows the region that was calculated from the high strength region from the initial strength distribution curve. The curve of *R = 10 mm* just shows the region that was calculated from the low strength region from the initial strength distribution curve. Only the curve of *R = 5 mm* shows all of the three regions. It is seen

from Figure 6.1 that the curve shifts to the right with increasing radius.

With the time axis on the order of year or minute, the failure probability curve for long-term reliability (Figure 6.2) and short-term reliability (Figure 6.3) can be easily obtained. In both pictures the curves are almost flat. Compared to the influence of time, the bend radius has a great influence on fiber reliability.

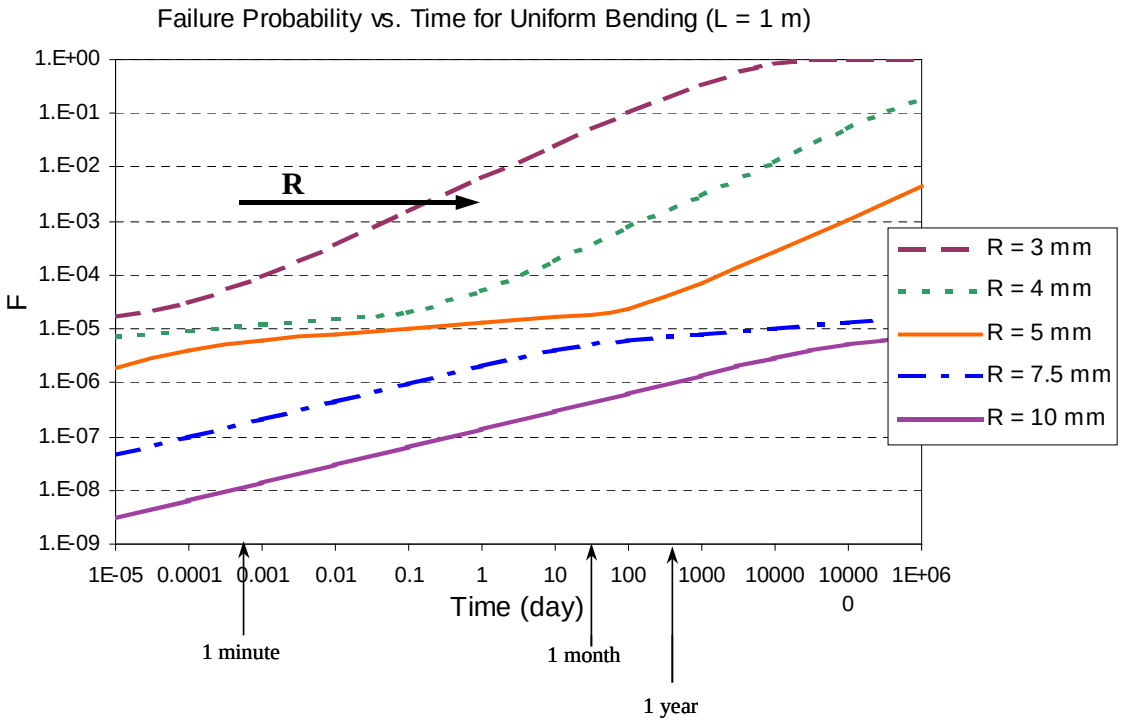

Figure 6.1 Failure probability of 1 m fiber under different bend radii

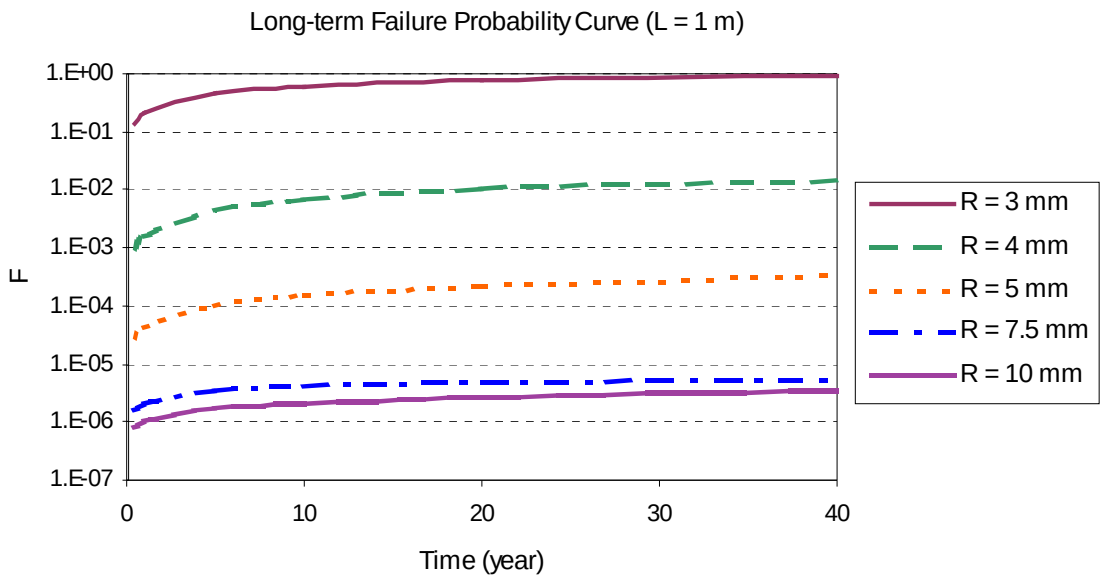

Figure 6.2 Long-term failure probability of 1 m fiber under different bend radii

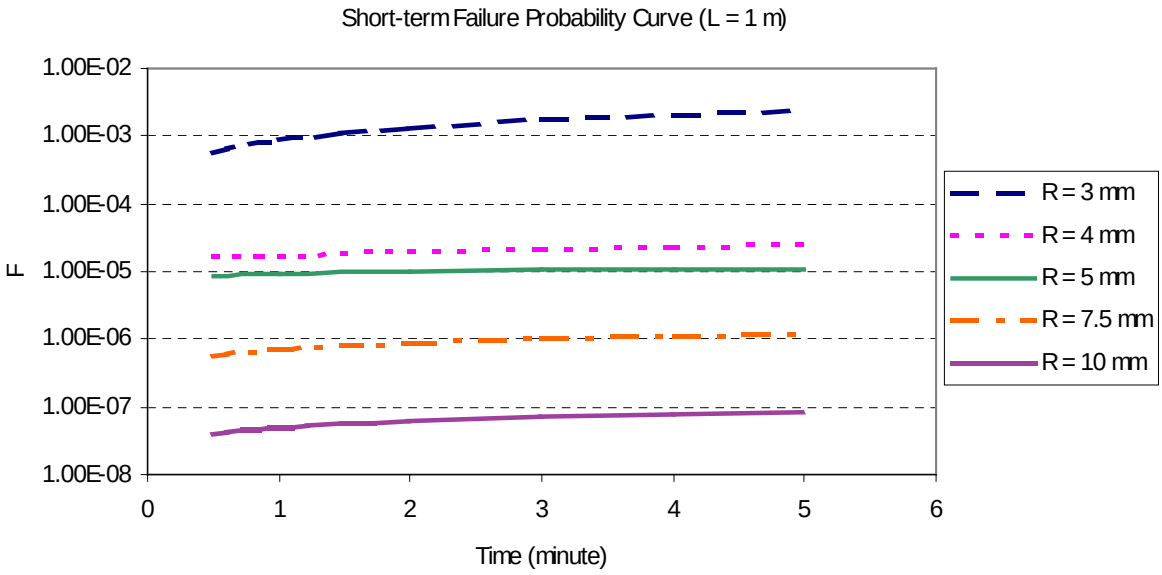

Figure 6.3 Short-term failure probability of 1 m fiber under different bend radii

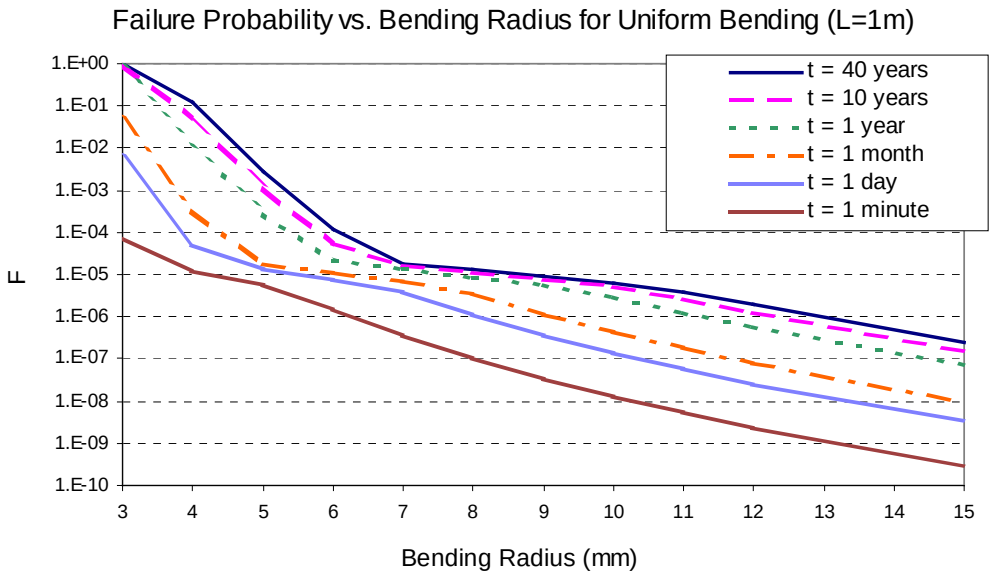

Figure 6.4 Failure probability vs. bend radius of 1 m fiber for different lifetimes

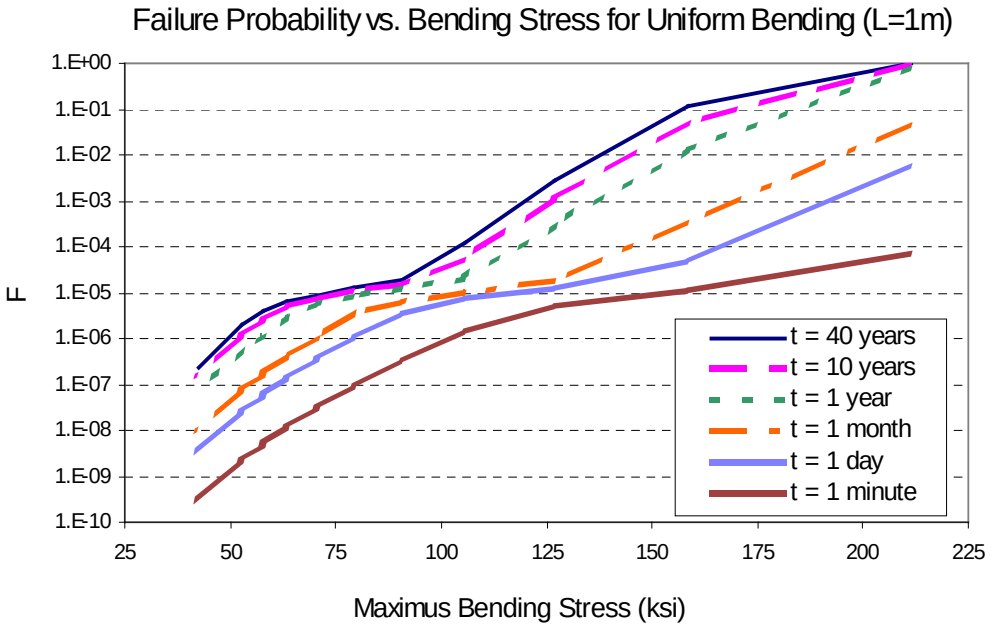

Figure 6.5 Failure probability vs. maximum bending stress of 1 m fiber for different lifetimes

Figure 6.4 shows the failure probability change with bend radius for different lifetimes, on the order of minute to year. Figure 6.5 shows the failure probability change with the maximum bending stress.

6.2 Side-Pull Test

The side-pull test is a kind of proof test applied in industry to minimize the number of fiber breaks during the optoelectronic component manufacturing process. It is discuss here to show how the new reliability assessment method can be used to solve a practical problem.

In a fiber optic component, the root of the fiber pigtail is vulnerable to stress during handling. High fallout due to fiber breaks at the fiber roots has been reported during optical circuit package manufacturing processes. These fiber breaks are the result of momentary and accidental side-pull events. A simple 500 g side-pull test is employed in industry. But, it has been found that simply passing a 500 g side pull test is not sufficient to assure that there will be no fiber breaks at the strain relief boot in the manufacturing environment.

Generally, rubber strain relief boots of various designs are employed to provide some protection to the fiber roots. C.C. Chang, et.al., from CIENA Corporation, contend that the side-pull test should not only put a direct requirement on the strength of tested fiber, but also require a minimum bend radius limited by the relief boot. They contend

the boot is a “bend limiter” rather than a “strain relief” [C.C.Chang, 2002].

In Chang’s paper, an approach is proposed to evaluate the strain relief boot. First, they calculate the minimum bend radius corresponding to a side-pull load based on Corning’s guideline, then they use a specific experiment procedure and algorithm to measure the minimum bend radius obtained by a specific relief boot. Figure 6.6 shows the minimum bend radius verse side-pull load obtained by Chang, et.al., for a failure probability roughly equal to 1 ppm for side-pull events totaling less than 1 minute in duration.

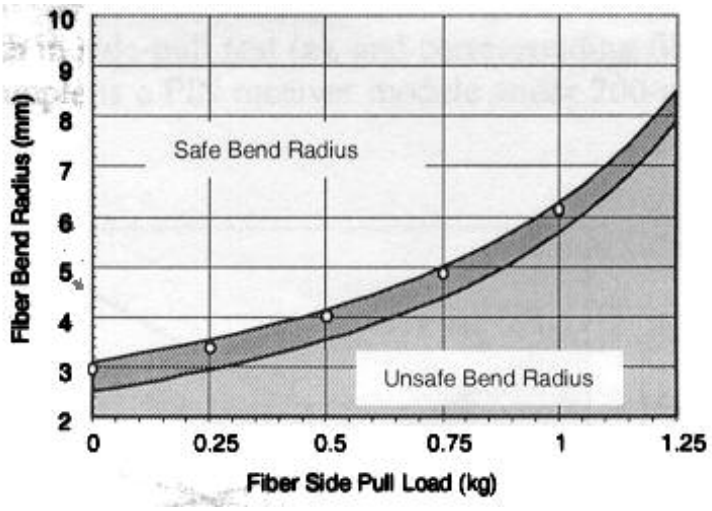

Figure 6.6 Criterion of fiber bend radius vs. side-pull load (after Chang)

What concerns us here is the minimum bend radius. It is easy to find that the way Chang calculated the minimum bend radius in side-pull test is theoretically incorrect or at least not accurate. Chang’s method is briefly described in the following paragraph.

From Corning's guideline [Castilone, 2001], a 3 mm radius bend of 1/2 turn (180^{o}) maintained for 1 minute has a failure probability of less than 0.5 ppm (1 ppm = 10^{-6}). The bending stress of a 3 mm radius bend is approximately 223 ksi. Considering a 500 g side-pull event, the applied tensile stress on the fiber is 57.8 ksi. The side pull event is actually a combination of tensile stress and bending stress event. So to ensure the failure probability less than 0.5 ppm in 1 minute, the bending induced stress should be less than 223 - 57.8 = 165.2 ksi, which corresponds to a bend radius of about 4 mm. Similarly, they got the minimum allowable bend radii for 1 ppm failure probability under 1000 g, 750 g, and 250 g side-pull loads as 6.2 mm, 4.9 mm, and 3.4 mm, respectively. And these data are shown in the criterion curvature in Figure 6.6.

Obviously they didn't take into consideration the influence of fiber length. According to the previous discussion, at a low F level, the failure probability is proportional to the fiber length. Thus, if the failure probability of a 1/2 turn (180^{o}) at 3 mm bend radius is 0.5 ppm, then for a side-pull event, which can be approximated by a 1/4 turn (90^{o}), at 3 mm bend radius, the failure probability will be 0.25 ppm. And the stress analysis needs to be improved too. From Corning's guidelines, a 3 mm bend radius (223 ksi bending stress) is designated as a stress situation like Figure 6.7(a) shows, where only the upper half circle (arc APB) is subjected to tensile stress caused by bending. But the stress situation caused by a side-pull event (57.8 ksi tensile stress + 165.3 ksi bending stress) is actually like what Figure 6.7(b) shows, where part of the

lower circle is subjected to tensile stress too — arc A'PB' is subjected to tensile stress. Therefore, simply using the guideline as Chang did will bring inaccuracy.

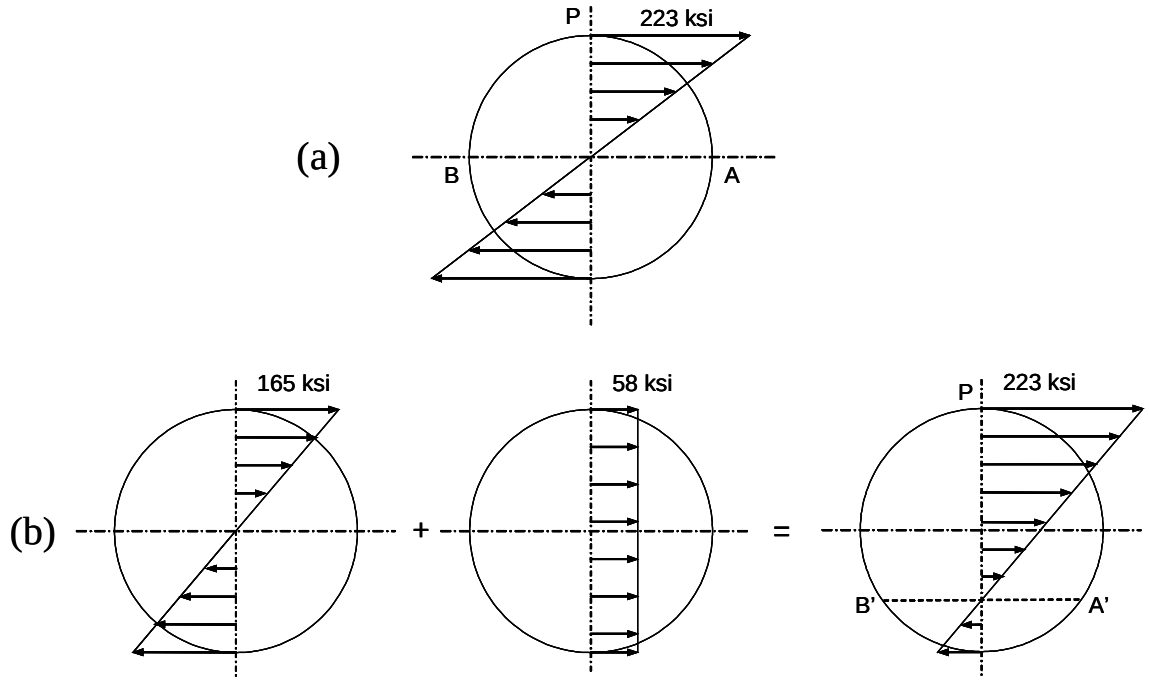

Figure 6.7 (a) Fiber cross section stress situation for pure bending with 3 mm radius (223 ksi)

(b) Fiber cross section stress situation for a 500 g side-pull and 3 mm bend radius (165+58=223 ksi)

Table 6-5 Allowable bend radius values for side-pull test

Side-pull load (g)	minimum allowable bend radius (mm)	minimum allowable bend radius from Chang (mm)
0	2.1	3
250	2.4	3.4
500	2.7	4
750	3.1	4.9
1000	3.7	6.2
1250	4.7	8.4 (guessed from plot)

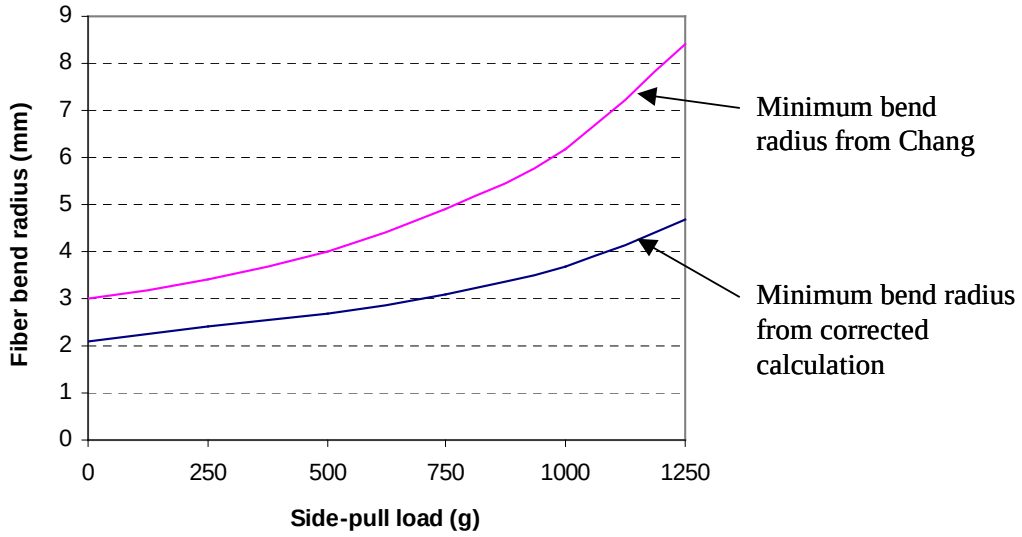

Figure 6.8 Criterion of fiber bend radius vs. side-pull load

The minimum bend radius for a failure probability roughly equal to 1 ppm of 1 minute side-pull event was calculated based on the method developed in Chapter 5,

using the accurate stress analysis shown in Figure 6.7(b). The result is shown in Figure 6.8, compared with Chang's result. From Figure 6.8, Chang's result is much more conservative than the accurate result.

6.3 Summary

With the bending fiber reliability assessment approach developed, guidelines for industrial application are established in this chapter. Furthermore, with the reliability assessment curves, one can get more than just the guidelines. Among the four parameters, fiber length (L), bend radius (R), lifetime (t), and failure probability (F), any one can be calculated given the other three.

The side-pull test is another example, showing how the reliability assessment method developed in this thesis can be used to solve a practical problem in industry. The result could be used to manufacture or evaluate relief boots more accurately.

Chapter 7

CONCLUSIONS AND FUTURE WORK

Optical fiber reliability issues have been researched for decades. There are 'fragmented' theories scattered in the literature. This dissertation is believed to be the first to systematically put together, expand, and correct all the relevant optical fiber mechanical failure theories. It presents an exact approach for optical fiber reliability assessment due to mechanical breakage.

The mechanical failure, or breakage, of optical fibers must be avoided to ensure reliability of fiber-based systems. The first stress event in a fiber's lifetime is the proof test. It is generally assumed that the proof test truncates the strength distribution at the proof test stress level, and historically no one has documented failures stresses below the proof stress level. But, this is not consistent with theoretical analysis result that after proof test the strength of fiber may be much less than the proof test stress level. This dissertation resolves this apparent contradiction by reviewing the theory and conducting a probabilistic assessment.

With the trend of using optical fiber in computer and switching gear backplanes, a new potential mechanical reliability problem arises due to the necessary bends introduced in the optical fibers. Theories about instantaneous failure assessment for optical fiber in bending has been developed, without taking into consideration of static

fatigue, but practically static fatigue plays an non-neglected role in fiber reliability. The bending with fatigue problem is a new subject. This dissertation is the first in the literature that fully discusses this subject. The dissertation reviews existing theories and then develops a new analytic approach to assess the mechanical reliability of optical fibers under bending loads and static fatigue conditions. This new analytic approach is verified through a simple static two-point bend experiment.

7.1 Conclusions

After the correction and improvement of existing post-proof test strength theories, presented in Chapter 3, some basic misconceptions involved with proof testing are resolved from a probabilistic point of view. The analysis concludes that for Corning SMF-28 fiber theoretically only one optical fiber out of a billion, $F=10^{-9}$, which passes the proof test, may have a post-proof strength less than the proof stress value. More precisely, only one fiber in a million will experience any post-proof stress strength degradation of more than 6%. Thus practically speaking from a probabilistic standpoint, the proof test basically has negligible strength degradation influence.

Through proof test simulation, this dissertation examines the parameters of the proof test. The proof stress level has the strongest influence on both the pre- and post-proof strengths. The proof test dwell time is the second most important parameter. From a practical probabilistic standpoint, the proof-test unloading rate and loading rate has

very little influence on the post-proof strength distribution, even though theoretically it is shown that the absolute minimum possible post-proof strength is determined by the unloading rate.

It is mathematically shown in this dissertation that the fiber strength distribution is greatly influenced by fiber length, and at a low F (failure probability) level, F is directly proportional to fiber length, L. This relationship between F and L clearly indicates that the readily available strength distribution data from Corning for 20 m fiber gauge lengths must be used with caution for assessing the strength of short length fibers.

After reviewing existing theories about the instantaneous reliability assessment of optical fibers in bending, a new analytic approach is developed to assess the mechanical reliability of optical fibers under bending loads, taking into consideration the effect of static fatigue. Static fatigue is the phenomena in glass where sub-critical crack lengths can grow under a load level less than that which would instantaneous failure. The basic idea of this new approach is to non-uniformly degrade the fiber surface strength due to the non-uniform bending stress, and then use the weakest link theory to integrate over the entire surface of the fiber to get the total failure probability.

Long-term and short-term reliability calculations using the new proposed approach are discussed in Chapter 4. A discussion of the practical implications of the calculations helps to explain the underlying mathematics. From the calculation results, the bend radius has a much stronger influence on the failure probability than time, the length of time the fiber is held at a particular bend radius. There are three regions in the

failure probability, F, verses bend radius, R, or F verses maximum stress, σ_{max}, curves. These three regions correspond respectively to the high-strength region, low-strength region, and the proof test truncation region from the initial strength distribution curve.

A relatively simple static two-point bend experiment was conducted to verify the new reliability assessment approach of fiber bending including the effect of static fatigue. The approach is used to perform a lifetime prediction for 2.5 mm and 2.7 mm diameter fiber bends in the two-point bend fixture. The prediction results are a good match with the measured lifetimes. The predictions are conducted with an approximate uniform bending stress analysis as well as with a more accurate non-uniform bend radius stress analysis. Not surprisingly the more accurate stress analysis leads to a better lifetime prediction.

The two-point bend experiments also used to demonstrate that an initial tensile test strength distribution is not needed. For some applications, a simple bending test can be used along with some corresponding extrapolation to get the fiber's initial strength distribution. Using this procedure it must be remembered that the bending test data can only give a small part of the initial strength distribution, because the procedure only tests very short lengths of fiber.

Using the bent fiber reliability assessment approach developed, guidelines for industrial application are established in chapter 6. Furthermore, the reliability assessment curves provide more flexibility. Among the four parameters, fiber length (L), bend radius (R), lifetime (t), and failure probability (F), any one can be calculated given

the other three.

The optical component fiber pig tail side-pull test is another example discussed in the dissertation that shows how the newly developed reliability assessment method can be used to solve a practical problem that is currently an issue in industry. The results can be used to help manufacture optical component bend limiting boots or assess current boots more accurately.

7.2 Future Work and Directions

There are still many issues related to optical fiber reliability assessment worth further research. Some of them are briefly indicated here.

To make an accurate reliability assessment of a specific fiber, the initial strength distribution of this kind of fiber must be known. It is important to note that the strength distribution is most strongly influenced by the manufacturing process. Thus the strength distribution of the fiber in question needs to be known not in a generic manner, but from a particular manufacturing lot or at least site and date. In this dissertation, calculations are based on the initial strength distribution of single mode fiber manufactured by Corning, and tested in year 2000. To get the initial strength distribution, Corning did arduous tensile testing using many kilometers of fiber. For the reliability assessment of another kind of optical fiber, maybe just with a different dimension, or a new generation optical fiber with improved quality, the tedious tensile test has to be done again.

Keeping track of the initial strength distributions and making it readily available for reliability assessment is critical. There are many issues associated with the tensile test itself.

B and *n* are two important crack growth constants, or stress corrosion parameters, indicating the crack growth behavior. In the calculation of this dissertation, *B* and *n* values used are predicted from Glaesemann's experiment of high speed testing of abraded optical fiber in ambient environment. There are some uncertainties surrounding the values of *B* and *n*. It is contended that *B* and *n* are temperature and humidity dependent, and the values from high-speed tests are different from that of the long-term low-stress fatigue.

The failure discussed in this dissertation is caused by pure mechanical breakage, no other factor has been taken into consideration, such as heat, optical power. It has been recently reported that the combination of moderate optical powers (500 mW) and tight bends (13 mm) can prove catastrophic for optical fibers [Sikora, 2003], according to research carried out by BT Exact in the UK. Researchers in BT proposed that the damage is caused by an increase in temperature that occurs when the power leaks out of the fiber at a bend and is absorbed by its coating. This either causes the fiber coating to burn off leaving the silica beneath exposed or if the temperature is high enough (around 1100°C) the fiber itself deforms giving rise to a large permanent optical loss. The failure occurs more rapidly as the power level rises and the fiber diameter shrinks. So bringing in more factors in the fiber reliability problem and making more accurate assessment is

one direction of future work.

It has been found that in a nuclear reactor severe embrittlement of optical protective jacket will leads to premature mechanical failure of fiber itself [Berghmans, et.al., 1996], weather or not the radiation will cause embrittlement of optical fiber itself need further research.

Appendix A

STRENGTH DEGRADATION CURVE DURING PROOF TEST BASED ON THE TWO-REGION MODEL

constants

$n_1 \quad 28 \qquad B_1 \quad 1.86\,10^{7} \quad GPa^2S$

$n_2 \quad 2.25 \qquad B_2 \quad 4.39\,10^{3} \quad GPa^2S$

$r \quad 0.81$

Prooftest

$_p \quad 0.69 \quad GPa$

$t_p \quad 0.3 \quad sec \qquad t_l \quad 0.1$

$t_u \quad 0.1 \qquad v_u \quad \frac{p}{t_u} \qquad v_u \quad 6.9 \quad GPa / s$

$$\text{strength}(S_i, k) := \begin{array}{l} \text{region} \leftarrow 1 \\ T_0 \leftarrow 0 \\ \sigma_0 \leftarrow 0 \\ S_0 \leftarrow S_i \\ rr_0 \leftarrow 0 \\ \Delta t_l \leftarrow \frac{t_l}{k} \\ \Delta t_p \leftarrow \frac{t_p}{k} \\ \Delta t_u \leftarrow \frac{t_u}{k} \\ B \leftarrow 0 \end{array}$$

for $j \in 1..3 \cdot k$

break if $B = 1$

if $j \le k$

$T_j \leftarrow T_{j-1} + \Delta t_1$

$\sigma_j \leftarrow \frac{\sigma_p}{t_1} \cdot T_j$

$S_j \leftarrow \left[S_i^{n_1-2} - \frac{1}{B_1} \cdot \frac{\sigma_p^{n_1} \cdot (T_j)^{n_1+1}}{t_1^{n_1} \cdot (n_1+1)} \right]^{\frac{1}{n_1-2}}$

$rr_j \leftarrow \frac{\sigma_j}{S_j}$

if $k < j \le 2k$

$T_j \leftarrow T_{j-1} + \Delta t_p$

$\sigma_j \leftarrow \sigma_p$

if region = 1

$S_j \leftarrow \left[(S_{j-1})^{(n_1-2)} - \frac{1}{B_1} \cdot \sigma_p^{n_1} \cdot \Delta t_p \right]^{\frac{1}{n_1-2}}$

$rr_j \leftarrow \frac{\sigma_j}{S_j}$

region $\leftarrow 2$ if $rr_j > r$

if $rr_j > 1$

$B \leftarrow 1$

break

if region = 2

$S_j \leftarrow \left[(S_{j-1})^{(n_2-2)} - \frac{1}{B_2} \cdot \sigma_p^{n_2} \cdot \Delta t_p \right]^{\frac{1}{n_2-2}}$

$rr_j \leftarrow \frac{\sigma_j}{S_j}$

if $rr_j > 1$

$B \leftarrow 1$

break

if $2k < j \le 3k$

$T_j \leftarrow T_{j-1} + \Delta t_u$

$\sigma_j \leftarrow \frac{\sigma_p}{t_u} \cdot \left[t_1 + t_p + t_u - (T_j) \right]$

if region = 1

$$S_j \leftarrow \left[S_i^{n_1-2} - \left[\frac{1}{B_1} \cdot \sigma_p^{n_1} \cdot \left(t_p + \frac{t_1 + t_u}{n_1 + 1} \right) \right] + \frac{1}{B_1} \cdot \sigma_p^{n_1} \cdot \frac{\left(t_1 + t_p + t_u - T_j \right)^{n_1+1}}{\left(n_1 + 1 \right) \cdot t_u^{n_1}} \right]^{\frac{1}{n_1-2}}$$

$rr_j \leftarrow \frac{\sigma_j}{S_j}$

region $\leftarrow 2$ if $rr_j > r$

if $rr_j > 1$

$B \leftarrow 1$

break

if region = 2

$$S_j \leftarrow \left[\left(S_{j-1} \right)^{(n_2-2)} - \frac{1}{B_2} \cdot \left(\sigma_j \right)^{n_2} \cdot \Delta t_u \right]^{\frac{1}{n_2-2}}$$

$rr_j \leftarrow \frac{\sigma_j}{S_j}$

if $rr_j > 1$

$B \leftarrow 1$

break

$$\begin{pmatrix} T \\ \sigma \\ S \end{pmatrix}$$

Input:

Initial Strength before proof test is:

S_i 168.5534267808781 kpsi

$S_i \quad \frac{S_i}{100} 0.69 \qquad S_i \quad 1.163 \quad \text{GPa}$

Result:

X strength S_i 100

T X_0 X_1 GPa S X_2 GPa

$\frac{}{0.69} 100$ kpsi S $\frac{S}{0.69} 100$ kpsi

$S_f \quad S_{300} \qquad S_f \quad 44.042$ kpsi

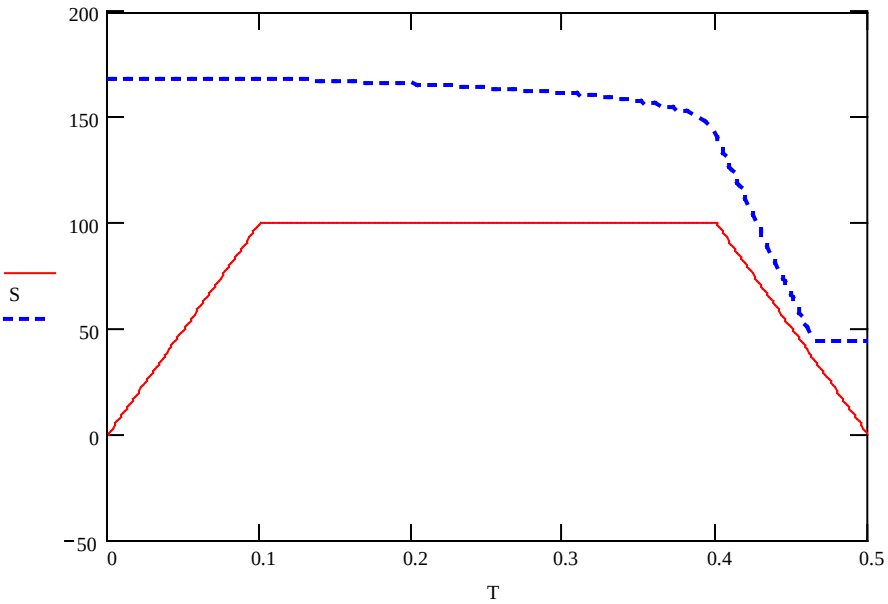

Figure A.1 An actual strength degradation behavior during proof test from simulation

Appendix B

THE TIME DERIVATIVE OF STRENGTH DURING PROOF TEST

From the definition of fiber strength,

$$S = \frac{K_{Ic}}{Y\sqrt{a}} \tag{B-1}$$

Take time derivative at both sides,

$$\frac{dS}{dt} = -\frac{K_{Ic}}{2Y} \cdot a^{-\frac{3}{2}} \cdot \frac{da}{dt} \tag{B-2}$$

From Eq.(B-1) yields

$$a^{-\frac{1}{2}} = \frac{S \cdot Y}{K_{Ic}} \tag{B-3}$$

From the crack growth model

$$\frac{da}{dt} = AK_I^{\,n} \tag{B-4}$$

Substituting Eq.(B-3) and (B-4) into Eq.(B-2) yields

$$\frac{dS}{dt} = -\frac{S^3 \cdot Y^2}{2K_{Ic}^{\,2}} \cdot A \cdot K_I^{\,n} \tag{B-5}$$

From the definition of stress intensity factor,

$$\left.\begin{aligned} K_I &= Y \cdot \sigma \cdot \sqrt{a} \\ K_{Ic} &= Y \cdot S \cdot \sqrt{a} \end{aligned}\right\} \Rightarrow K_I = \frac{\sigma}{S} \cdot K_{Ic} \tag{B-6}$$

Substituting Eq.(B-6) into (B-5) yields

$$\frac{dS}{dt} = -\frac{1}{2} \cdot A \cdot Y^2 \cdot {K_{Ic}}^{n-2} \cdot S^3 \cdot \left(\frac{\sigma}{S}\right)^n \tag{B-7}$$

Define

$$B = \frac{1}{(n-2) \cdot A \cdot Y^2 \cdot {K_{Ic}}^{n-2}} \tag{B-8}$$

So finally,

$$\frac{dS}{dt} = -\frac{1}{B(n-2)} \cdot S^3 \cdot \left(\frac{\sigma}{S}\right)^n \tag{B-9}$$

It is easy to plot the dS/dt curve in MathCAD. Following is the worksheet from MathCAD.

Constants:

$n \quad 20$

$B \quad 10^{7} \quad \text{GPa}^2\ \text{S} \qquad B \quad \frac{B}{0.69^2}\ 10^{4} \quad B \quad 2.1 \quad 10^{3} \quad \text{kpsi}^2\ \text{S}$

$p \quad 100 \quad \text{kpsi}$

$$d(S) \quad \frac{1}{B\,(n \quad 2)}\ S^{3} \quad \frac{p}{S}^{n}$$

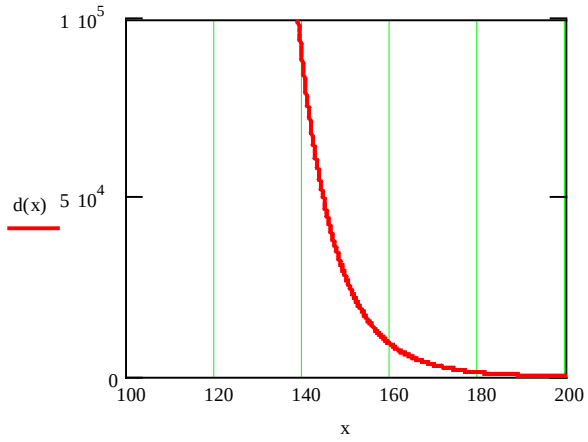

Figure B.1 The actual strength time derivative during the proof test from simulation

Appendix C

THE MINIMUM POST-PROOF STRENGTH FROM TWO-REGION CRACK GROWTH MODLE

Based on Fuller‘s method, Glaesemann solved the minimum post-proof strength problem for the two-region model. But his result is not complete, there is a small but important scenario he didn’t address explicitly. The complete solution will be given here.

According to Appendix B, the time derivative of strength along the proof test profile is

$$\frac{dS}{dt} = -\frac{1}{2} AY^2 K_{Ic}{}^{n_i-2} \left(\frac{\sigma}{S}\right)^{n_i} S^3 \tag{C-1}$$

For the situation of that the fiber just survive the proof test, there is a point where the *S(t)* curve is tangent to the unloading stress profile (Figure C.1) named $S_{*\min}$

$$\frac{dS}{dt} = -\dot{\sigma}_u \tag{C-2}$$

$$S(t) = \sigma(t) = S_{*\min} \tag{C-3}$$

Substituting Eq.(C-2) and (C-3) into Eq.(C-1) yields

$$S_{*\min}{}^3 = \frac{2}{AY^2 K_{Ic}{}^{n_i-2}} \cdot \dot{\sigma}_u \tag{C-4}$$

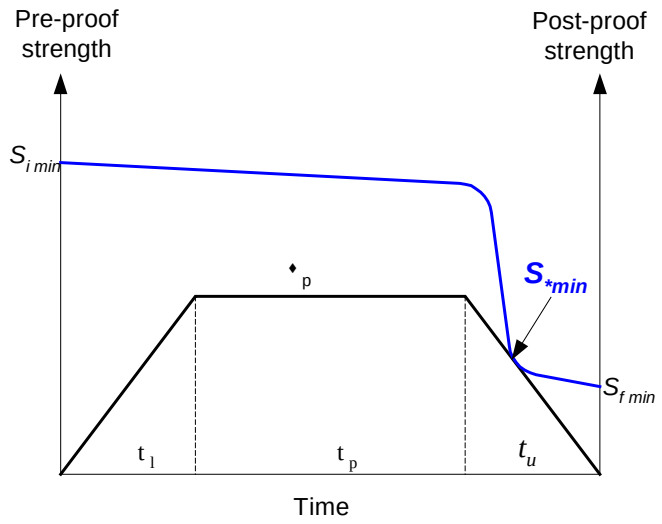

Figure C.1 The situation that just survives the proof test

Another crack growth constant B is defined as

$$B_i \equiv \frac{2}{(n_i - 2)AY^2 K_{Ic}^{\,n_i - 2}} \tag{C-5}$$

Substituting B into Eq.(C-4) yields

$$S_{*\min}^{\;3} = (n_i - 2)B_i\dot{\sigma}_u \tag{C-6}$$

It is certainly in crack growth region II when *S(t)* curve touches $\sigma(t)$ curve, so the subscript for n and B is "2" in Eq.(C-6), which would be

$$S_{*\min}^{\;3} = (n_2 - 2)B_2\dot{\sigma}_u \tag{C-7}$$

But there is a special case that needs to be taken into account: for a very high unloading rate, the tangent point calculated from Eq.(C-4) could be higher than the

proof stress, i.e., $S_{*\min} > \sigma_p$, as curve "a" in Figure C.2. This is the scenario missed in Glaesemann's solution. This situation could be solved conceptually.

Obviously, curve "a" is not a 'just survive' case, because it actually doesn't touch the proof test stress profile. One certainly can lower the pre-proof strength to get a lower knee point, until the knee point reaches the proof test stress level σ_p. The curve cannot be lowered further, because the unloading rate is so high that it not possible to find a tangent point, which is lower than the proof test stress level σ_p to satisfy Eq.(C-4). So mathematically curve "a" is the solution for high unloading rate case but physically curve "b" is the correct solution, whose $S_{*\min} = \sigma_p$.

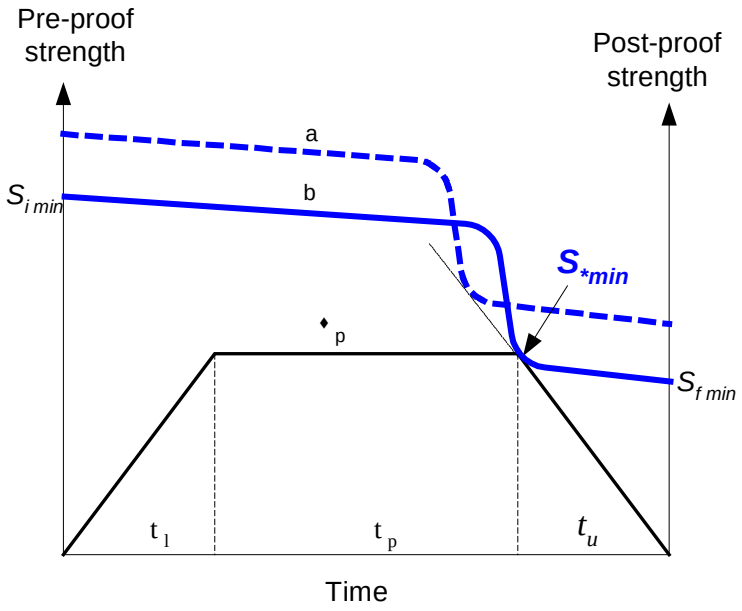

Figure C.2 The situation where the calculated $S_{*\min}$ is higher than the proof stress

So the calculation of S_{*min} depends on parameter ,

$$\alpha = \frac{\sigma_p^{\ 3}}{B_2(n_2 - 2)\dot{\sigma}_u} \tag{C-8}$$

if $\alpha > 1$, then $S_{*\min} = \sqrt[3]{B_2(n_2 - 2)\dot{\sigma}_u}$

if $\alpha < 1$, then $S_{*\min} = \sigma_p$

Then S_{*min} is reduced through dynamic fatigue at a constant stressing rate to S_{fmin}, by two steps, 1) In region II, $S_{*min} \rightarrow S_r$; 2) In region I, $S_r \rightarrow S_{fmin.}$ Here, S_r is the fiber inert strength at the cross point of region I and region II, where

$$r = \frac{\sigma_r}{S_r} \tag{C-9}$$

where σ_r is the applied proof stress and at that time.

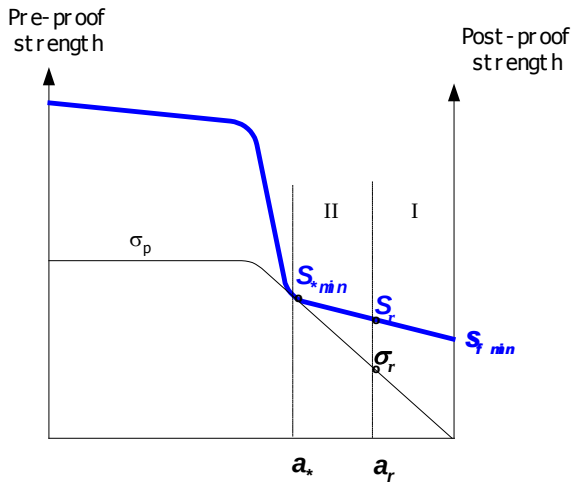

Figure C.3 The situation where the calculated $S_{*\min}$ is higher than the proof stress

1) In region II, S_{*min}, a_* → S_r, a_r

$$\frac{da}{dt} = A_2 K_I^{\,n_2} = A_2[Y(S_{*\min} - \dot{\sigma}_u t)\sqrt{a}]^{n_2} \tag{C-10}$$

$$a^{-n_2/2} da = A_2 Y^{n_2} \dot{\sigma}_u^{\,n_2} (\frac{S_{*\min}}{\dot{\sigma}_u} - t)^{n_2} dt \tag{C-11}$$

$$\int_{a_*}^{a_r} a^{-n_2/2} da = A_2 Y^{n_2} \dot{\sigma}_u^{\,n_2} \int_0^{(S_{*\min} - \sigma_r)/\dot{\sigma}_u} (\frac{S_{*\min}}{\dot{\sigma}_u} - t)^{n_2} dt \tag{C-12}$$

$$\frac{2}{n_2 - 2} \cdot a^{1-n_2/2} \Bigg|_{a = a_*}^{a = a_r} = A_2 Y^{n_2} \dot{\sigma}_u^{\,n_2} \frac{1}{n_2 + 1} \cdot (\frac{S_{*\min}}{\dot{\sigma}_u} - t)^{n_2+1} \Bigg|_{t = 0}^{t = \frac{S_{*\min}}{\dot{\sigma}_u}} \tag{C-13}$$

$$a_* = (\frac{K_{Ic}}{Y S_{*\min}})^2 \tag{C-14}$$

$$a_r = (\frac{K_{Ic}}{Y S_r})^2 \tag{C-15}$$

Subtituting Eq.(C-14) and (C-15) into (C-13) and simplifying the equation yields,

$$\frac{2}{n_2 - 2} \cdot \left[S_{*\min}^{\,n_2 - 2} - S_r^{\,n_2 - 2} \right] = A_2 K_{Ic}^{\,n_2 - 2} Y^2 \frac{1}{\dot{\sigma}_u (n_2 + 1)} \cdot \left[S_{*\min}^{\,n_2 + 1} - (S_r r)^{n_2 + 1} \right] \tag{C-16}$$

Substituting B2 into Eq.(C-16) and simplifying it yields

$$S_{*\min}^{\,n_2 - 2} \left[1 - \frac{S_{*\min}^{\,3}}{B_2 (n_2 + 1) \dot{\sigma}_u} \right] = S_r^{\,n_2 - 2} \left[1 - \frac{S_r^{\,3} r^{n_2 + 1}}{B_2 (n_2 + 1) \dot{\sigma}_u} \right] \tag{C-17}$$

2) In region I, S_r, a_r → S_{fmin}, a_f

$$\frac{da}{dt} = A_1 K_I^{\ n_1} = A_1[Y(\sigma_r - \dot{\sigma}_u t)\sqrt{a}]^{n_1} \tag{C-18}$$

$$a^{-n_1/2} da = A_1 Y^{n_1} \dot{\sigma}_u^{\ n_1} (\frac{\sigma_r}{\dot{\sigma}_u} - t)^{n_1} dt \tag{C-19}$$

$$\int_{a_r}^{a_f} a^{-n_1/2} da = A_1 Y^{n_1} \dot{\sigma}_u^{\ n_1} \int_0^{\sigma_r/\dot{\sigma}_u} (\frac{\sigma_r}{\dot{\sigma}_u} - t)^{n_1} dt \tag{C-20}$$

$$\frac{2}{n_1 - 2} \cdot a^{1-n_1/2} \Bigg|_{a=a_r}^{a=a_f} = A_1 Y^{n_1} \dot{\sigma}_u^{\ n_1} \frac{1}{n_1 + 1} \cdot (\frac{\sigma_r}{\dot{\sigma}_u} - t)^{n_1+1} \Bigg|_{t=0}^{t=\frac{\sigma_r}{\dot{\sigma}_u}} \tag{C-21}$$

$$a_f = (\frac{K_{Ic}}{Y S_{f\min}})^2 \tag{C-22}$$

Subtituting Eq.(C-22) into (C-21) and simplifying the equation yields,

$$\frac{2}{n_1 - 2} \cdot \left[S_r^{\ n_1 - 2} - S_{f\min}^{\ n_1 - 2} \right] = A_1 K_{Ic}^{\ n_1 - 2} Y^2 \frac{1}{\dot{\sigma}_u (n_1 + 1)} \cdot \frac{\sigma_r^{\ n_1 + 1}}{\dot{\sigma}_u} \tag{C-23}$$

$$\frac{1}{B_1} = \frac{n_1 - 2}{2} A_1 K_{Ic}^{\ n_1 - 2} Y^2 \tag{C-24}$$

Finally the minimum post-proof strength is derived

$$S_{f\min}^{\ n_1 - 2} = S_r^{\ n_1 - 2} - \frac{(S_r r)^{n_1 + 1}}{B_1 (n_1 + 1) \dot{\sigma}_u} \tag{C-25}$$

So the minimum post-proof strength is calculated as follows. First find out S_{*min}

$$\alpha = \frac{\sigma_p{}^3}{B_2(n_2 - 2)\dot{\sigma}_u} \tag{C-26}$$

if $\alpha > 1$, then $S_{*\min} = \sqrt[3]{B_2(n_2 - 2)\dot{\sigma}_u}$

if $\alpha < 1$, then $S_{*\min} = \sigma_p$

Then derive S_{fmin} from S_{*min} by two steps

$$\begin{cases} S_{*\min}{}^{n_2-2}\left[1 - \dfrac{S_{*\min}{}^3}{B_2(n_2+1)\dot{\sigma}_u}\right] = S_r{}^{n_2-2}\left[1 - \dfrac{S_r{}^3 r^{n_2+1}}{B_2(n_2+1)\dot{\sigma}_u}\right] \\ S_{f\min}{}^{n_1-2} = S_r{}^{n_1-2} - \dfrac{(S_r r)^{n_1+1}}{B_1(n_1+1)\dot{\sigma}_u} \end{cases} \tag{C-27}$$

REFERENCES

1. M. Abramowitz and I. A. Stegun, "Handbook of Mathematical Functions", Dover, New York, 1965
2. Janet L. Armstrong and M. John Matthewson, "Humidity Dependence of the Fatigue of High-Strength Fused Silica Optical Fibers", *Journal of the American Ceramic Society*, Vol. 38, No. 12, p. 3100-3108, Dec. 2000
3. F. Berghmans, F. Vos, M. Decreton, L. Van Den Durpel, D. Marloye, I. Vervimp, "Optical Fiber Semiconductor Absorption Temperature Sensor for Temperature Monitoring in a Gas-cooled Nuclear Reactor", *SPIE Vol. 2839, p. 182-190, Fiber Optic and Laser Sensors XIV*, Denver, August, 1996
4. G. M. Bubel and M. J. Matthewson, "Optical Fiber Reliability Implications of Uncertainty in the Fatigue Crack Growth Model", *Optical Engineering*, Vol. 30, No. 6, p. 737-745, June 1991
5. M. M. Bubnov, S. L. Semjonov, "B-Value and Optical Fiber Lifetime", *Materials Research Society Symposium Proceeding*, Vol. 531, p. 231-241, 1998
6. R. J. Castilone, "Mechanical reliability: applied stress design guidelnes," *Corning White Paper 5053*, 2001
7. R. J. Castilone, G. S. Glaesemann, T. A. Hanson, "Extrinsic Strength Measurements and Associated Mechanical Reliability Modeling of Optical Fiber", *16th Annual National Fiber Optic Engineers Conference*, Denver CO. Auguest, 2000
8. C. C. Chang, et. al., "Evaluation on Fiber Boot of Optical Component by Bend Radius Measurement in Side Pull Test", CIENA Corporation, 2002

9. S. F. Cowap and S. D. Brown, "Static Fatigue Testing of a Hermatically Sealed Optical Fiber," *Journal of American Ceramic Society*, Vol. 70, No. 4, p. C67-8, April 1987

10. V. Eitel and F. Oberlies, "Eigige Eigenschaften des Glasfadens (Some properties of glass fibers)," *Glastech. Ber*., Vol. 15, p. 228-231, 1937

11. P. W. France, M. J. Paradine, M. H. Reeve, and G. R. Newns, "Liquid Nitrogen Strengths of Coated Optical Fibres," *Journal of Material Science*, Vol. 15, No. 4, p. 825-830, April 1980

12. E.R. Fuller Jr., S. M. Wiederhorn, J. E. Ritter Jr., P. B. Oates, "Proof Testing of Ceramics, Part 2 Theory", *Journal of Materials Science*, Vol. 15, p. 2282-2295, 1980

13. G. S. Glaesemann, "Method for Obtaining Long-length Strength Distributions for Reliability Prediction", *Optical Engineering*, Vol. 30, No. 6, p. 746-748, June 1991

14. G. S. Glaesemann, "Optical Fiber Failure Probability Predictions from Long-length Strength Distributions", *40th International Wire & Cable Symposium*, p. 819-825, 1991

15. G. S. Glaesemann, "Advancements in Mechanical Strength and Reliability of Optical Fibers", *SPIE, Vol. CR73, Reliability of Optical Fibers and Optical Fiber Systems*, Boston, Sept, 1999

16. G. S. Glaesemann, D. A. Clark, T. A. Hanson, D. J. Wissuchek, "High Speed Strength Testing of Optical Fiber", *Materials Research Society Symposium Proceedings*, Vol. 531, p. 249-260, 1998

17. G. S. Glaesemann, R. J. Castilone, "The Mechanical Reliability of Corning Optical Fiber in Bending," *Corning White Paper 3690*, 2002

18. W. Griffioen, et. Al., "COST 218 Evaluation of Optical Fibre Lifetime Models", *SPIE Vol. 1791, Optical Materials Reliability and Testing*, pp. 190-201, 1992

19. W. Griffioen, "Strippability of Optical Fibers," *Proc. 11th An. Euro. Fibre Optic Comm. & Networks*, p. 239-244, 1993

20. S. T. Gulati, "Nonlinear Bending of Strong Glass Fibers," for abstract see *Am. Seram. Soc. Bull.*, Vol. 60, No. 8, p. 862, 1981

21. T. A. Hanson, "Analysis of the Proof Test with Power Law Assumptions", *SPIE Vol. 2074*, p. 108-119, 1994

22. T. A. Hanson, G. S. Glaesemann, "Incorporating Multi-region Crack Growth into Mechanical Reliability Predictions for Optical Fibers", *Journal of Material Science*, Vol. 32, p. 5305-5311, 1997

23. M. John Matthewson, Charles R. Kurkjian, and Suresh T. Gulati, "Strength Measurement of Optical Fibers by Bending", *Journal of American Ceramic Society*, Vol. 69, No. 11, p. 815-821, 1986

24. M. J. Matthewson and C. R. Kurkjian, "Static Fatigue of Optical Fibers in Bending", *Journal of American Ceramic Society*, Vol. 70, No. 9, p. 662-68, 1987

25. M. J. Matthewson and G. J. Nelson, "A Novel Four-point Bend Test for Strength Measurement of Optical Fibers and Thin Beams: Part II: Statistical Analysis," *Journal of Lightwave Technology*, Vol.14, No.4, p. 555-63, April 1996

26. M. John Matthewson, "Optical Fiber Reliability Models", *SPIE Fiber Optics Reliability and Testing, Critical Reviews*, Vol. CR50, p. 3-31, 1999

27. M. John Matthewson, "Optical Fiber Mechanical Testing Techniques", *SPIE Fiber Optics Reliability and Testing*, Critical Reviews, Vol. CR50, p. 32-59, 1999

28. Y. Mitsunaga, Y. Katsuyama, Y. Ishida, "Reliability Assurance for Long-length Optical fibre Based on Proof Testing", *Electronics Letters*, Vol. 17, No. 16, p. 567-568, 6th Auguest 1981

29. G. J. Nelson, M. J. Matthewson and B. Lin, “A Novel Four-point Bend Test for Strength Measurement of Optical Fibers and Thin Beams: Part I: Bending Analysis,” *Journal of Lightwave Technology*, Vol.14, No.4, p. 555-63, April 1996

30. J. E. Ritter, K. Jakus, and P. R. Panat, “Impact Damage and Strength Degradation of Fused Silica, Reliability of Photonics Materials and Structures”, Edited by E. Suhir, M. Fukuda, and C. R. Kurkjian, *Proceedings of the Materials Research Society*, Vol. 531, p. 53-58, San Francisco, 1998

31. E.S.R. Sikora, D. J. McCartney, K. Farrow, R. Davey, “Reduction in Fibre Reliability Due to High Optical Power”, Vol.39, No.14, p.1043-1044, July, 2003

32. D. Sinclair, “A Bending Method for Measurement of The Tensile Strength and Young’s Modulus of Glass Fibers,” *Journal of Applied Physics*, Vol. 21, p. 380-386, 1950

33. K. Yoshida, T. Satoh, N. Enomotok T. Yagi, H. Hihara, and M. Oku, “Fracture Origins of Optical Fibers Fabricated by Hybridized Process”, *Journal of Lightwave Technology*, Vol. 14, No. 11, p. 2506-2512, 1996

34. T. T. Volotinen, et. al., “Aging Behavior of Fibers”, *SPIE Passive Fiber Optic Components and Their Reliability, Berlin, Germany,* Vol.1973, p. 161-174, April 1993

35. T. T. Volotinen, et. al., “Reliability of Optical Fibers and Components: Achievements and Conclusions of COST 246”, *SPIE Optical Fiber Reliability and Testing, Boston*, Vol. 3848, p. 88-94, September 1999